Mikrostrukturna karakterizacija materijala primenom elektronskih i jonskih snopova

Institut za nuklearne nauke
“Vinča”

Laboratorija za atomsku fiziku

Nataša Bibić

Napredak u nauci uvek sledi povećanje moći rezolucije mernih uređaja. Eksteprimentalne metode koje koriste elektronske i jonske snopove doživele su značajan napredak u povećanju rezolucije, a time i u našem poznavanju strukturnih osobina široke klase materijala. Posebno zanačajan aspekt ovih uređaja je da omogućavaju bolje razumevanje veze između atomske strukture i fizičkih i hemijskih osobina materijala. Prezentacija obuhvata osnove interakcije elektrona i jona sa materijalima. Takodje, obuhvata karakteristike elektronskih mikroskopa (SEM,TEM) i spektroskopije Rutherfodovog povratnog rasejanja (RBS), eksperimentalnih tehnika koje se koriste za mikrostruktrunu karakterizaciju materijala.

Resolution

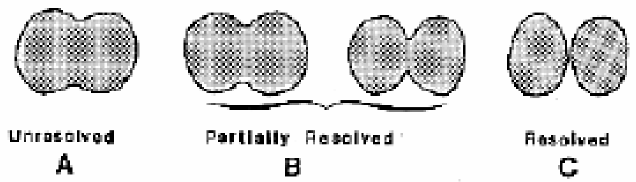

1-7. Illustration of resolution of two objects. As the resolution of these two objects improves (A—B—C), the objects can be independently visualized.

Light Microscopy

- Resolving limit

Eye	0.1 mm
Light microscope	0.2 µm
SEM	3 nm
TEM	0.2 nm

Evolution of Resolution

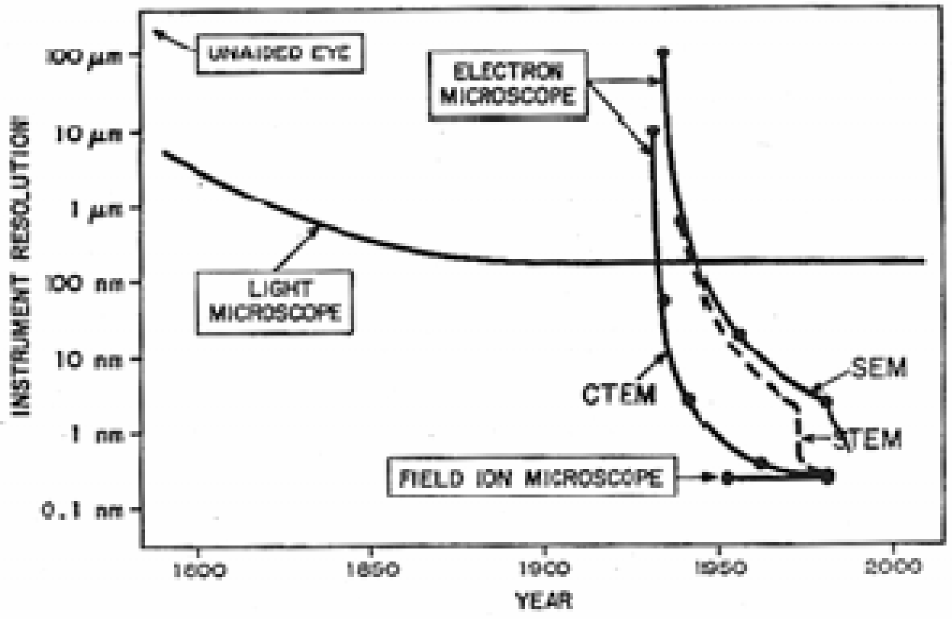

History:

First record of using glass lens for magnification was by an Arabian from what is now known as Iran, Alhazen, in the 10 and 11th century.

He contradicted Ptolemy's and Euclid's theory of vision that objects are seen by rays of light emanating from the eyes; according to him the rays originate in the object of vision and not in the eye. Because of his extensive research on vision, he has been considered by many as the father of modern optics.

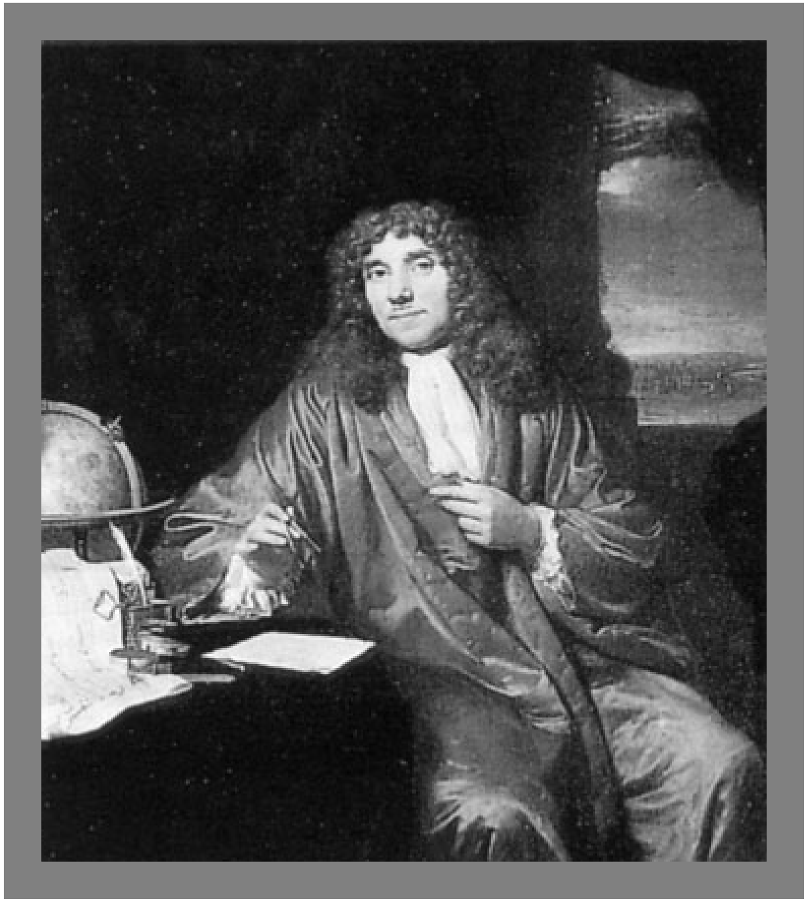

15th century on - Studies done with glass magnifiers to study objects in detail mostly as a curiosity by non-scientists - Antonie van Leeuwenhoek (linen draper) described three shapes of bacterial cells using his simple, single lens microscope (glass bead in metal holder).

Earliest Microscopes

- 1590 - Hans & Zacharias Janssen of Middleburg, Holland manufactured the first compound microscopes
- **1660** - Marcello Malpighi **circa 1660,** was one of the first great microscopists, considered the father embryology and early histology - observed capillaries in 1660
- 1665 - Robert Hooke (1635-1703)- book *Micrographia*, published in 1665, devised the compound microscope most famous microscopical observation was his study of thin slices of cork. He wrote:

> ***". . . I could exceedingly plainly perceive it to be all perforated and porous. . . these pores, or cells, . . . were indeed the first microscopical pores I ever saw, and perhaps, that were ever seen, for I had not met with any Writer or Person, that had made any mention of them before this."***

Earliest Microscopes

- 1673 - Antioni van Leeuwenhoek (1632-1723) Delft, Holland, worked as a draper (a fabric merchant); he is also known to have worked as a surveyor, a wine assayer, and as a minor city official.

- Leeuwenhoek is incorrectly called "*the inventor of the microscope*"
- Created a "simple" microscope that could magnify to about 275x, and published drawings of microorganisms in 1683
- Could reach magnifications of over 200x with simple ground lenses - however compound microscopes were mostly of poor quality and could only magnify up to 20-30 times. Hooke claimed they were too difficult to use - his eyesight was poor.
- Discovered bacteria, free-living and parasitic microscopic protists, sperm cells, blood cells, microscopic nematodes
- In 1673, Leeuwenhoek began writing letters to the Royal Society of London - published in *Philosophical Transactions of the Royal Society*
- In 1680 he was elected a full member of the Royal Society, joining Robert Hooke, Henry Oldenburg, Robert Boyle, Christopher Wren

Lister, Abbe, Zeiss & Schott

- In 1830, by **Joseph Jackson Lister** (father of Lord Joseph Lister) solved the problem of ***Spherical Aberration*** - caused by light passing through different parts of the same lens. He solved it mathematically and published this in the *Philosophical Transactions* in 1830
- **Ernst Abbe** together with **Carl Zeiss** published a paper in 1877 defining the physical laws that determined resolving distance of an objective. Known as Abbe's Law

  "minimum resolving distance *(d)* is related to the wavelength of light *(lambda)* divided by the $d = \frac{\lambda}{2 n \sin\theta}$ Numeric Aperture, which is proportional to the angle of the light cone *(theta)* formed by a point on the object, to the objective".
- **Abbe and Zeiss** developed oil immersion systems by making oils that matched the refractive index of glass. Thus they were able to make the a Numeric Aperture (N.A.) to the maximum of 1.4 allowing light microscopes to resolve two points distanced only 0.2 microns apart (the theoretical maximum resolution of visible light microscopes). **Leitz** was also making microscope at this time.
- Dr Otto Schott formulated glass lenses that color-corrected objectives and produced the first "apochromatic" objectives in 1886.

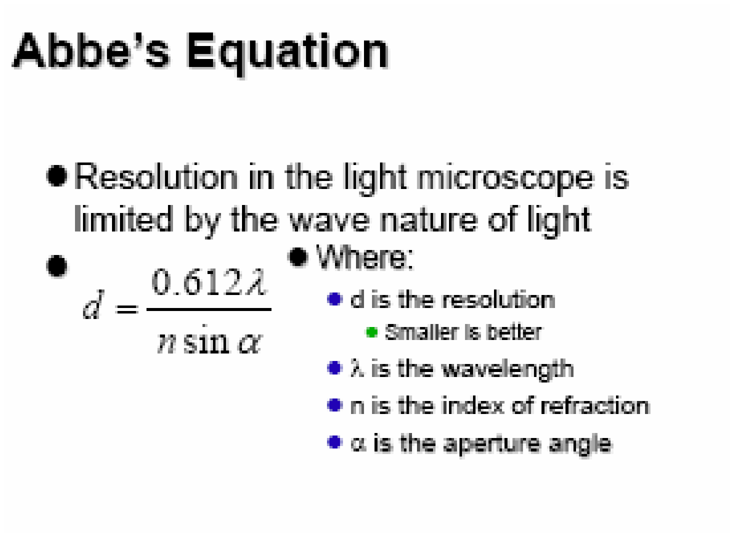

Abbe's Equation

- Resolution in the light microscope is limited by the wave nature of light
- $$d = \frac{0.612\lambda}{n \sin \alpha}$$
- Where:
  - d is the resolution
    - Smaller is better
  - λ is the wavelength
  - n is the index of refraction
  - α is the aperture angle

Origin of the Transmission Electron Microscope

DATE	NAME	EVENT
1897	J. J. Thompson	Discovers the electron
1924	Louis deBroglie	Identifies a wavelength to moving electrons $\lambda = h/mv$ where λ = wavelength h = Plank's constant m= mass v = velocity
1926	H. Busch	Magnetic fields act as lenses for electons
1929	E. Ruska	Ph.D thesis on magnetic lenses/pole piece
1931	Knoll & Ruska	First electron microscope built
1931	Davisson &Calbrick	Properties of electrostatic lenses
1934	Driest & Muller	Surpass resolution of the LM
1938	von Borries & Ruska	First practical EM (Siemens) - 10 nm resolution
1940	RCA	Commercial EM with 2.4 nm resolution
1945		1.0 nm resolution attained

J.J. Thomson's Plum Pudding Model of the Atom (1897)

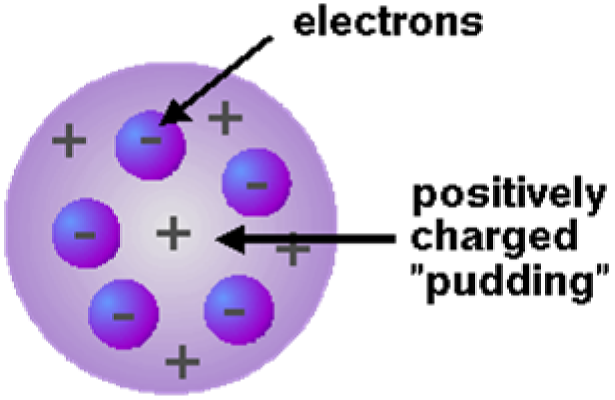

He proposed that the electrons are embedded in a positively charged 'pudding'

Rutherford’s a Scattering Experiment (1911)

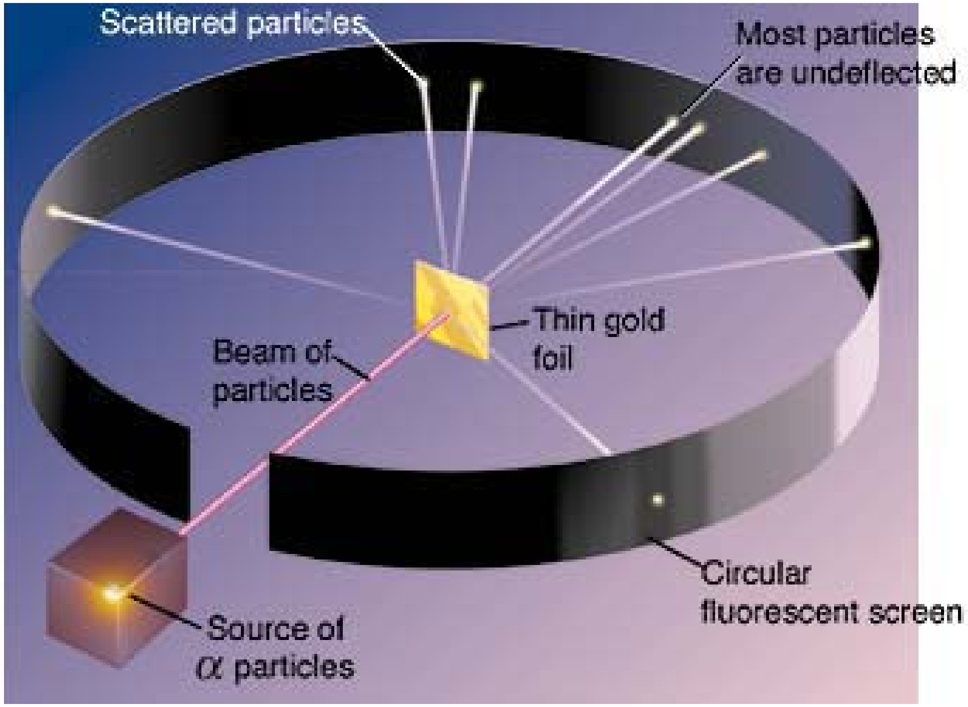

He found that, once in a while, the a-particles were scattered backwards by the target

video clip

Discovery of the Atomic Nucleus

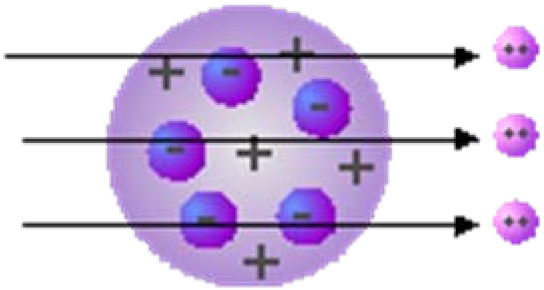

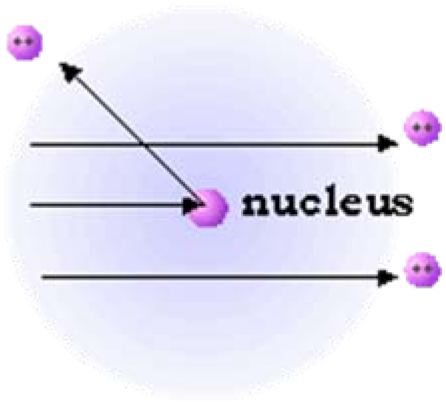

To explain the backscattering, the positive charge must be concentrated in a small region

Rutherford's Solar System Model of the Atom

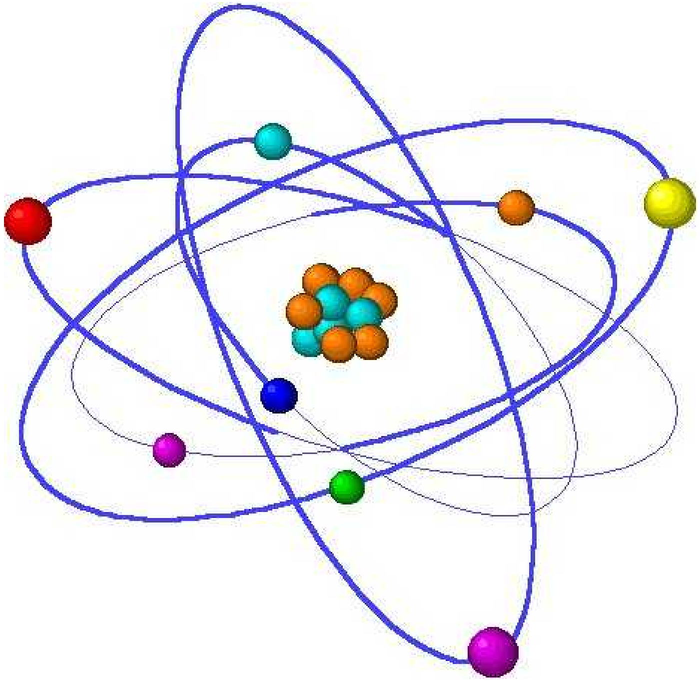

The atom consists of electrons orbiting around a small but dense central nucleus

Bohr’s Model of the Hydrogen Atom (1913)

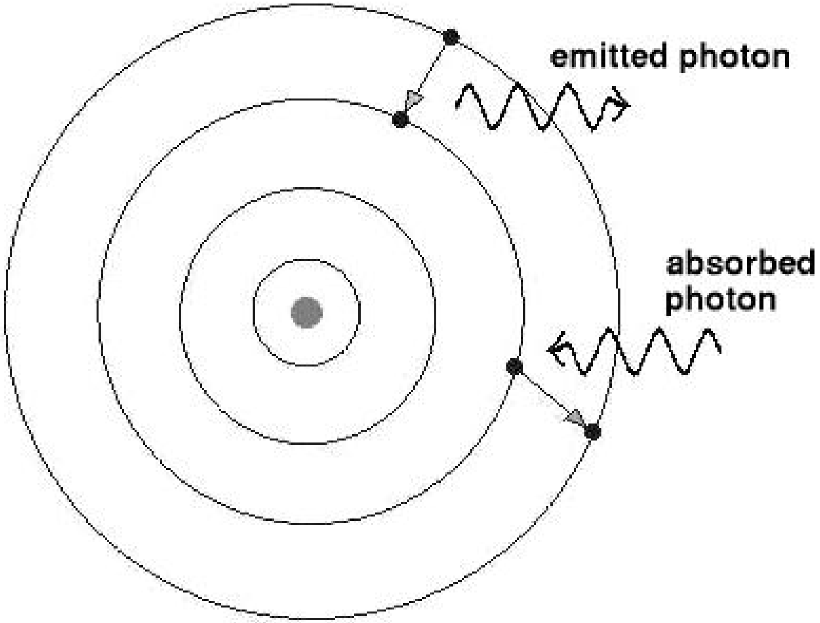

He proposed that only certain orbits for the electron are allowed

Cross Section of an Atom

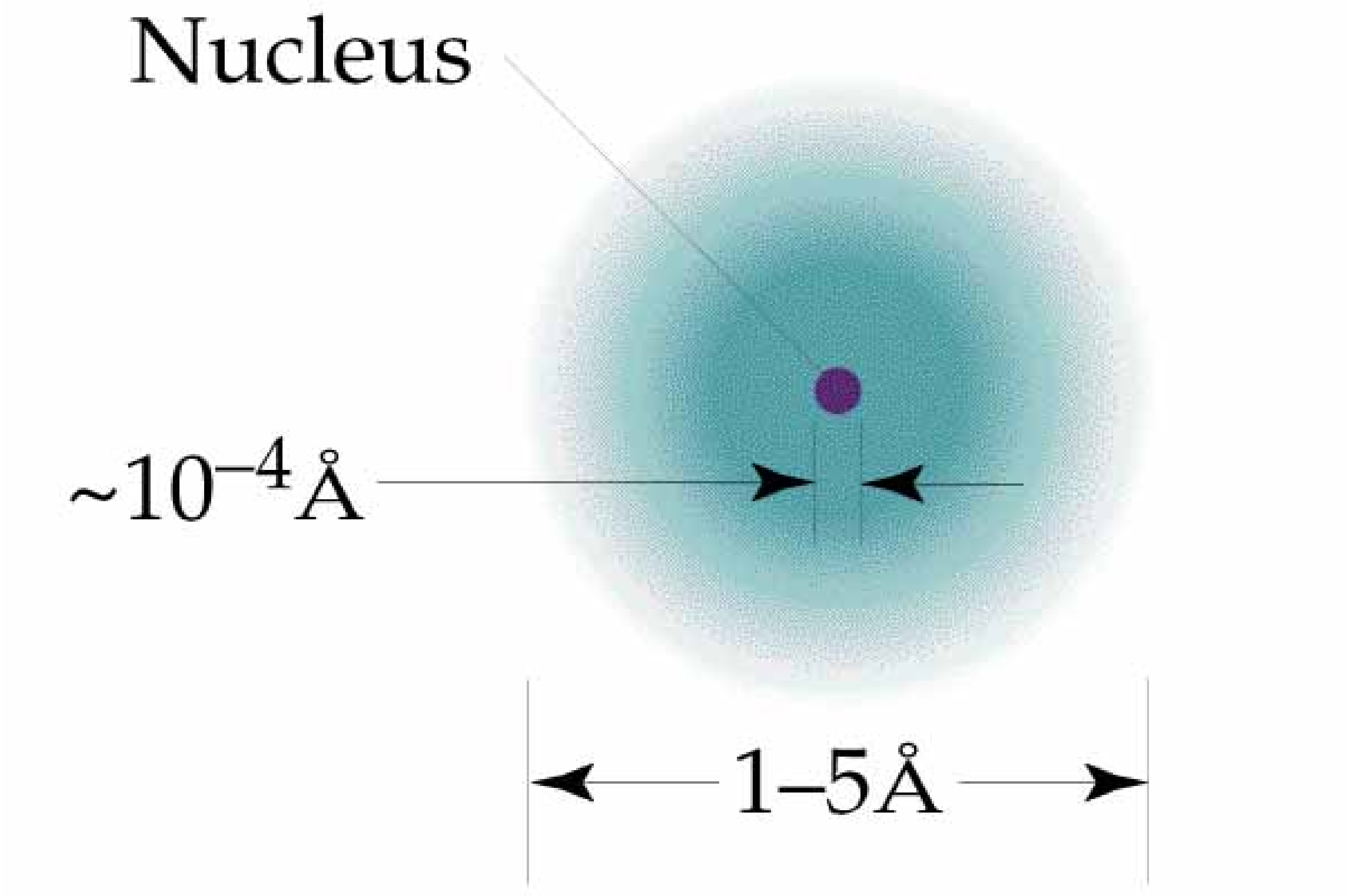

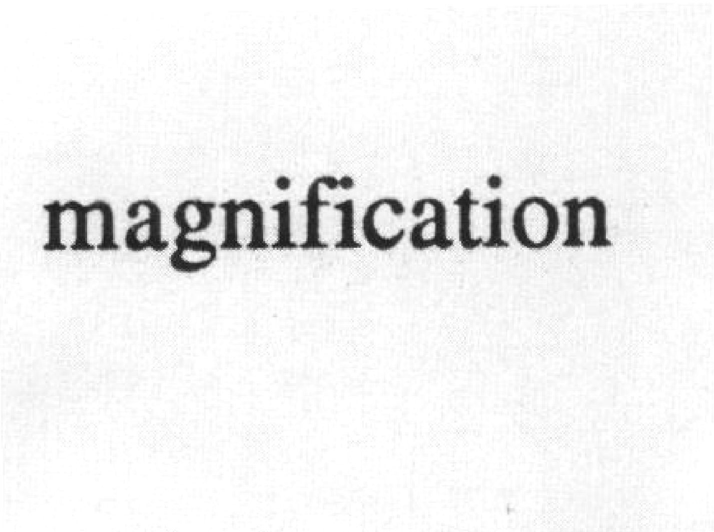

ft)

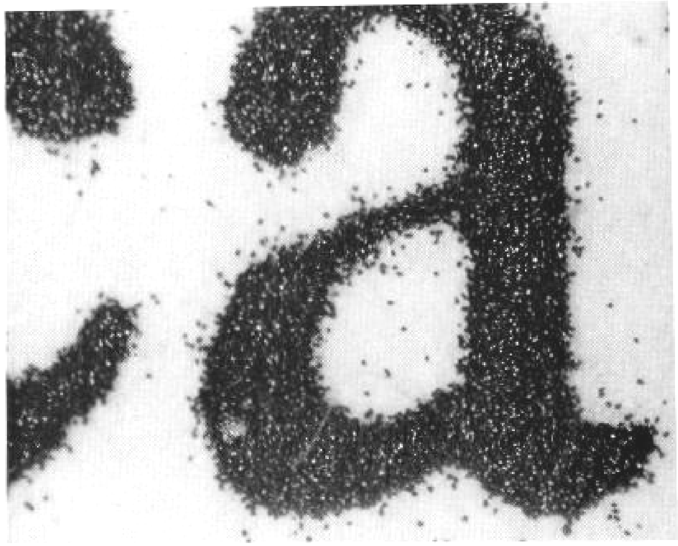

A (*Right*)

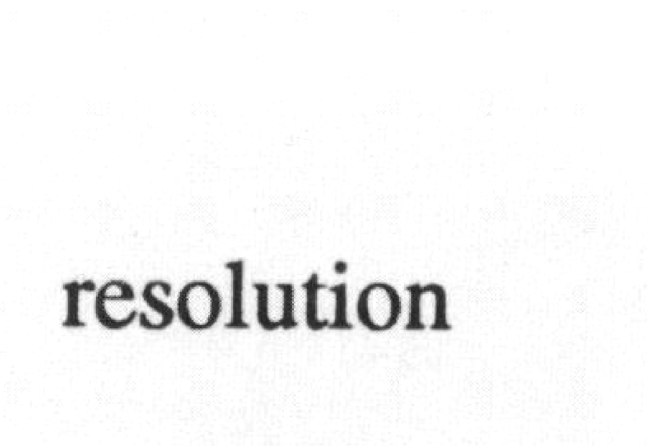

Examples:

(a) *Optical Microscope* –

λ = 50 nm (for white light Illumination)

n sin α = 0.135 (when fitted with an oil immersion lens)

Therefore, it is possible to achieve **a resolution** of about **250 nm** in Optical Microscopes.

(b) *Electron Microscope* –

De Broglie relationship relates the wavelength of electrons, λ, to their momentum, mv (m is the mass and v is velocity), by h – Planck’s constant, such that:

$$d = \frac{0.61 \times \lambda}{(n \sin \alpha)}$$

$$d = \frac{0.61 \times 500 \text{ nm}}{1.4 \text{ NA}} = \frac{217}{85} = 0.2 \ \mu\text{m}$$

Wavelength of electron beam = 0.005 nm
(10,000 times smaller than light)
Theoretical limit of resolution = 0.0025 nm
Practical limit of resolution = 0.1-0.2 nm

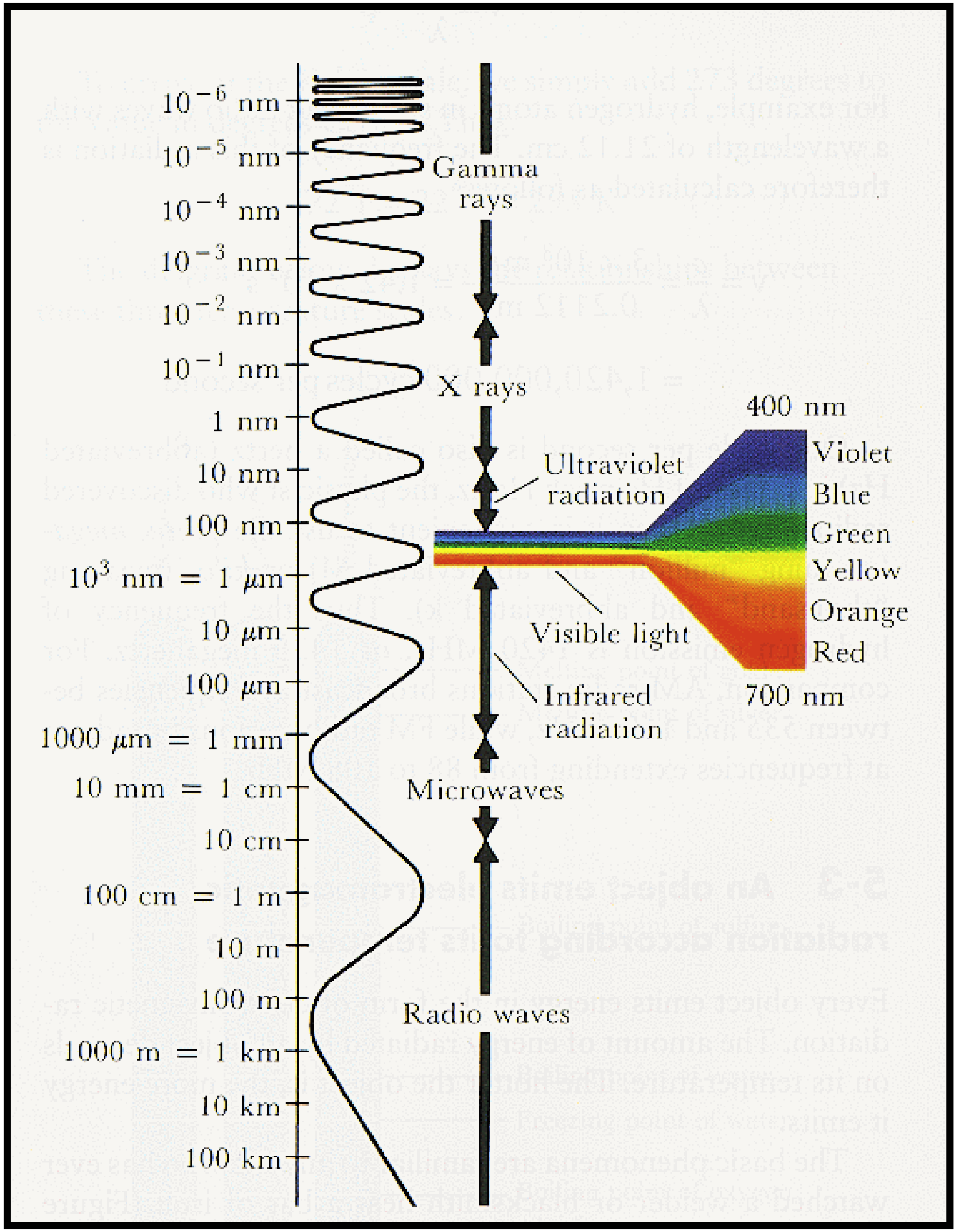

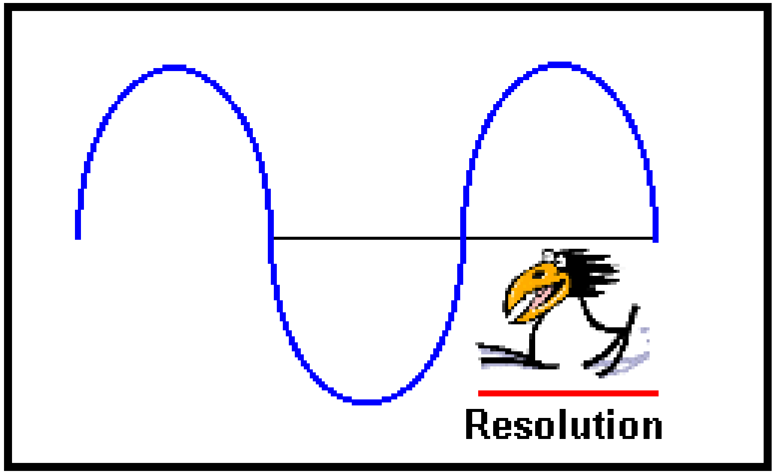

Resolution ≈ ½ λ

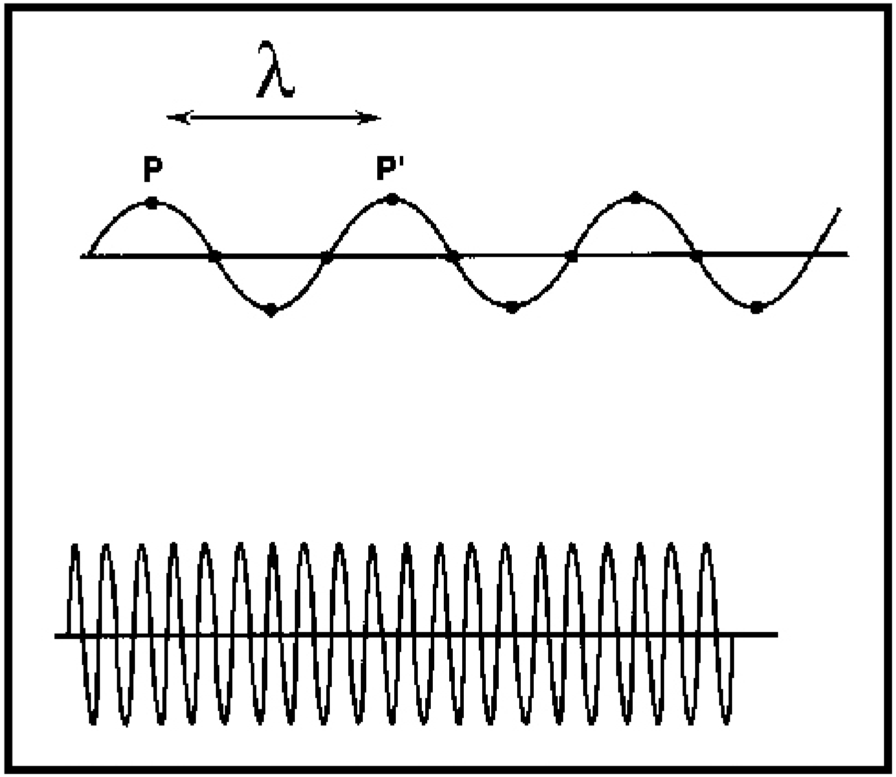

Resolution ≈ ½ λ
Resolution is limited to approx.
1/2 the wavelength of illuminating source

The greater the accelerating voltage the shorter the l

$$\lambda = \frac{h}{mv}$$

`v is velocity`

Therefore, a 50,000 volt (50 kV) electron

has a wavelength of 0.0055nm and

a 1MeV electron has a wavelength of 0.00123nm!

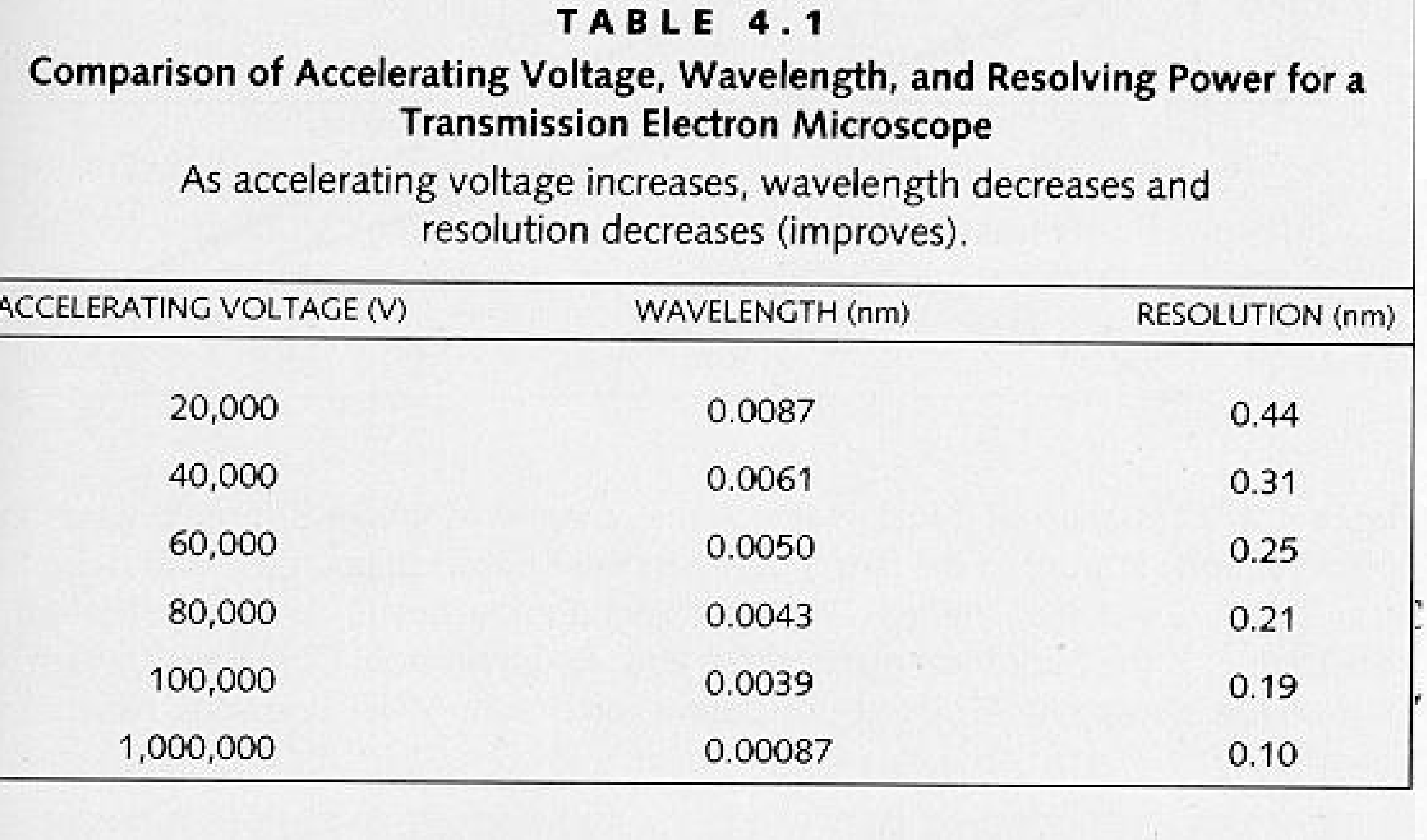

TABLE 4.1

Comparison of Accelerating Voltage, Wavelength, and Resolving Power for a Transmission Electron Microscope

As accelerating voltage increases, wavelength decreases and resolution decreases (improves).

ACCELERATING VOLTAGE (V)	WAVELENGTH (nm)	RESOLUTION (nm)
20,000	0.0087	0.44
40,000	0.0061	0.31
60,000	0.0050	0.25
80,000	0.0043	0.21
100,000	0.0039	0.19
1,000,000	0.00087	0.10

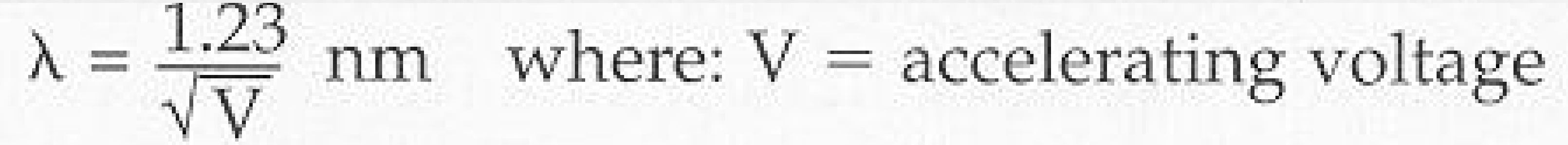

$$\lambda = \frac{1.23}{\sqrt{V}}\ \text{nm} \quad \text{where: } V = \text{accelerating voltage}$$

Wavelength = 0.005 nm

Particles as a Wave

In 1924 de Broglie suggested that electrons may have wave properties. The wave length of an electron is proposed to be *h/p* where p is the momentum of the electron.

- This expression is consistent with photon (*E=pc*) or p=h/ λ.
- Because of the Planck constant, the λ of macroscopic object is not detectable.
- Lower momentum particle is more wavelike.
- Higher energy wave is more particle like.

De Broglie waves:

$$\lambda = \frac{h}{p_{photon}} \rightarrow \frac{h}{p_{particle}} = \frac{h}{\gamma m v}$$

For electrons:

$$\lambda = \frac{h}{\sqrt{2mE}} = \frac{1.226}{\sqrt{E}} nm$$

Resolution of an electron microscope

An electron microscope is designed to resolve objects as small as 0.14 nm. What is the minimum energy of the electrons to be used in this instrument?

Solution: The Heisenberg uncertainty relation tells us that $\Delta p \ge \frac{\hbar}{2\Delta x}$

Then the momentum of the electrons itself cannot be smaller than this value. We obtain for the energy

$$E \ge \frac{(\Delta p)^2}{2m} \ge \frac{\hbar^2}{8m(\Delta x)^2} = \frac{(\hbar c)^2}{32\pi^2 mc^2(\Delta x)^2} = \frac{(197.3\,eV\mathrm{nm})^2}{8\times 5.11\times 10^5\,eV(0.14\,\mathrm{nm})^2} = 0.486eV$$

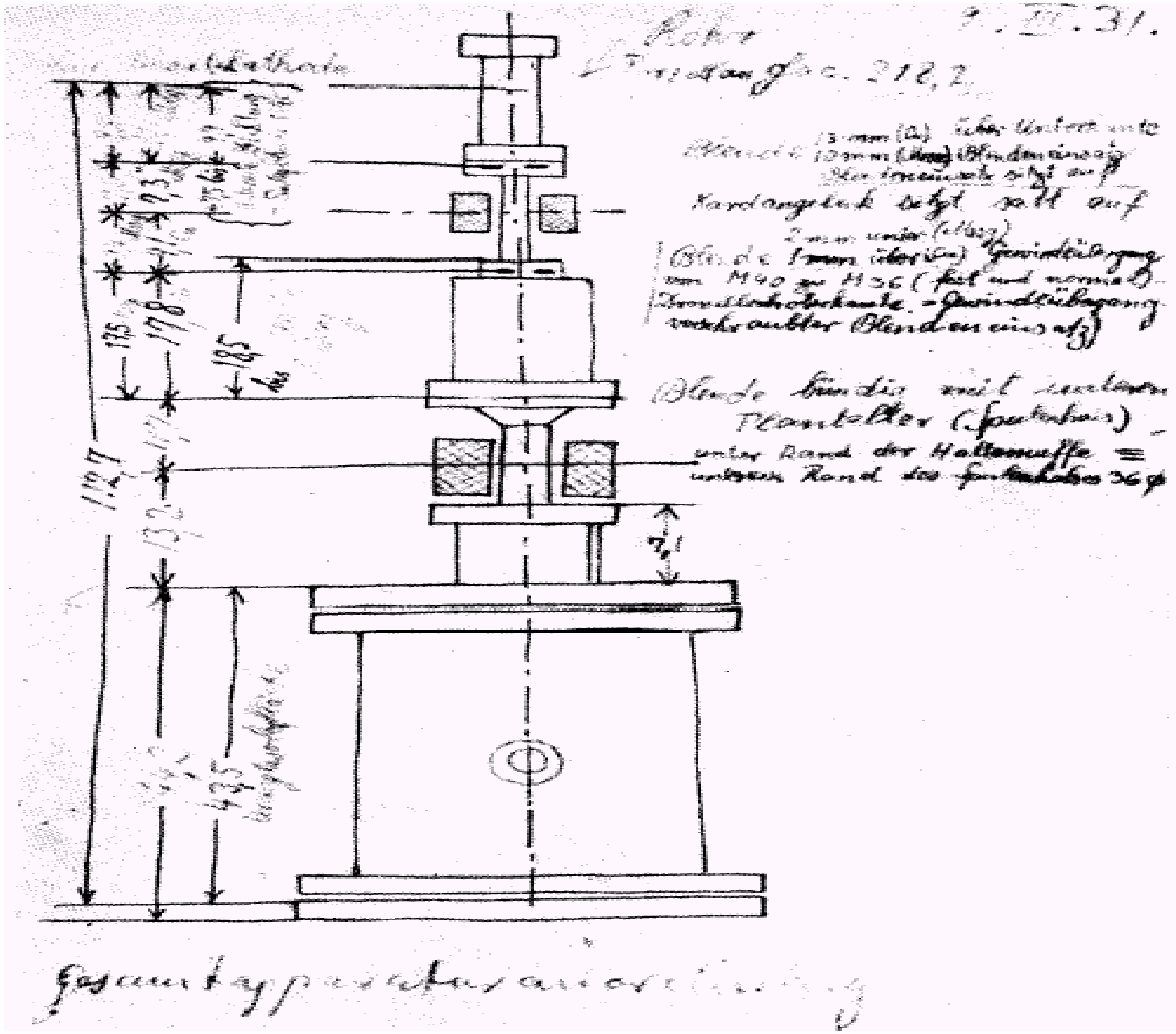

Fig. 2: Sketch by the author (9 March 1931) of the cathode ray tube for testing one-stage and two-stage electron-optical imaging by means of two magnetic electron lenses (electron microscope) [8].

- *1935 - **Max Knoll** demonstrates the theory of the scanning electron microscope*

*1938 - First scanning electron microscope produced by **von Ardenne***

Knoll and Ruska
1986 Nobel Prize winners

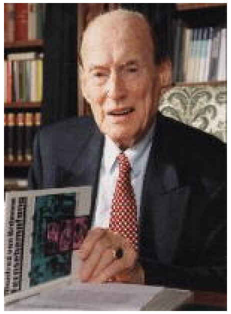

von Ardenne

*1939 - **Ruska** and **von Borries**, working for Siemens produce the first commercially available EM*

Electron Interactions

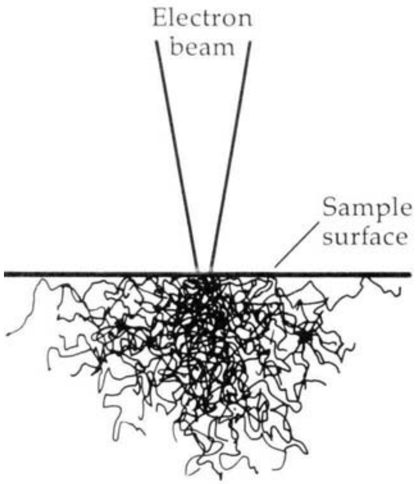

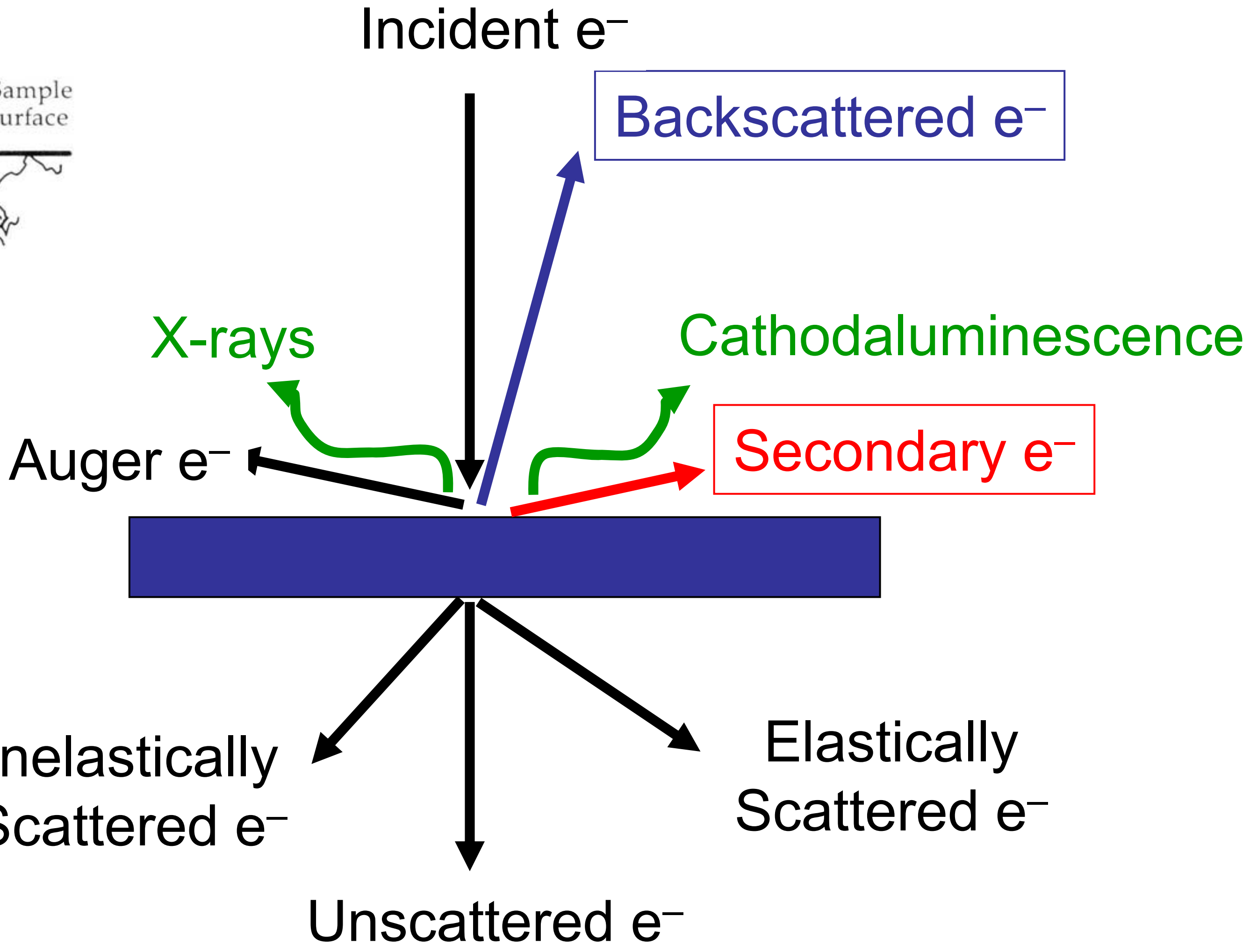
Incident e⁻

Backscattered e⁻

X-rays

Cathodaluminescence

Auger e⁻

Secondary e⁻

Inelastically Scattered e⁻

Elastically Scattered e⁻

Unscattered e⁻

Electrons are light mass particles, electrons are therefore scattered easily in all directions due to their interactions with the atomic electrons of the absorber material. This results into more energy loss per scattering event.

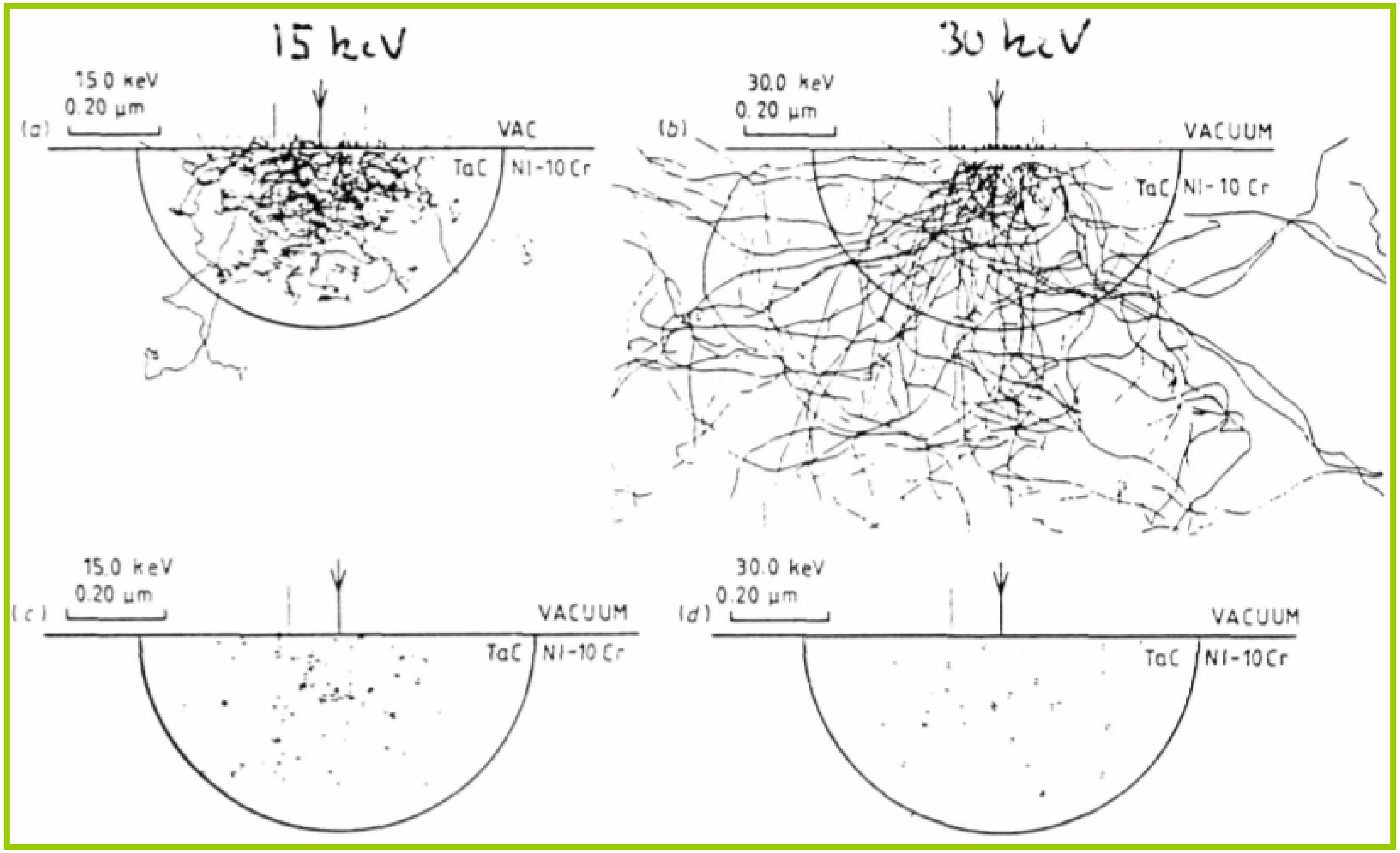

Signals for Imaging in the SEM and STEM

- ***Secondary electrons***
- ***Backscatter electrons***
- ***Auger electrons***
- ***X-rays***
- ***Transmitted Electrons***
  - ***Dark Field (DF)***
  - ***Bright Field (BF)***

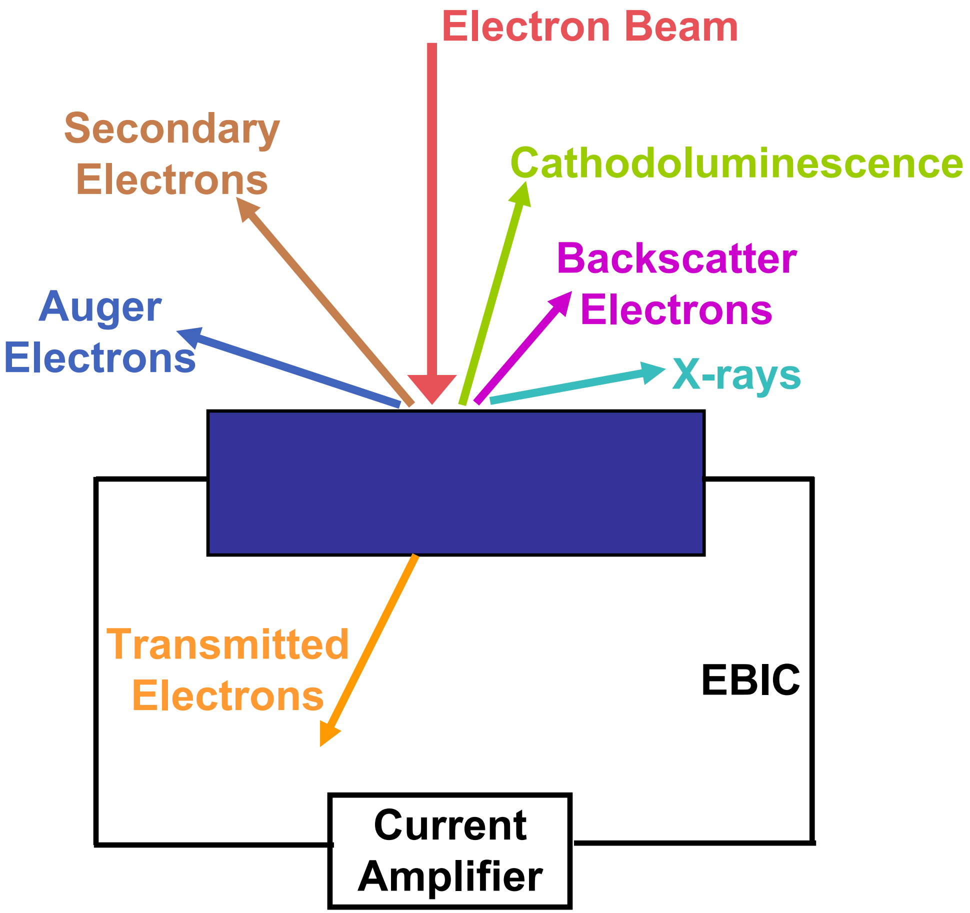

Scanning Electron Microscope

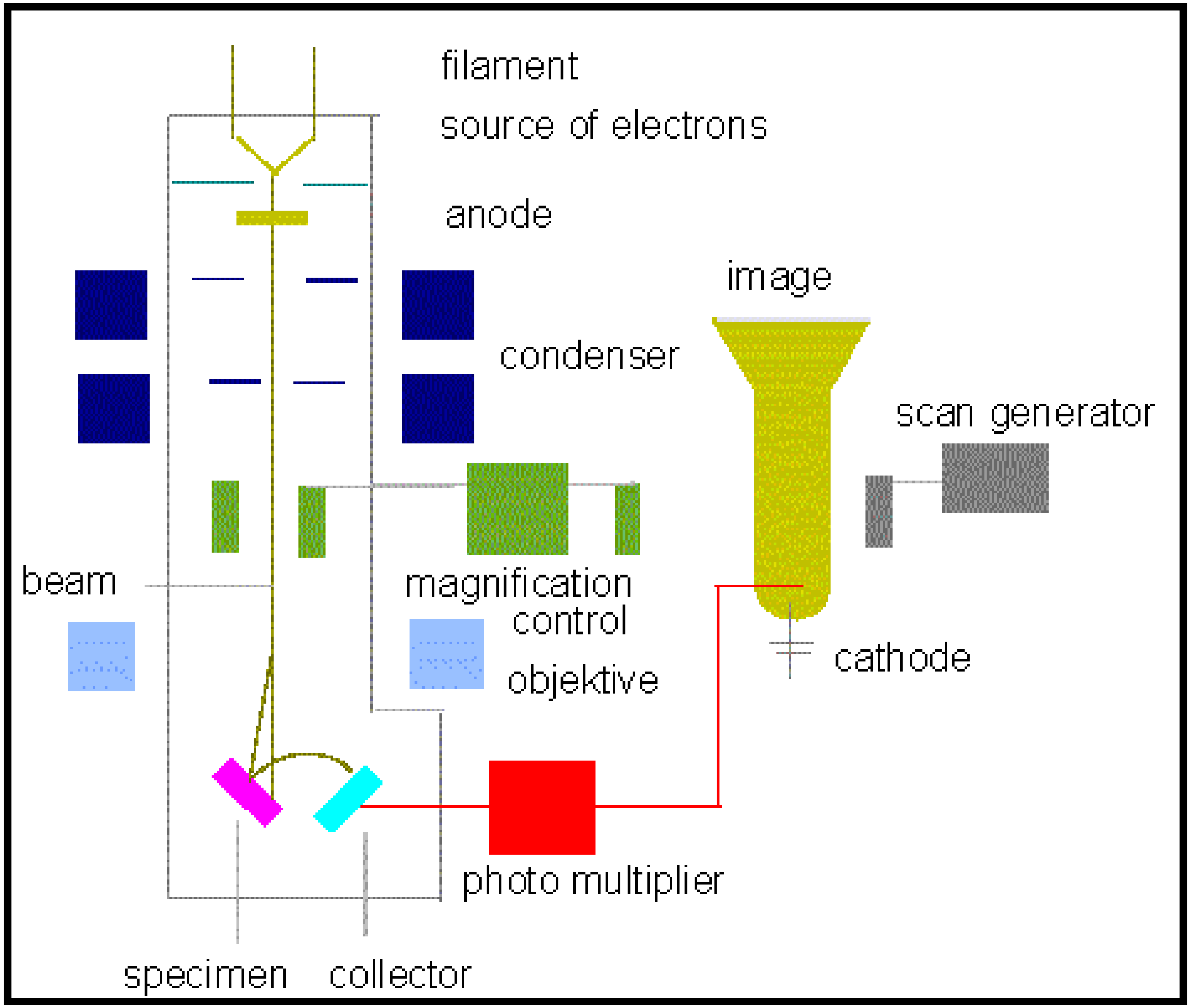

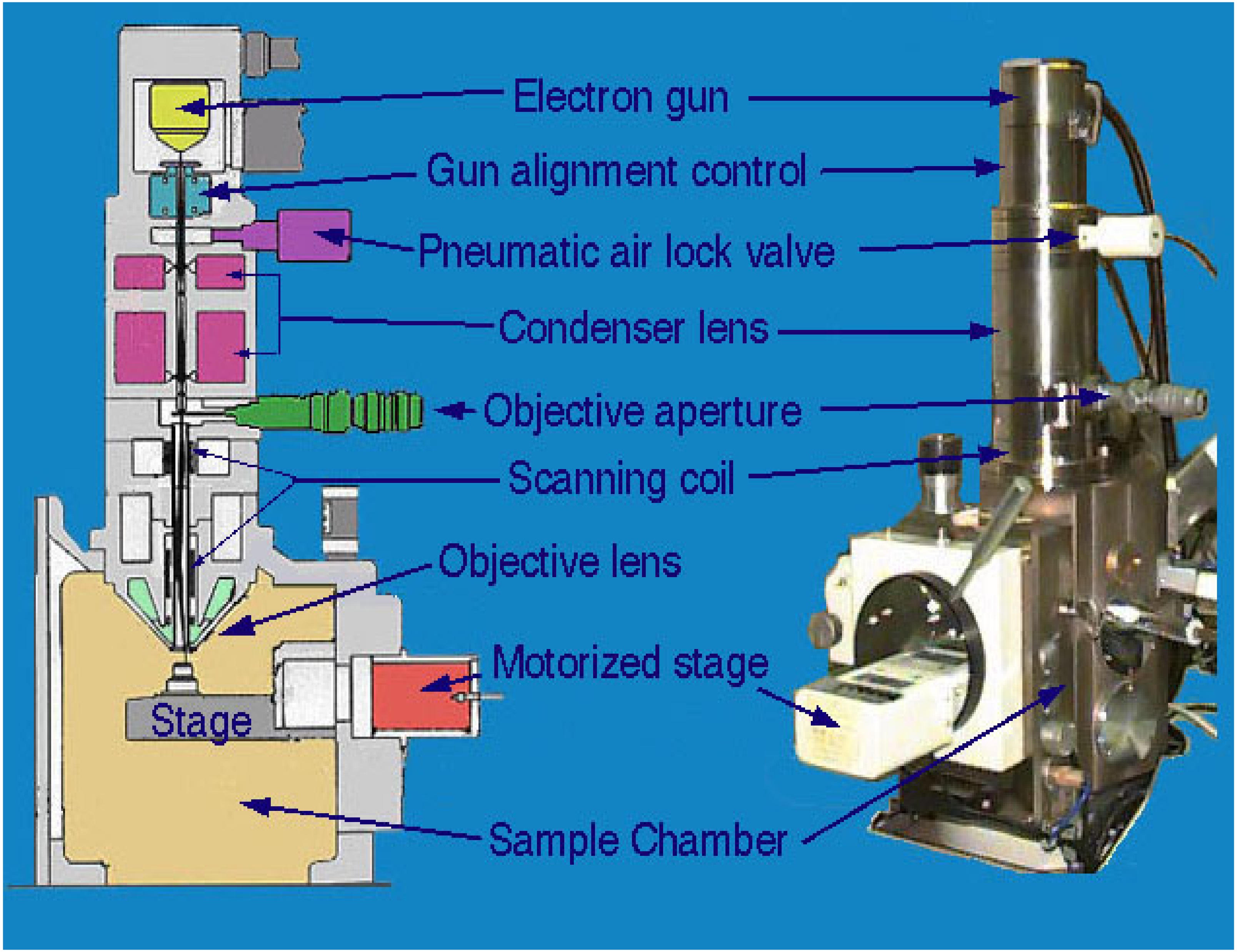

Electron gun

Gun alignment control

Pneumatic air lock valve

Condenser lens

Objective aperture

Scanning coil

Objective lens

Motorized stage

Sample Chamber

SEM Detector

FA-final aperture
SD-solid-state backscattered e detector
EDS-energy dispersive X-ray detector
WDS-wavelength dispersive X-ray spectrophotometer
PM-photomultiplier tube

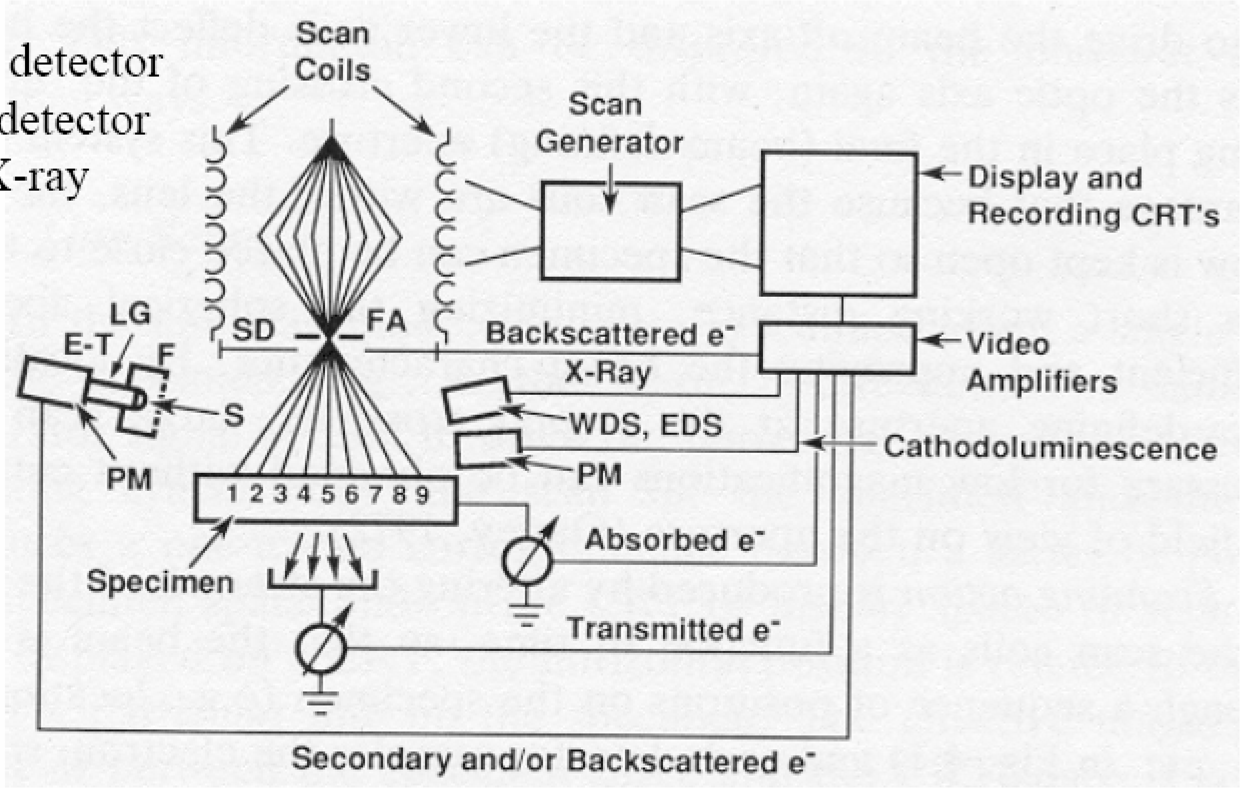

Mackay

Magnification

The magnification is changed simply by altering the size of the raster on the specimen. The magnification is merely the ratio of the viewing screen's linear size to the linear raster size.

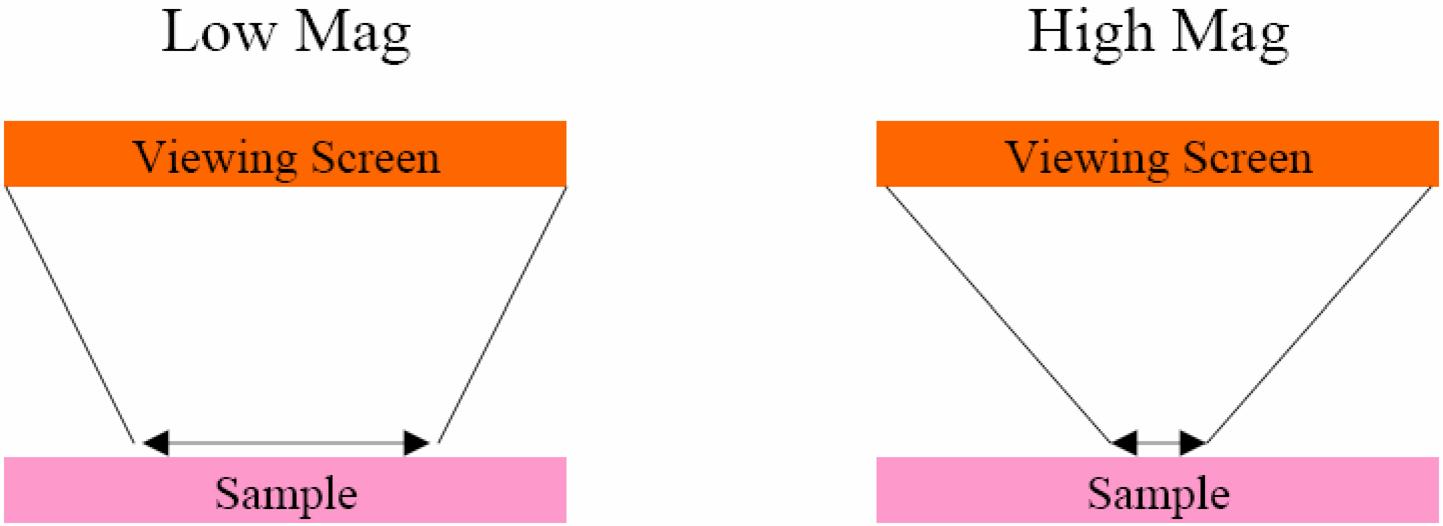

Secondary Electrons

MORE secondary e$^-$ escape

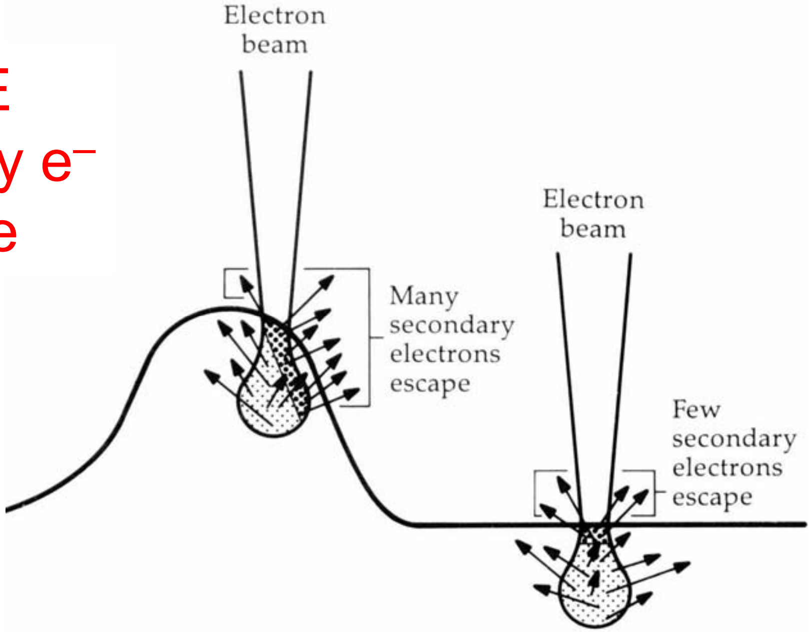

FEWER secondary e$^-$ escape

- ***Caused by incident electron passing "near" sample atom and ionizing an electron (inelastic process).***
- ***<u>Ionized electron</u> leaves sample with very <u>small kinetic energy</u> (5eV) and is called "<u>secondary electron</u>". (Each incident electron can produce several secondary electrons.)***
- ***<u>Production</u> of secondary electrons is <u>topography</u> related. Only secondaries near surface (<10 nm) exit sample.***

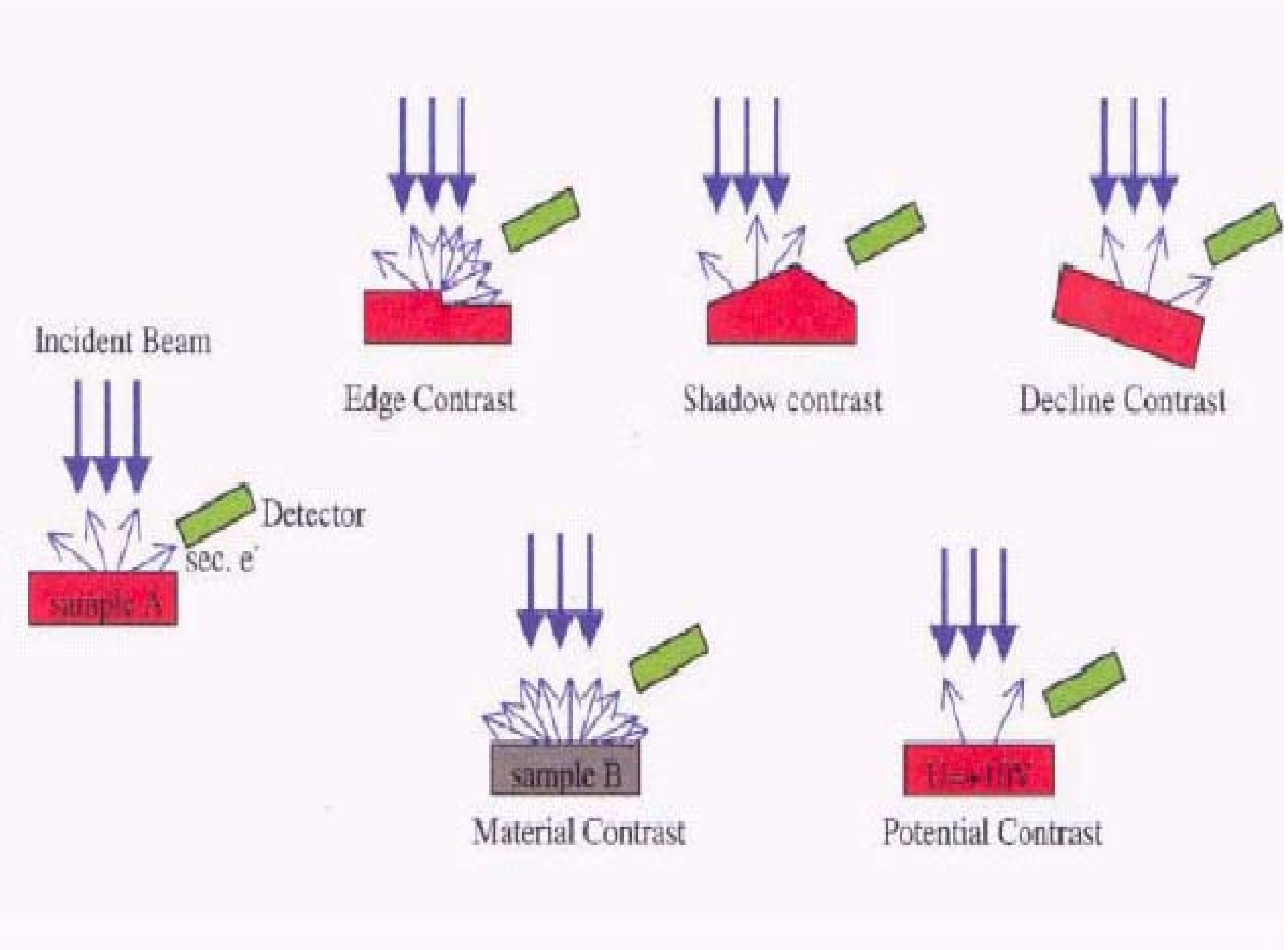
Edge Contrast
Shadow contrast
Decline Contrast
Incident Beam
Detector
sec. e
sample A
sample B
Material Contrast
U=+10V
Potential Contrast

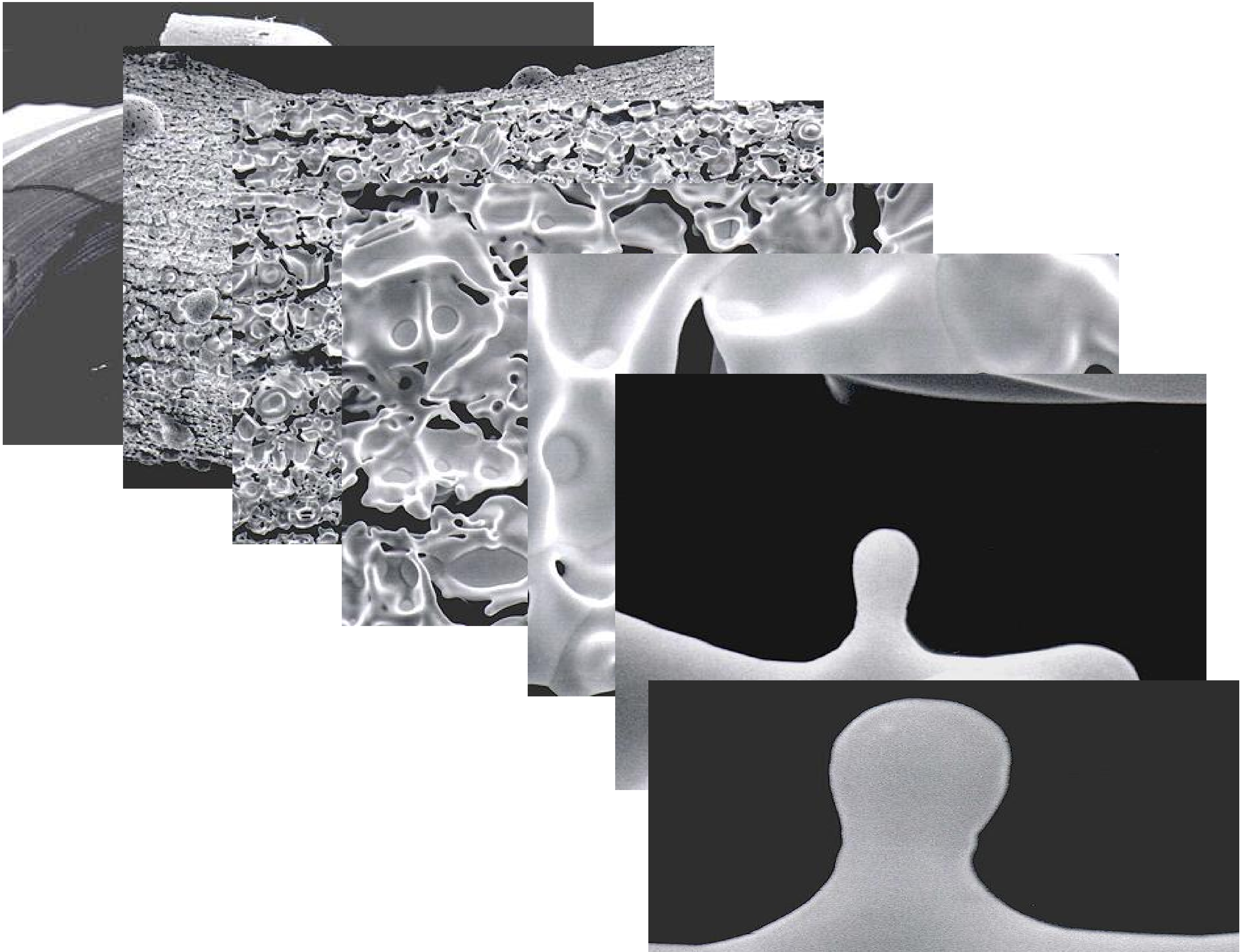

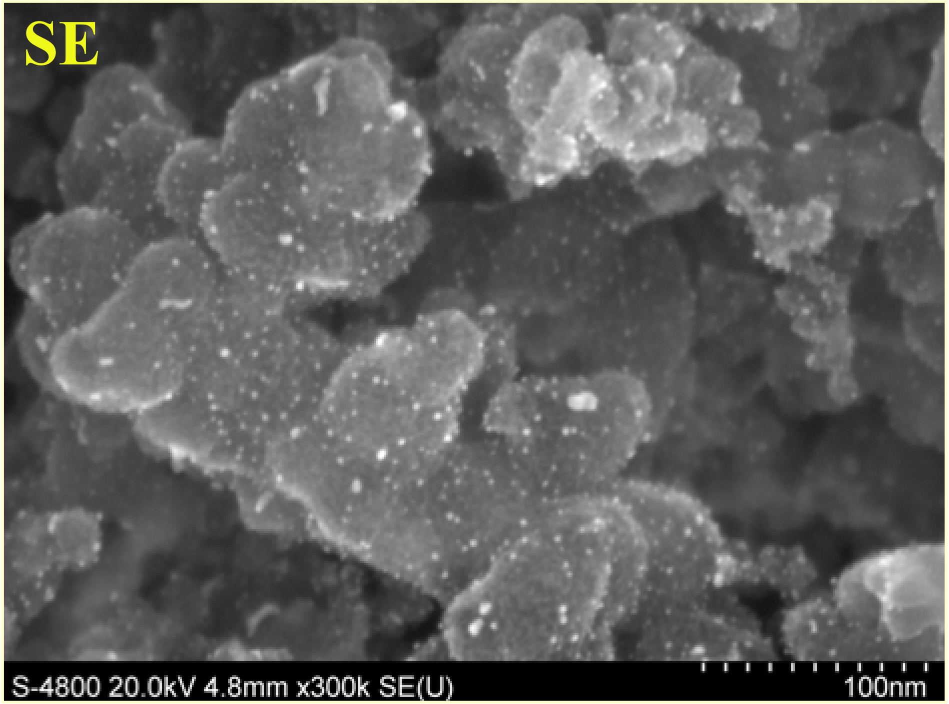

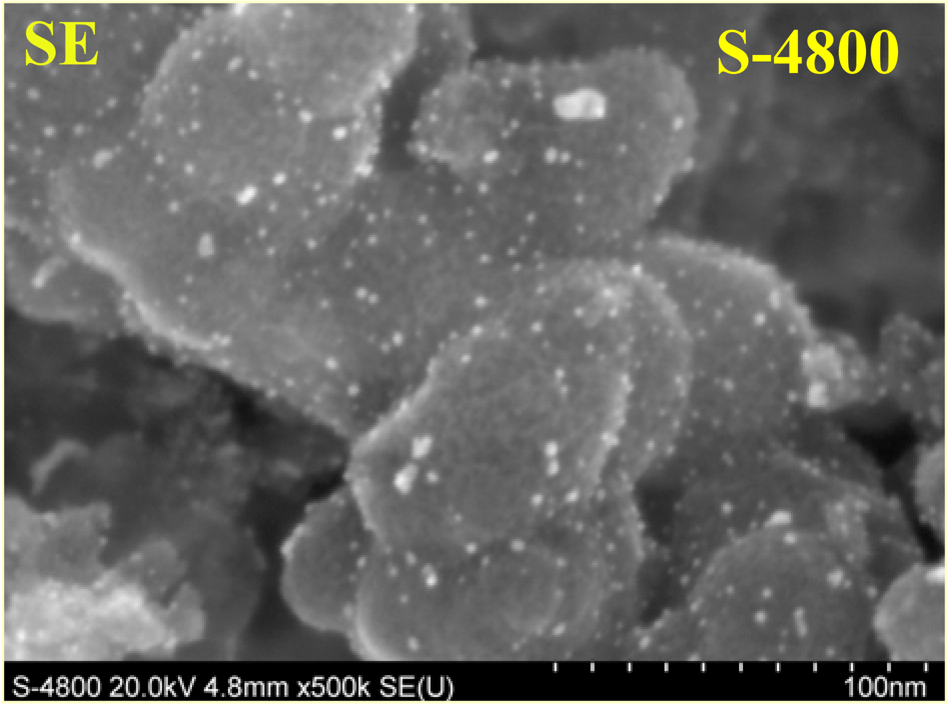

Catalyst(Pt /Carbon)

Vacc. : 20kV
Mag. : x300k – x800k
Comment : Uncoated

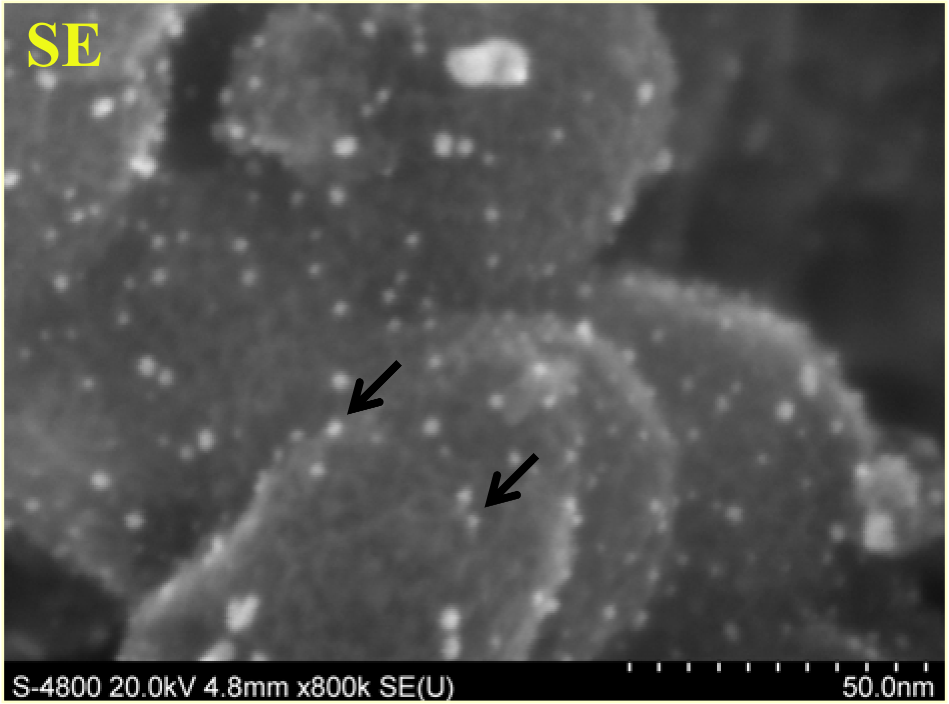

S-4800 **S-5200**

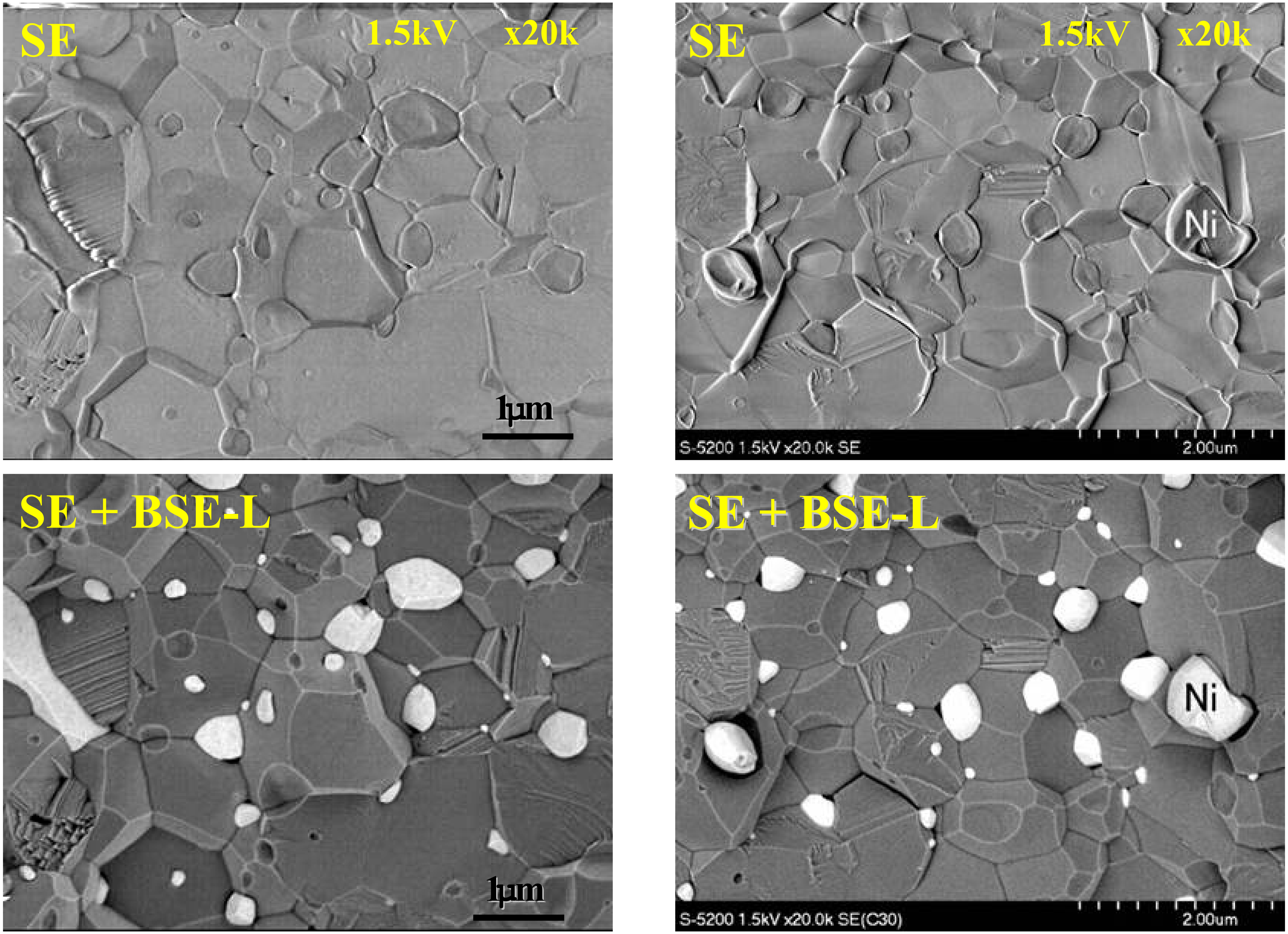

Al2O3 / Ni composite (courtesy by Dr. SEKINO, Osaka Univ.)

Signal Control (SE / SE+BSE-L / BSE-H)

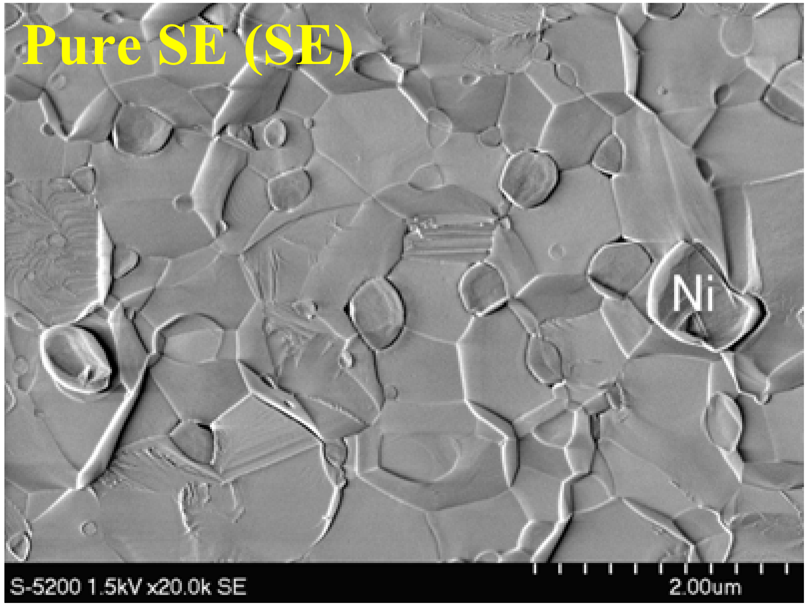

S-5200

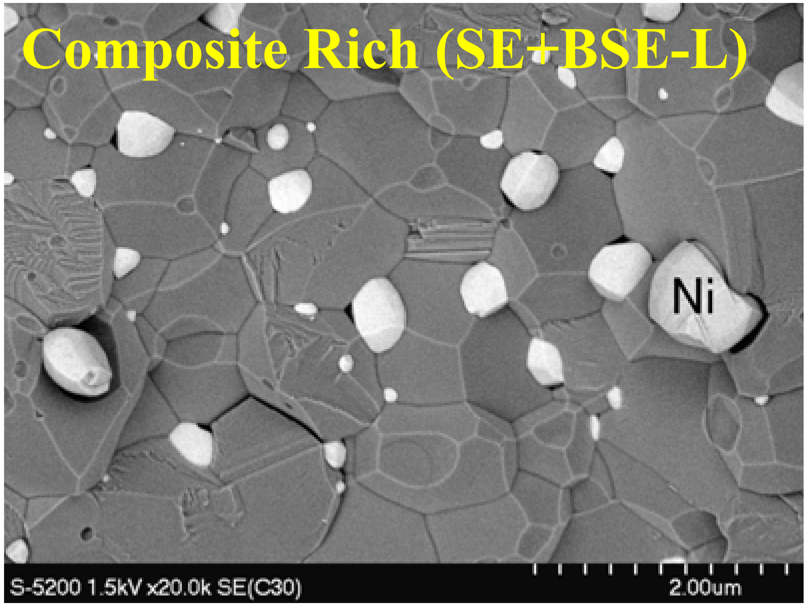

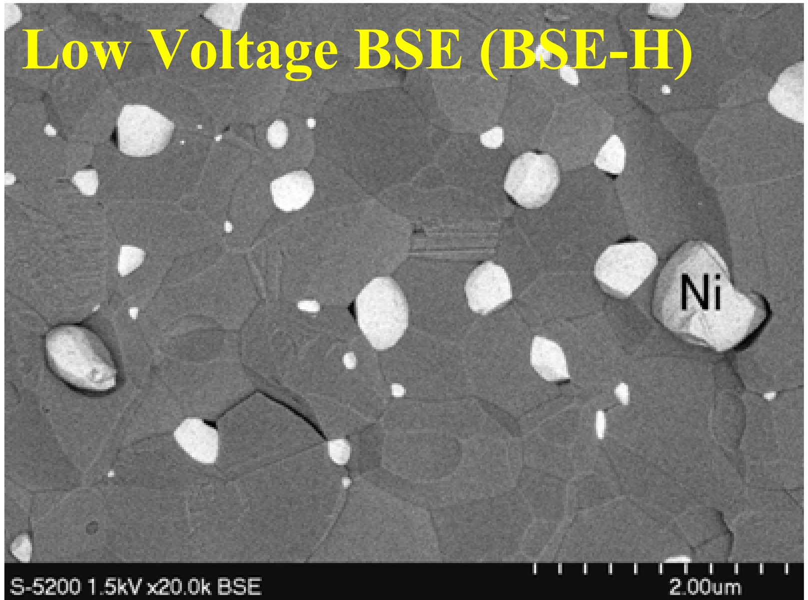

Alumina / Nickel Composite

Courtesy of Associate Prof.. T. Sekino,
ISIR, Osaka Univ.

SEMs are patterned after Reflecting Light Microscopes and yield similar information:

Topography
The surface features of an object or "how it looks", its texture; detectable features limited to a few nanometers

Morphology
The shape, size and arrangement of the particles making up the object that are lying on the surface of the sample or have been exposed by grinding or chemical etching; detectable features limited to a few nanometers

Composition
The elements and compounds the sample is composed of and their relative ratios, in areas ~ 1 micrometer in diameter

Crystallographic Information
The arrangement of atoms in the specimen and their degree of order; only useful on single-crystal particles >20 micrometers

X-ray Microanalysis

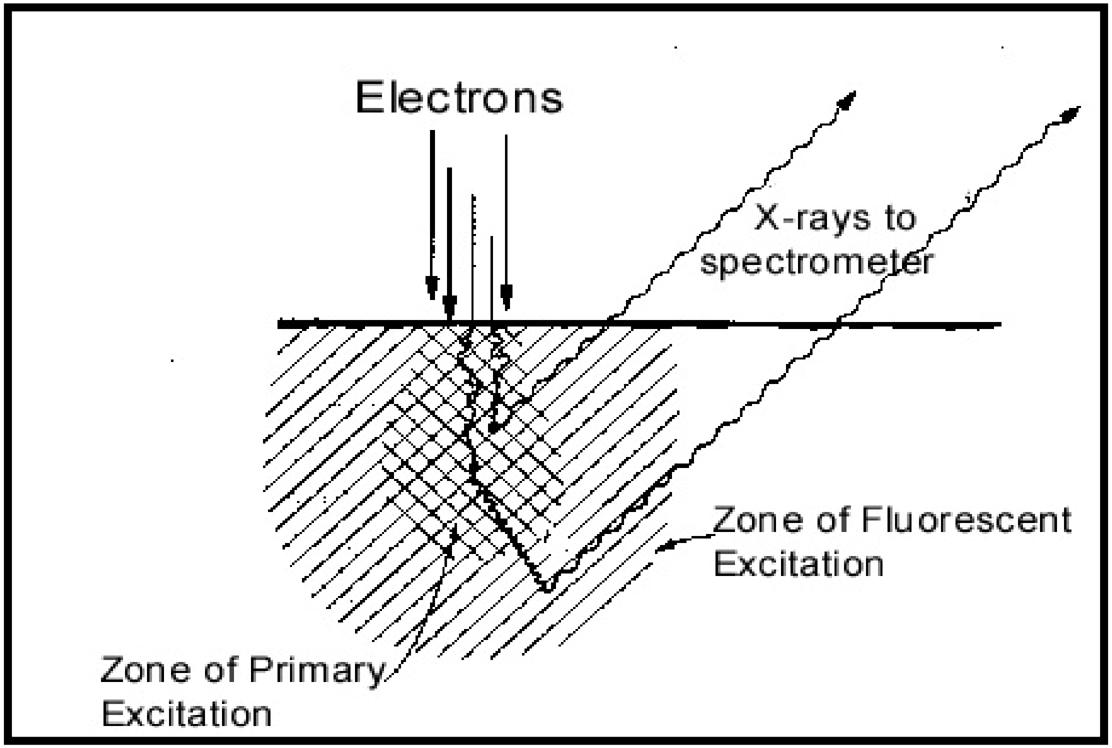

X-rays can have an energy nearly equal to that of the primary beam electron and thus can escape from very deep within the specimen

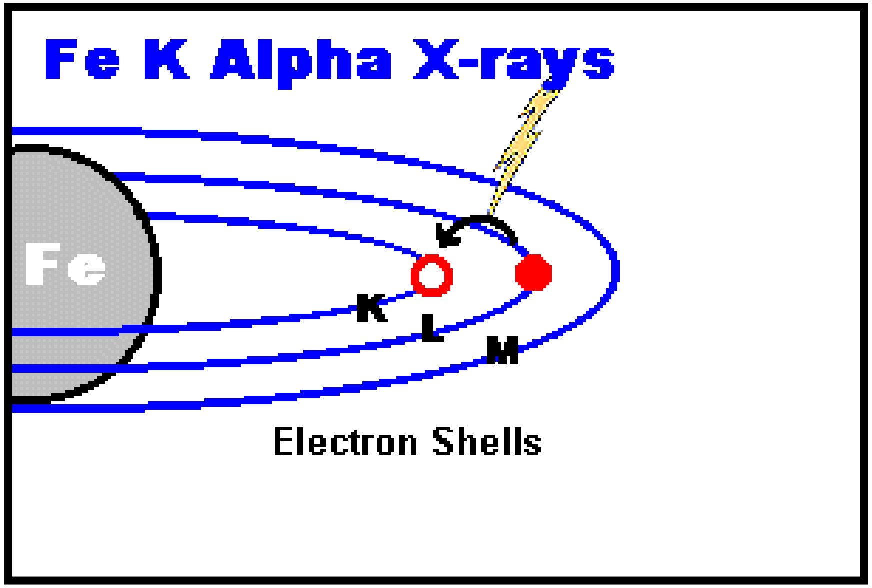

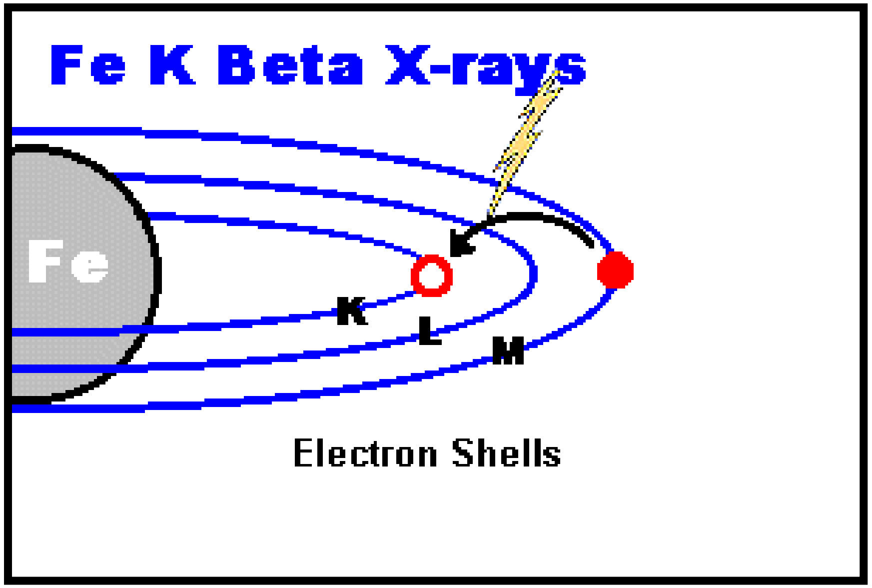

When an electron from a K-shell is replaced by one from the second closest shell (M), it is designated as a Kβ event

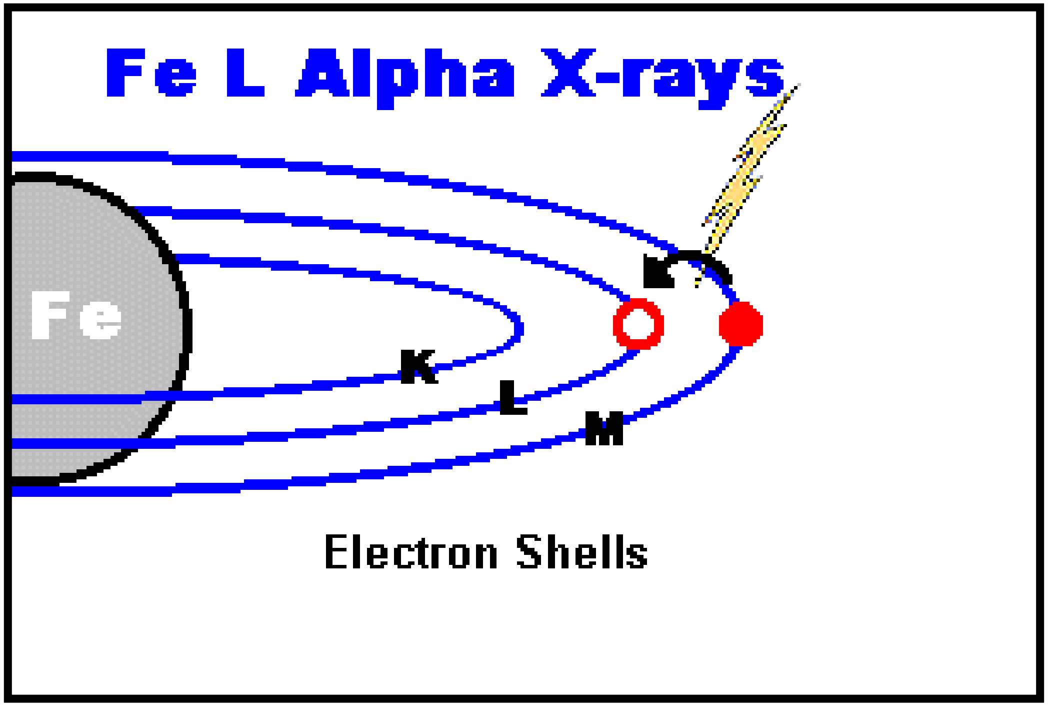

When an electron from a L-shell is replaced by one from the next closest shell (M), it is designated as a Lα event. The K shell will never donate its electron as this would require an increase in energy, not a drop.

X-ray Microanalysis

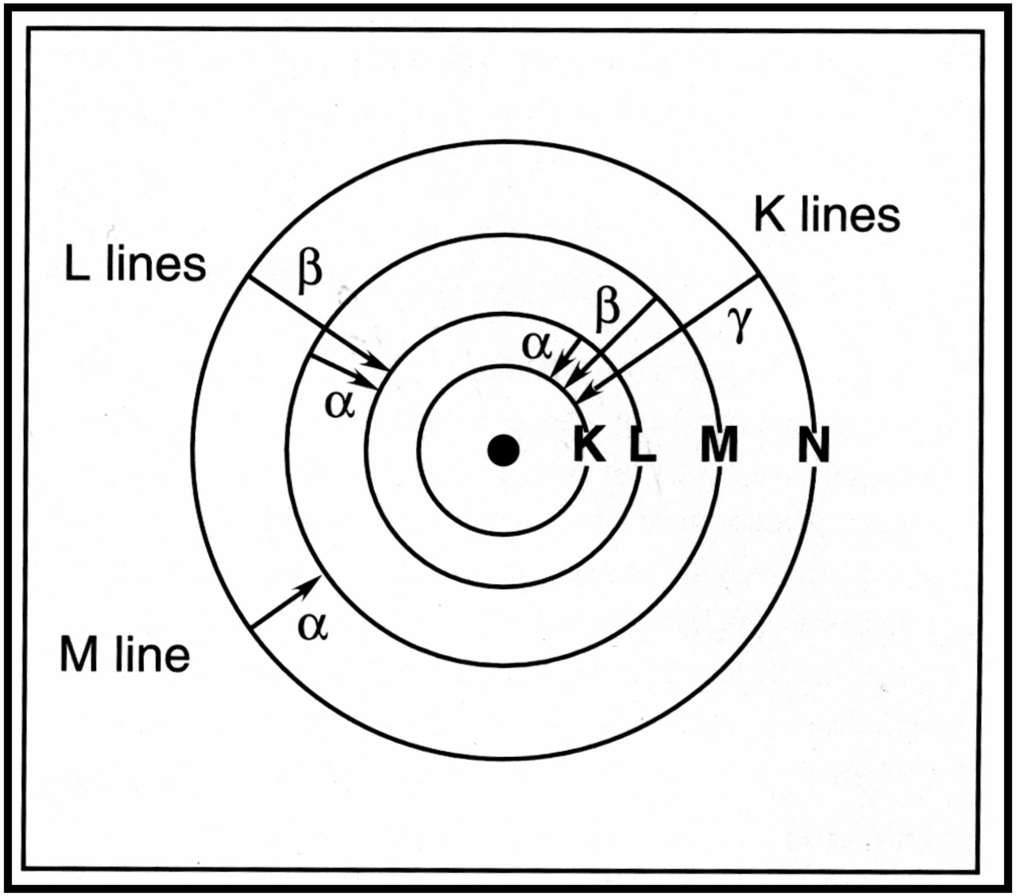

Certain events such as Mα, Lβ, and Kγ are only possible in atoms of sufficient atomic weight

Collection of X-rays

EDS

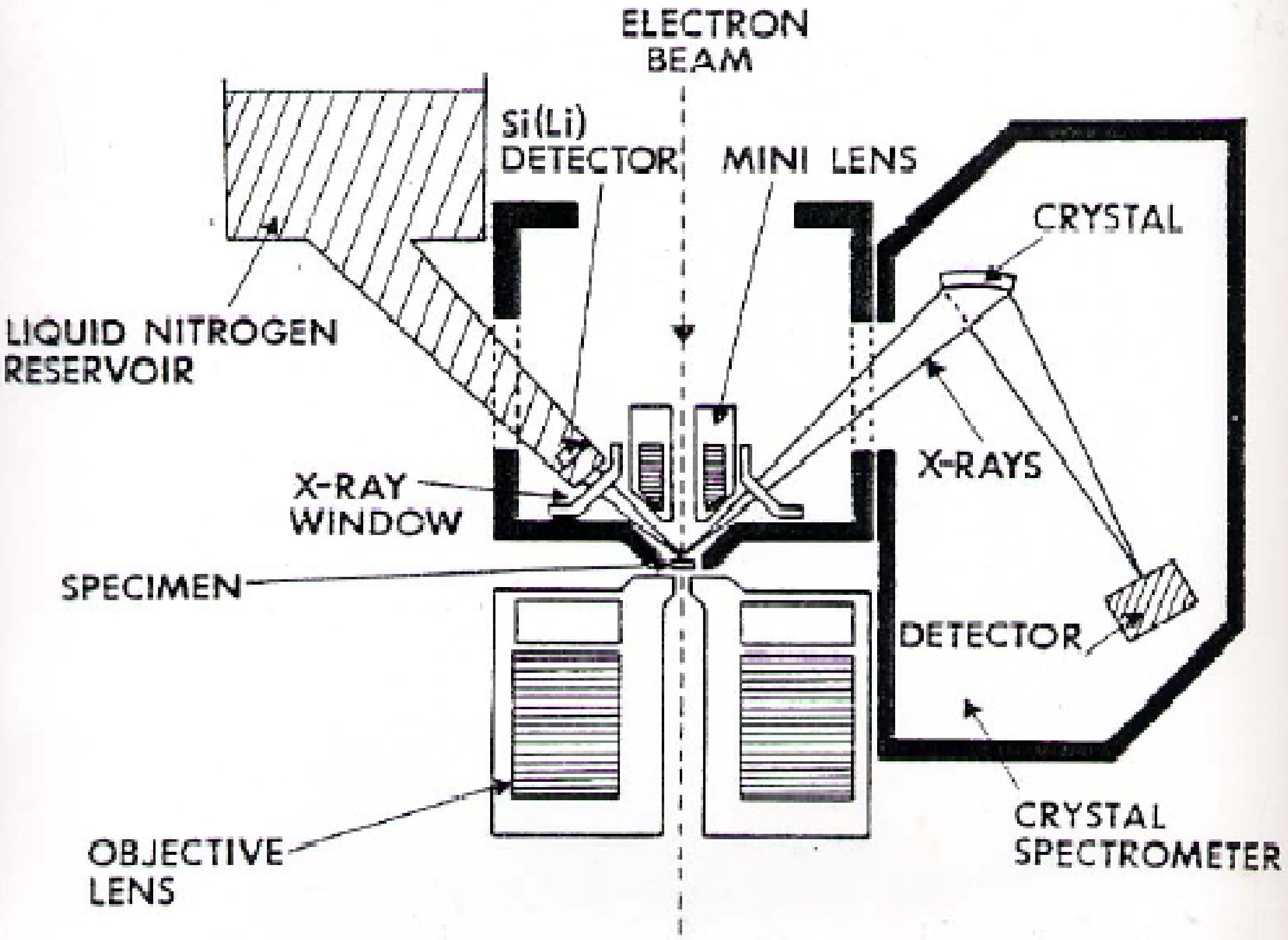

WDS

X-ray Detection

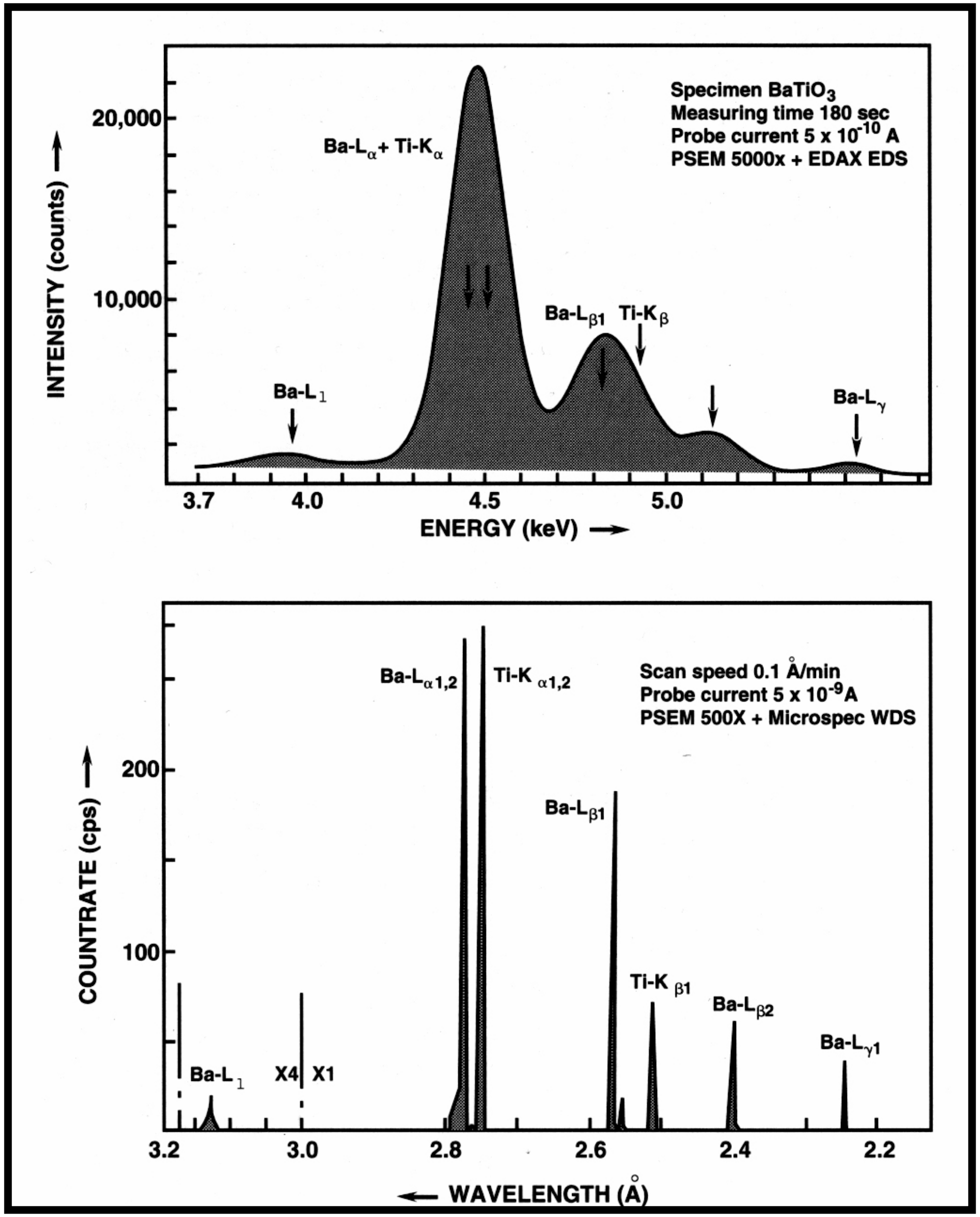

EDS = Energy
Dispersive
Spectroscopy

WDS = Wavelength
Dispersive
Spectroscopy

X-ray Microanalysis
Energy Dispersive Spectroscopy (EDS)

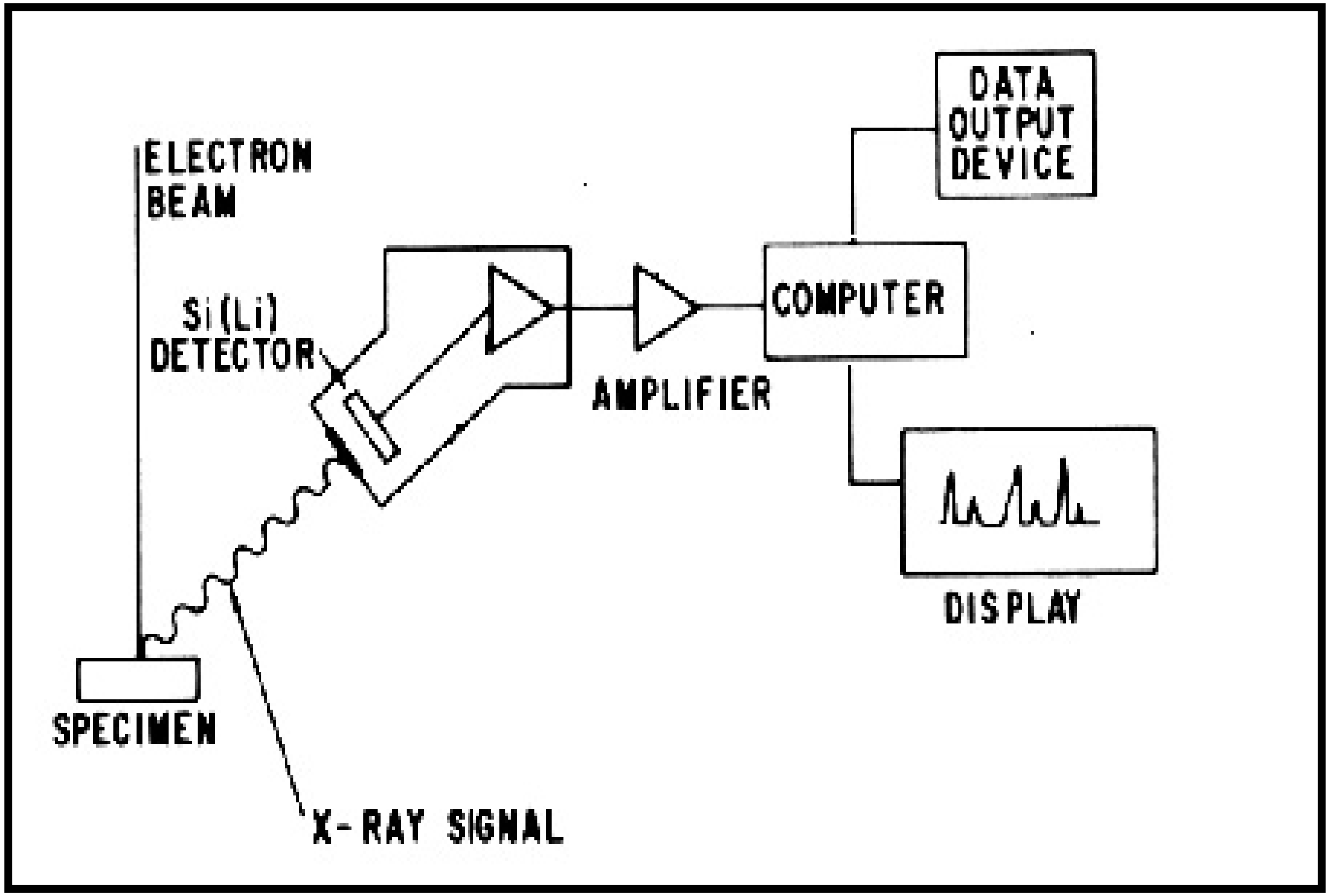

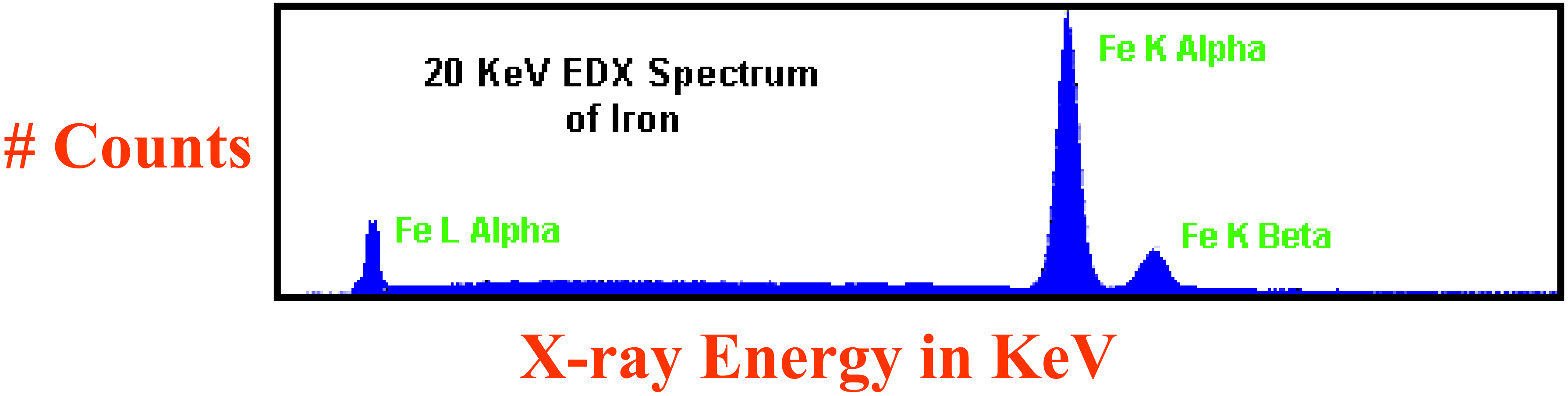

An X-ray spectrum for a sample is composed of all the possible signals for that given set of elements. These will differ in terms of energies (KeV) and probabilities (likelihood) scored as number of such signals collected over a given period of time.

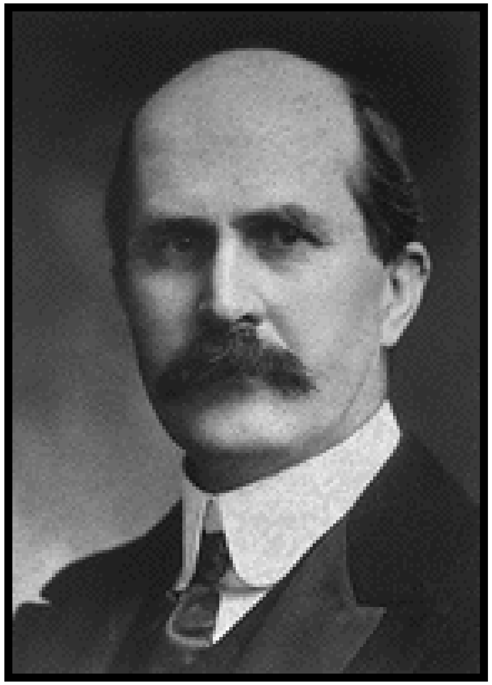

William Henry Bragg
1862 – 1942
Nobel Prize in Physics
1915

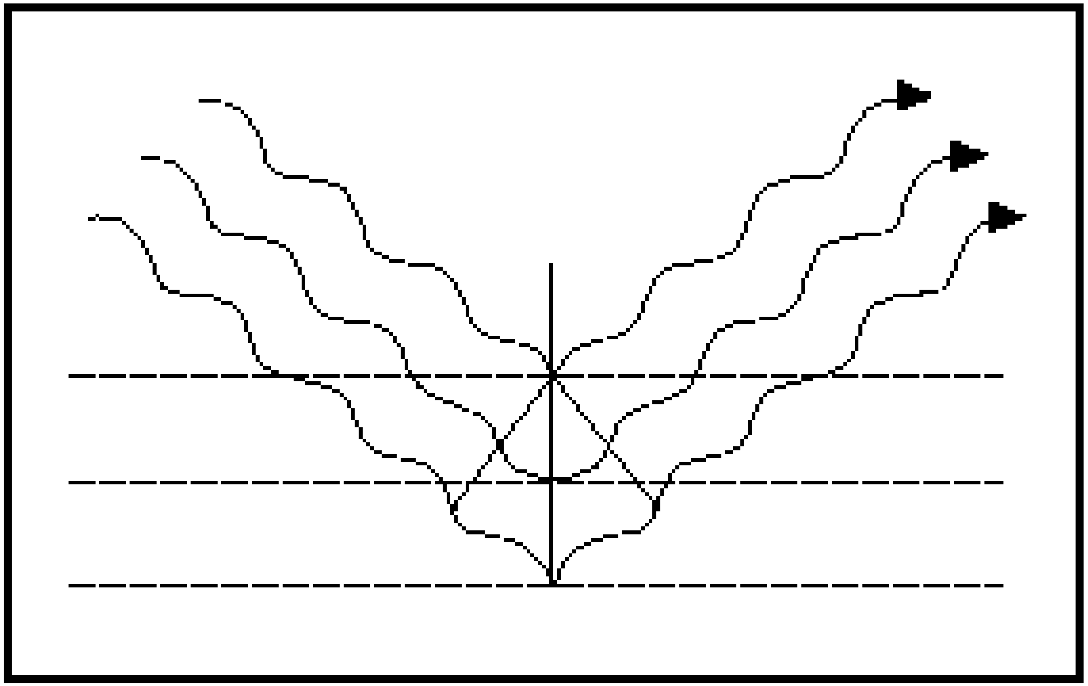

X-ray diffraction in a crystal.
Like an electron beam an X-ray has its own wavelength which is proportional to its energy

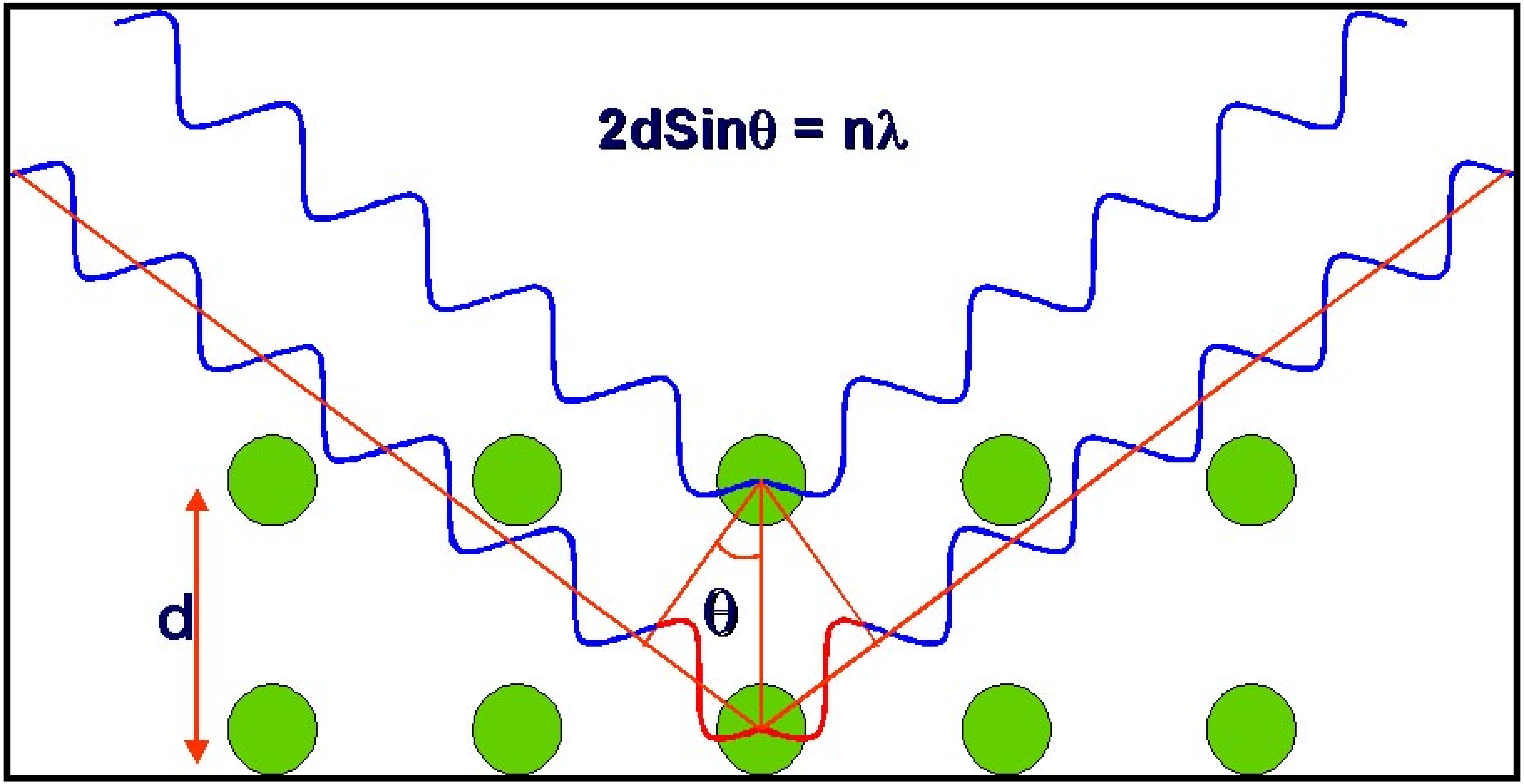

If a wavelength enters a crystal at the appropriate angle it will be diffracted rather than being absorbed or scattered by the crystal

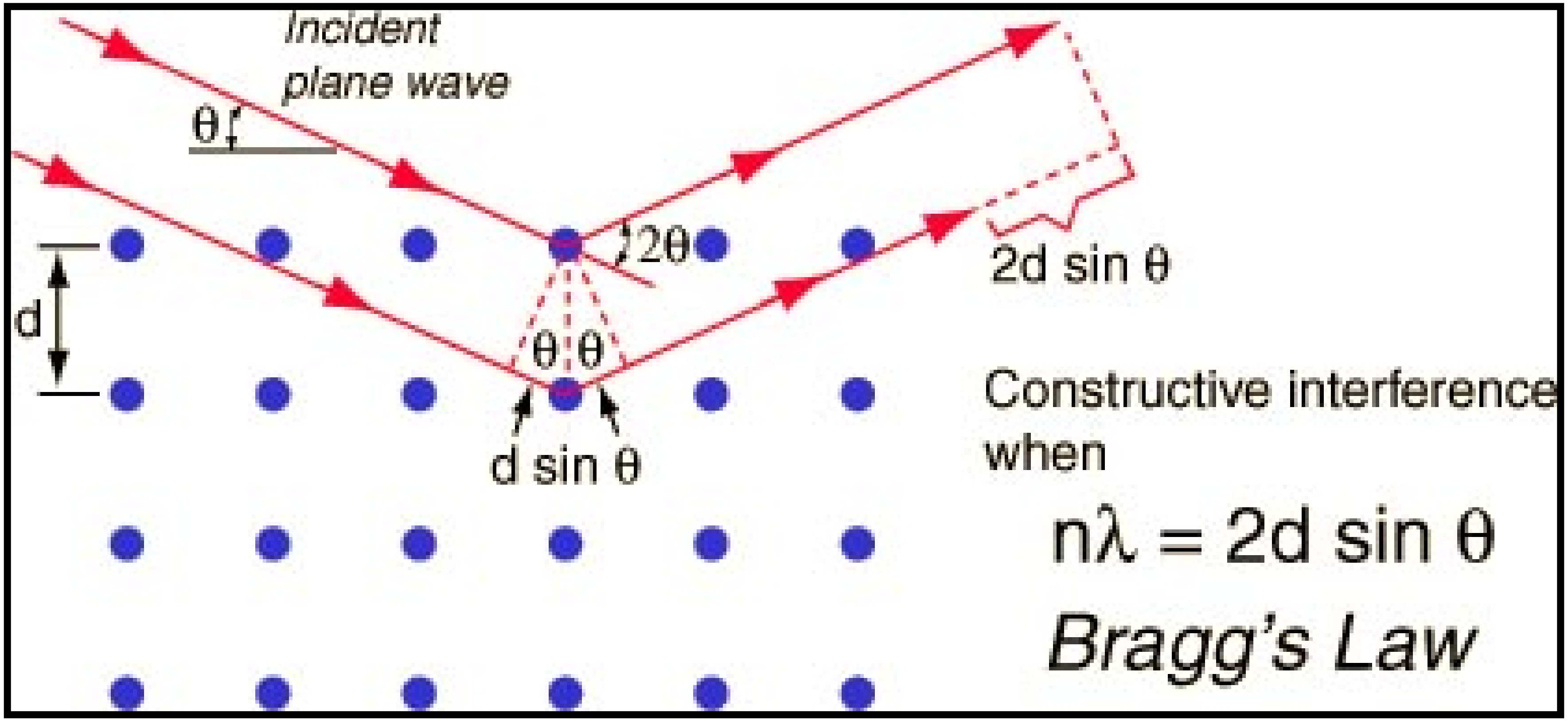

For a given wavelength λ there is a specific angle θ (Bragg's angle) at which diffraction will occur. Bragg's angle is determined by the d-spacing (interplanar spacing) of the crystal and the order of diffraction (n = 1, 2, 3….).

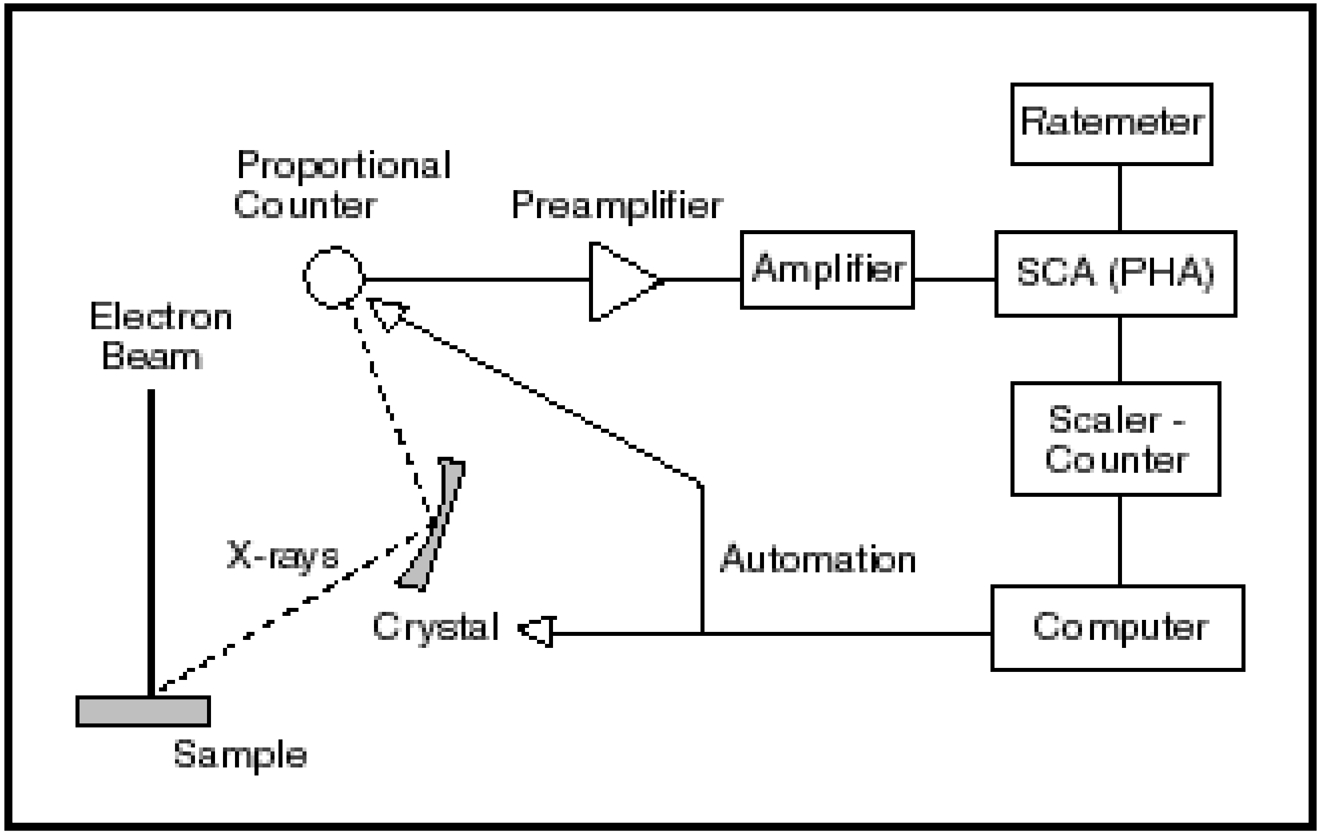

A WDS detector takes advantage of the fact that an X-ray of a given wavelength can be focused by a crystal if it encounters the crystal at the proper Bragg's angle.

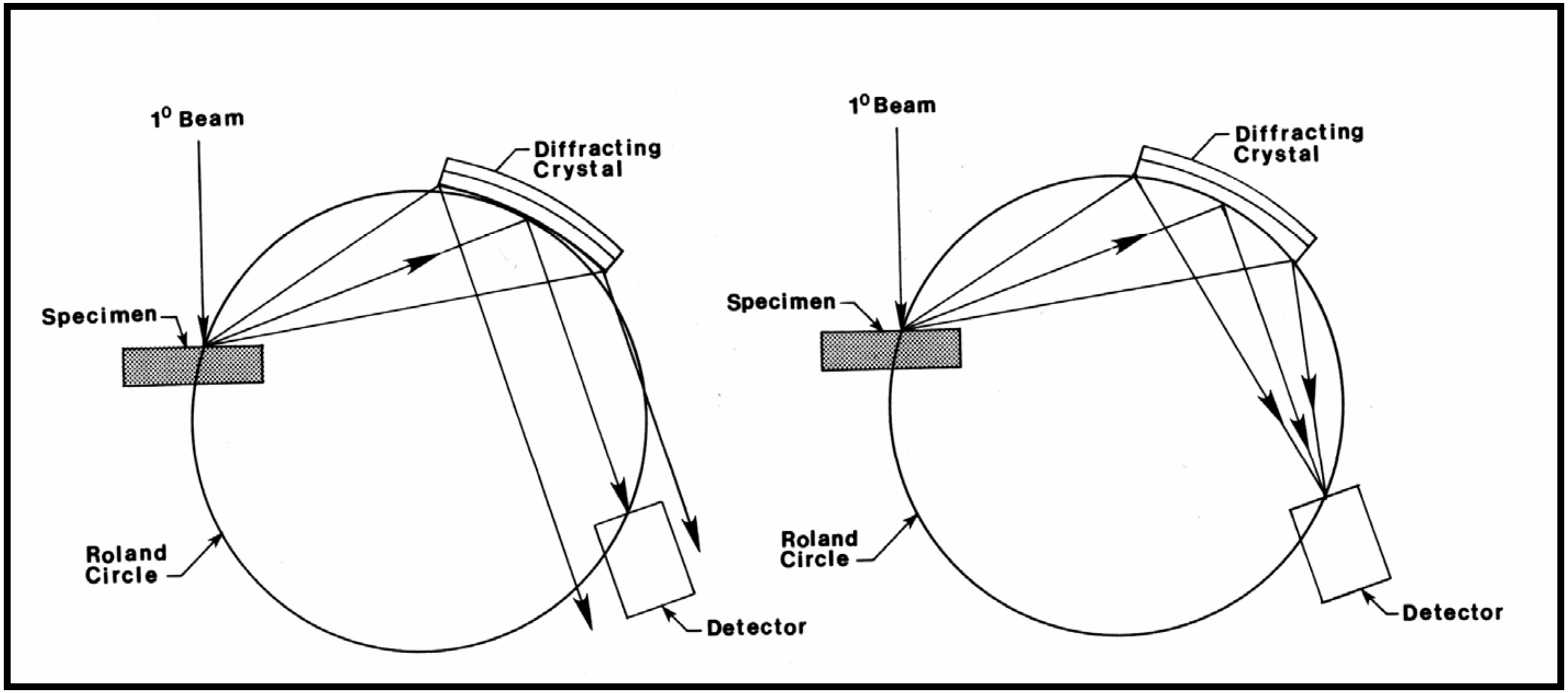

To change the Bragg's angle the diffracting crystal and detector can be moved together relative to the stationary specimen along a circle known as the Roland Circle

Applications of X-ray Microanalysis

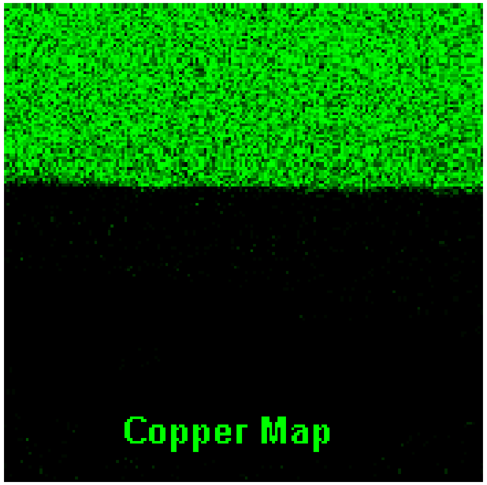

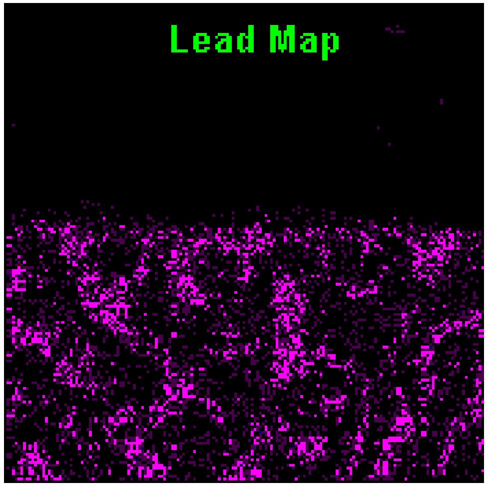

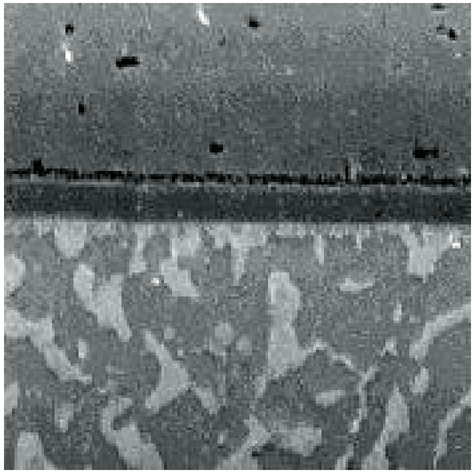

Secondary Electron

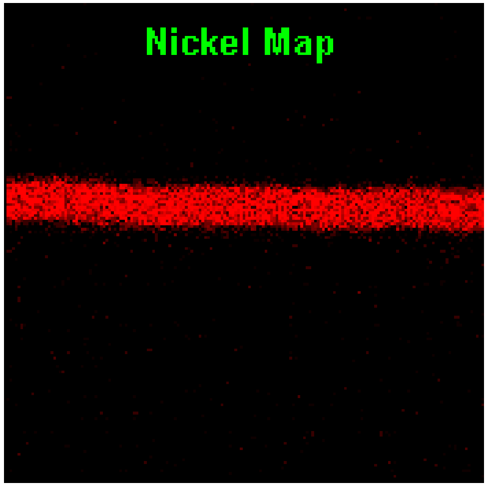

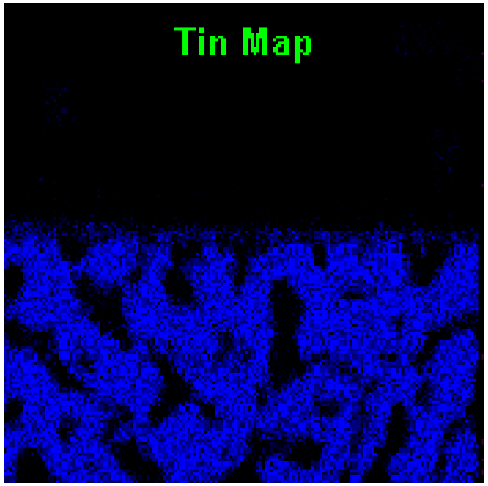

X-ray Mapping

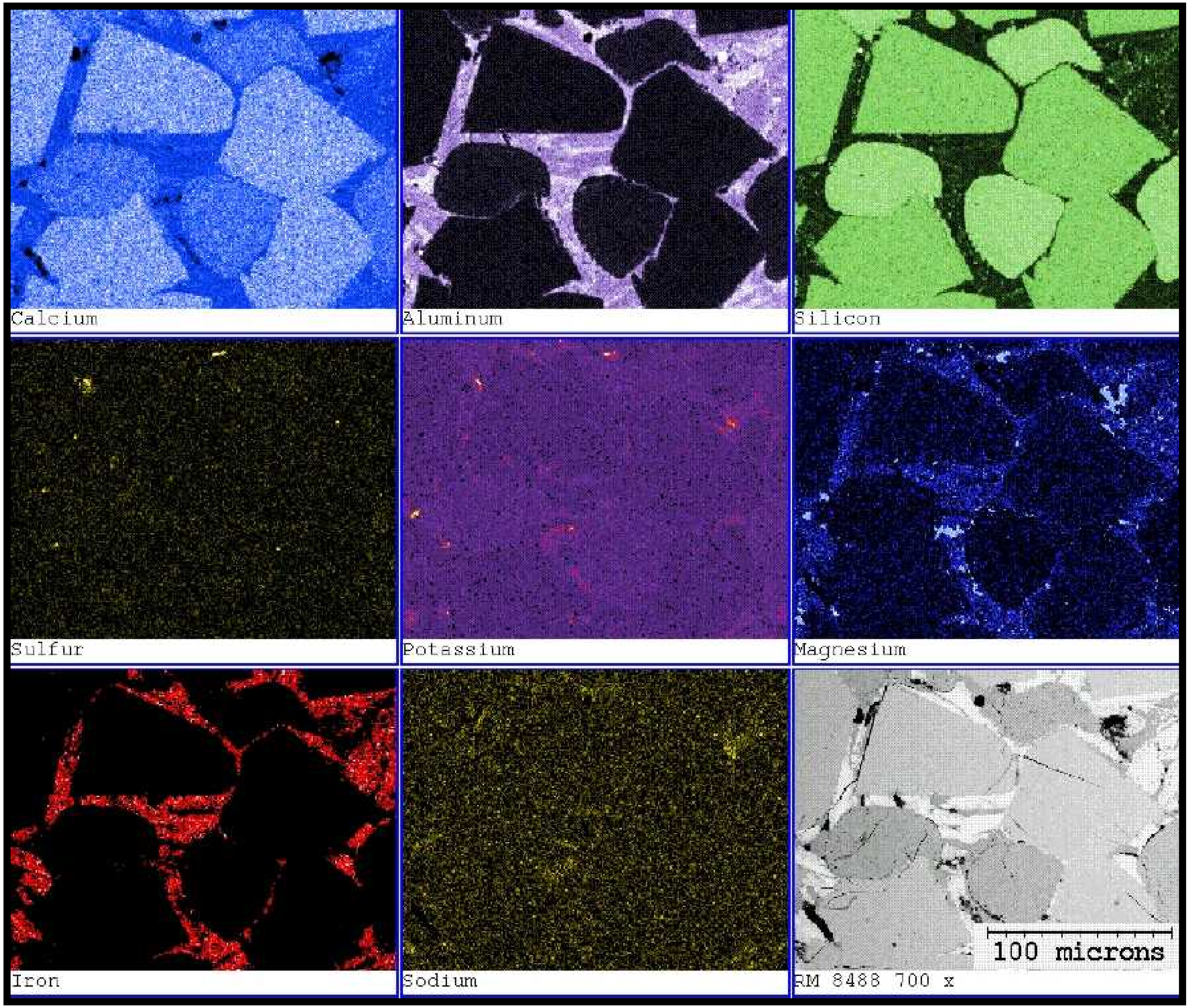

Laboratorija za atomsku fiziku

Philips SEM 501

The TEM

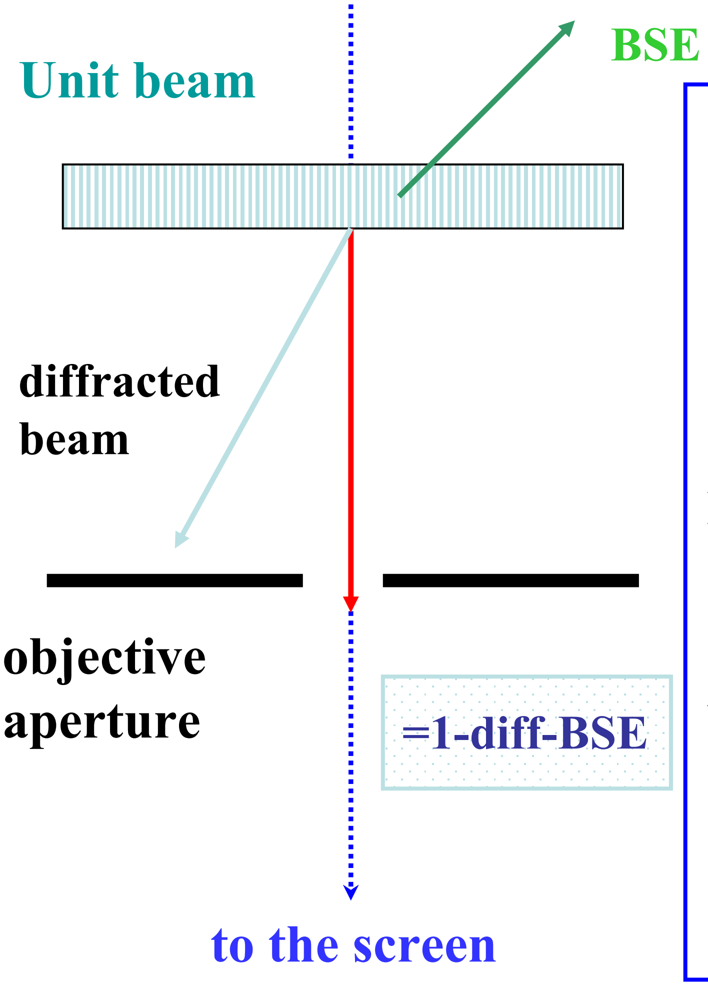

Unit beam

BSE

diffracted beam

objective aperture

=1-diff-BSE

to the screen

- ⌘ Samples must be thin (~100 nm) and beam energies must be high
- ⌘ With crystalline samples image detail comes mostly from Bragg diffraction
- ⌘ By choosing the aperture position either the diffracted beam (Dark Field) or the unscattered electrons (Bright Field) can be used to form the image

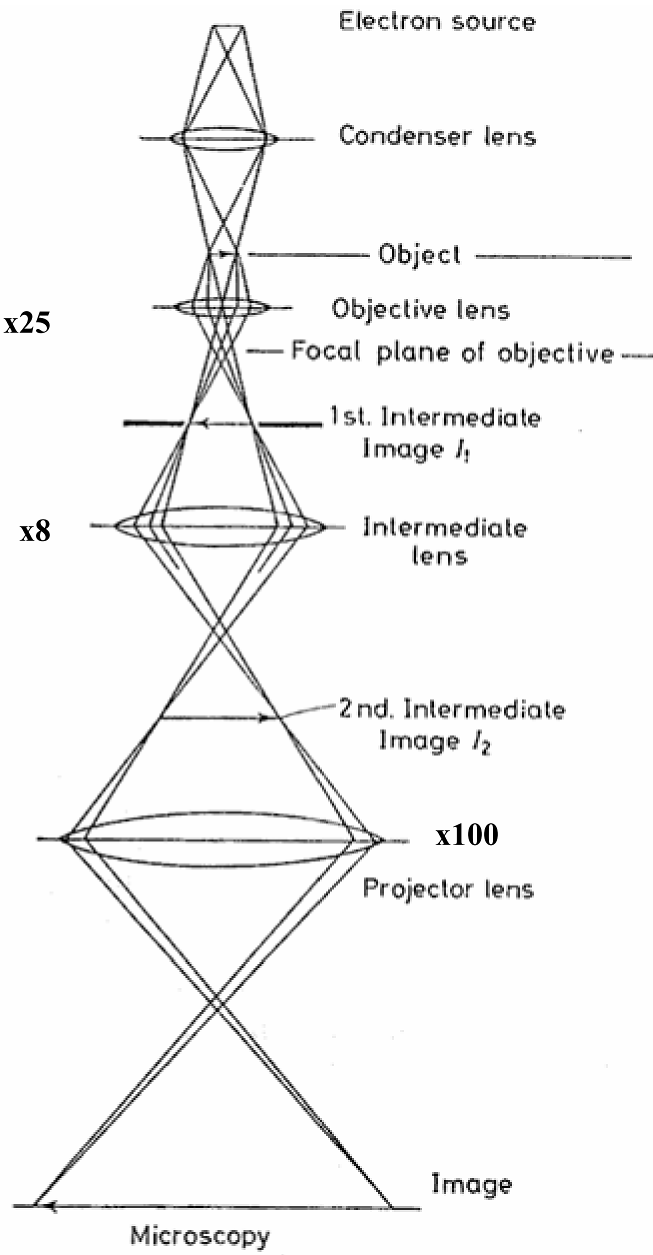

Materials Science

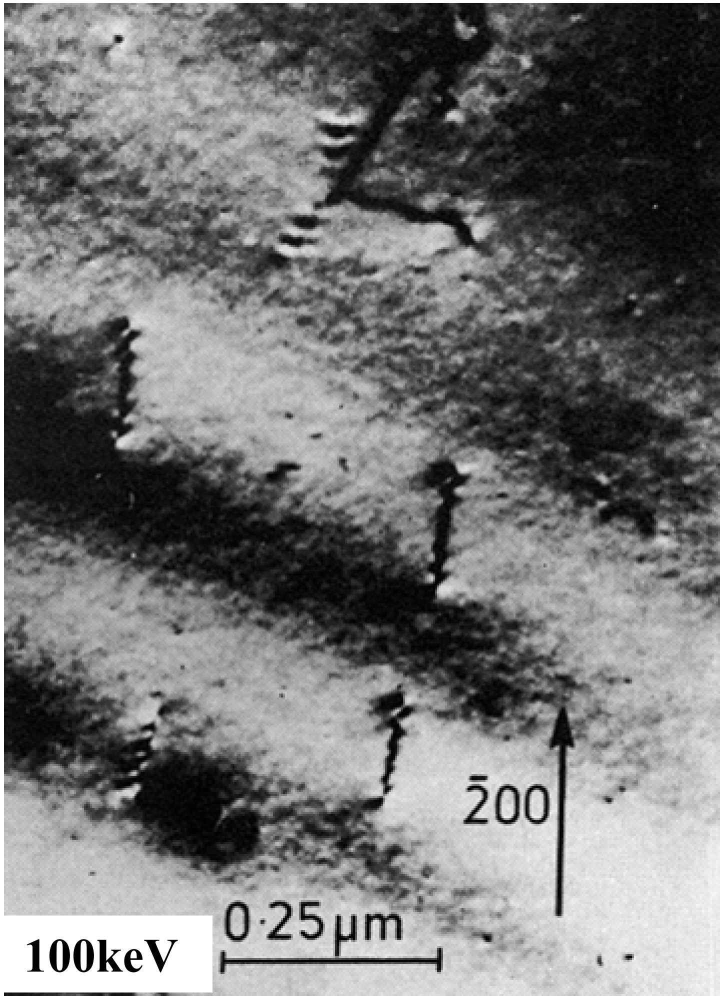

Screw dislocations in stainless steel

- *The TEM combination of diffraction and imaging provides a unique capability for understanding the properties of crystals, and of defects in crystalline materials*
- *The highly developed dynamical theory of diffraction permits detailed interpretation*
- *Imaging is possible from the meso- to the nanometer scale and the spatial resolution can now extend to the atomic level*
- *Requires specialized operators*

Transmission Electron Microscopy

$$\lambda \approx (150 / V)^{1/2} \text{ Angstroms}$$

Substituting 200 eV for V gives λ a of 0.87 Angstroms

For a beam of 100 KeV we get a wavelength of 0.0389 and a theoretical resolution of 0.0195 Angstroms!

But in actuality most TEMs will only have an actual resolution 2.4 Angstroms at 100KeV

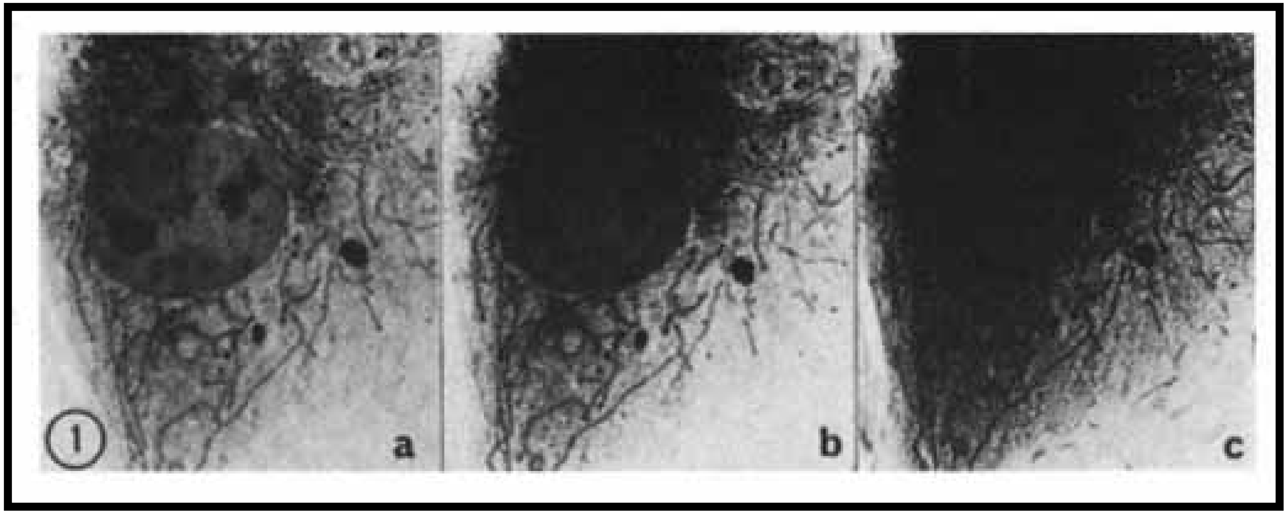

1 MeV **200 kV** **100kV**

TEM

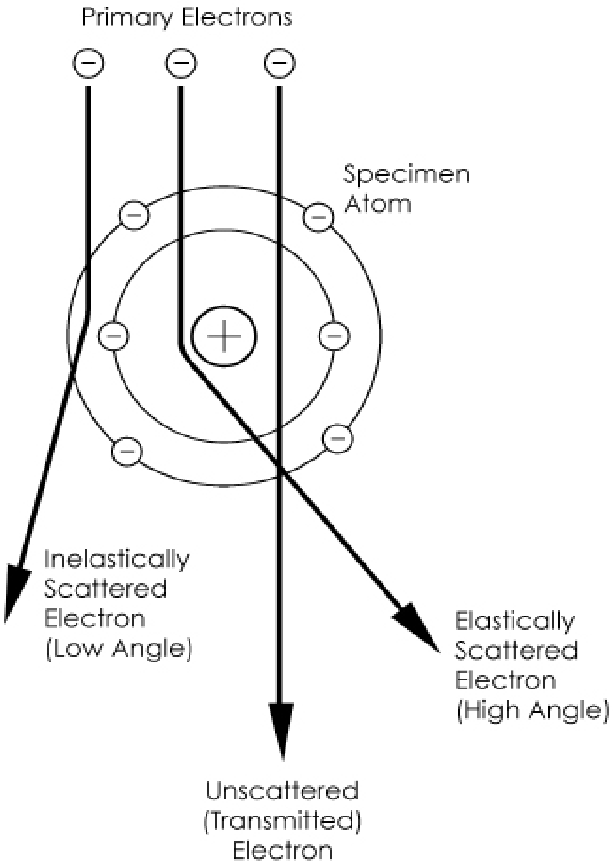
Primary Electrons
Specimen Atom
Inelastically Scattered Electron (Low Angle)
Elastically Scattered Electron (High Angle)
Unscattered (Transmitted) Electron

TEM

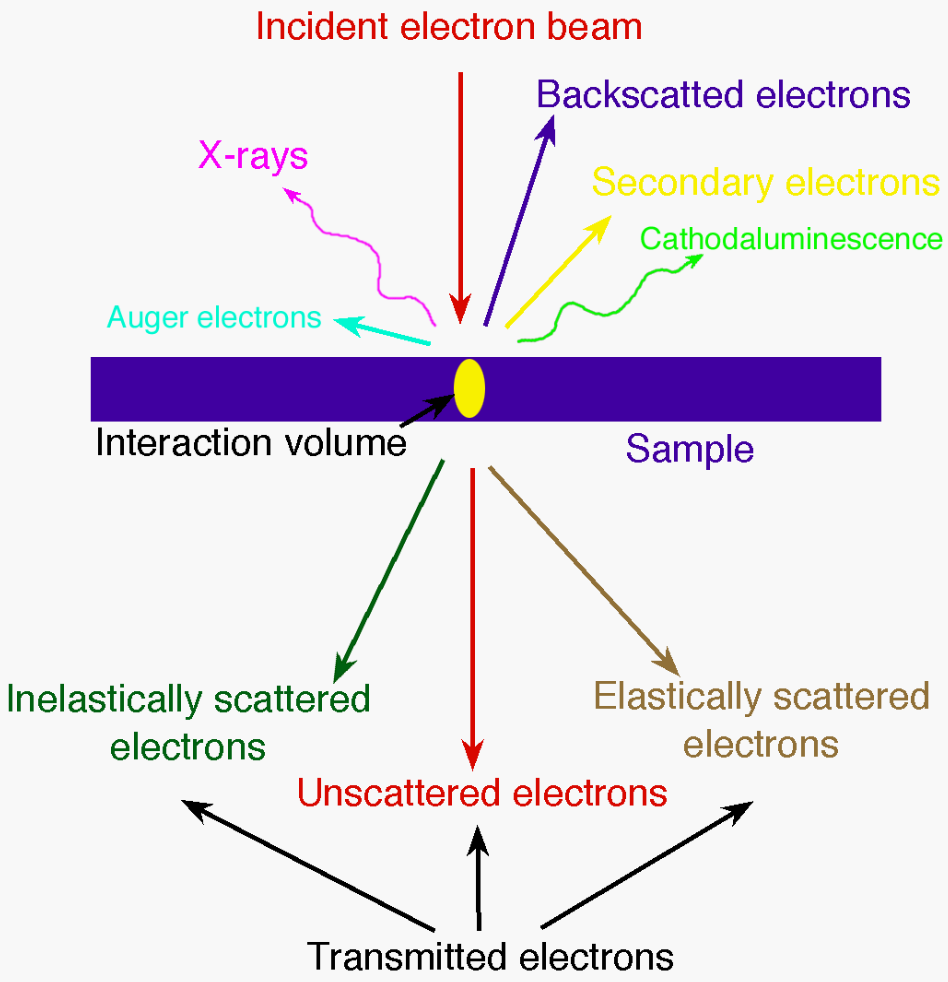
Incident electron beam
Backscatted electrons
X-rays
Secondary electrons
Cathodaluminescence
Auger electrons
Interaction volume
Sample
Inelastically scattered electrons
Elastically scattered electrons
Unscattered electrons
Transmitted electrons

Transmission Electron Microscopes:

Widely used in materials science and biological research

Capable of magnifying over a extremely wide range (~100 to >1,000,000 x)

Excellent spatial resolution (better than 1 nm)

Easy to use and very reliable

TEMs are patterned after Transmission Light Microscopes and will yield similar information.

Morphology

The size, shape and arrangement of the particles which make up the specimen as well as their relationship to each other on the scale of atomic diameters.

Crystallographic Information

The arrangement of atoms in the specimen and their degree of order, detection of atomic-scale defects in areas a few nanometers in diameter

Compositional Information (if so equipped)

The elements and compounds the sample is composed of and their relative ratios, in areas a few nanometers in diameter

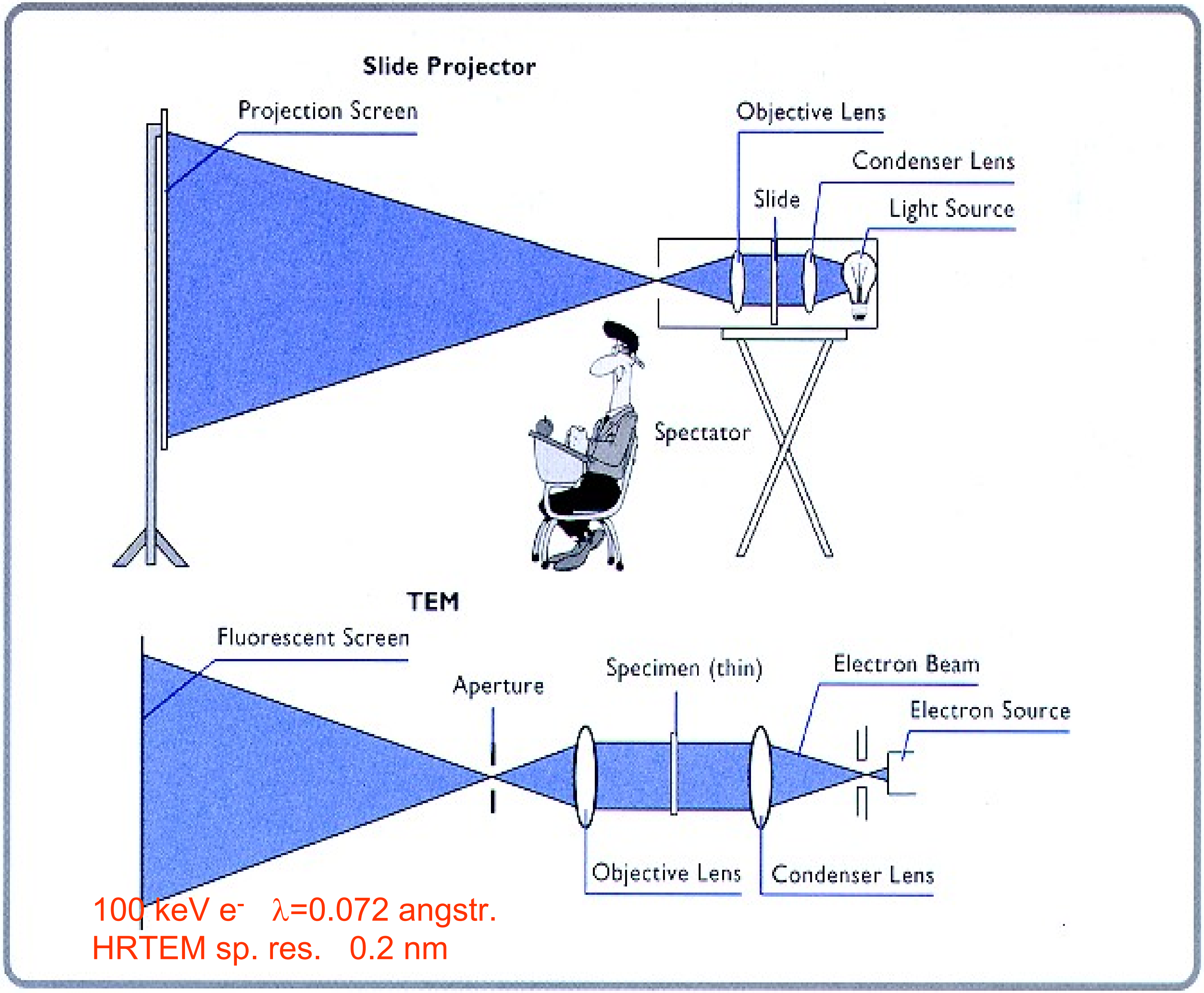

100 keV e^- λ=0.072 angstr.

HRTEM sp. res. 0.2 nm

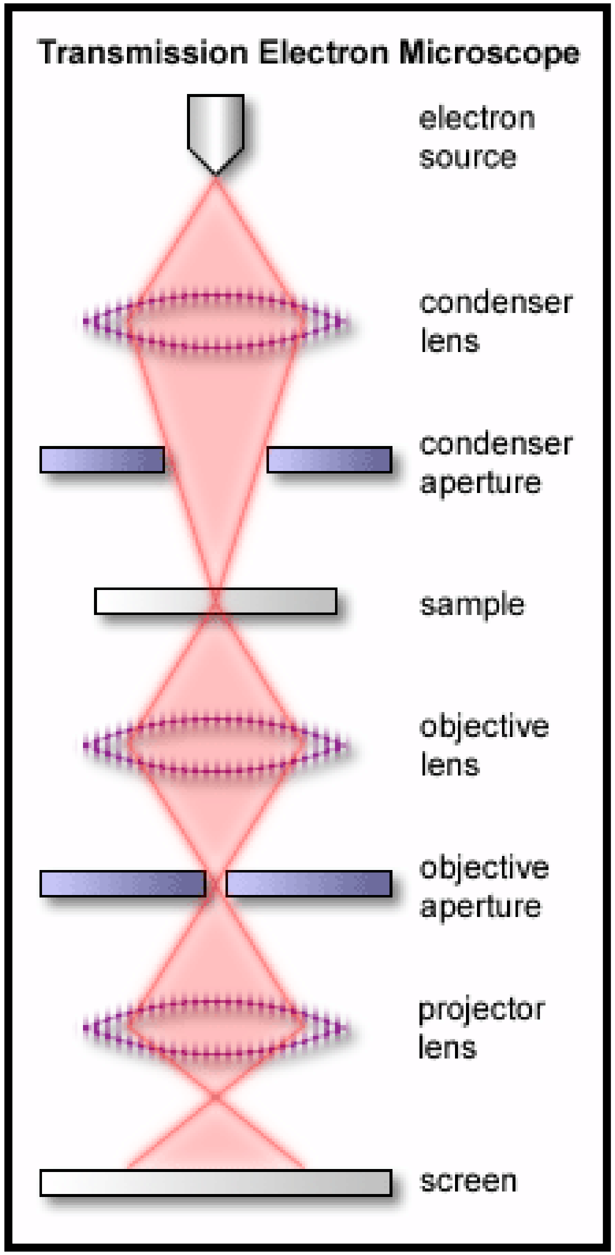

A simplified ray diagram of a TEM consists of an electron source, condenser lens with aperture, specimen, objective lens with aperture, projector lens and fluorescent screen.

Transmission Electron Microscope

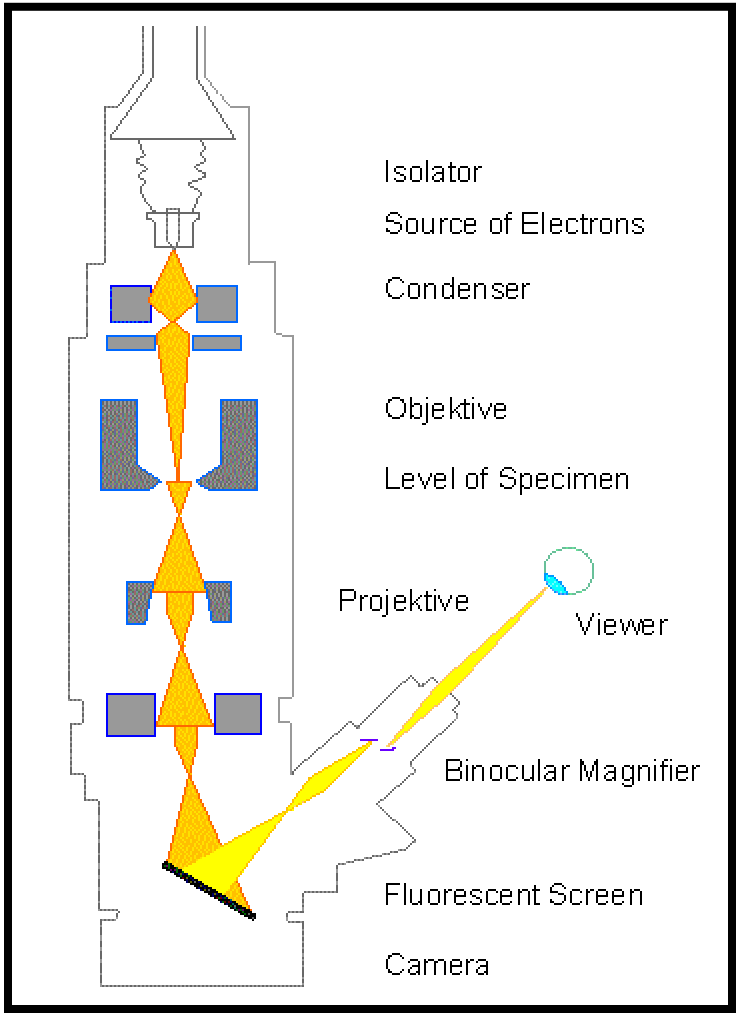

Basic premise of a TEM is to project a magnified image of the specimen onto a fluorescent screen where it can be viewed by the operator. The image itself is the result of beam electrons that are scattered by the specimen vs. those that are not.

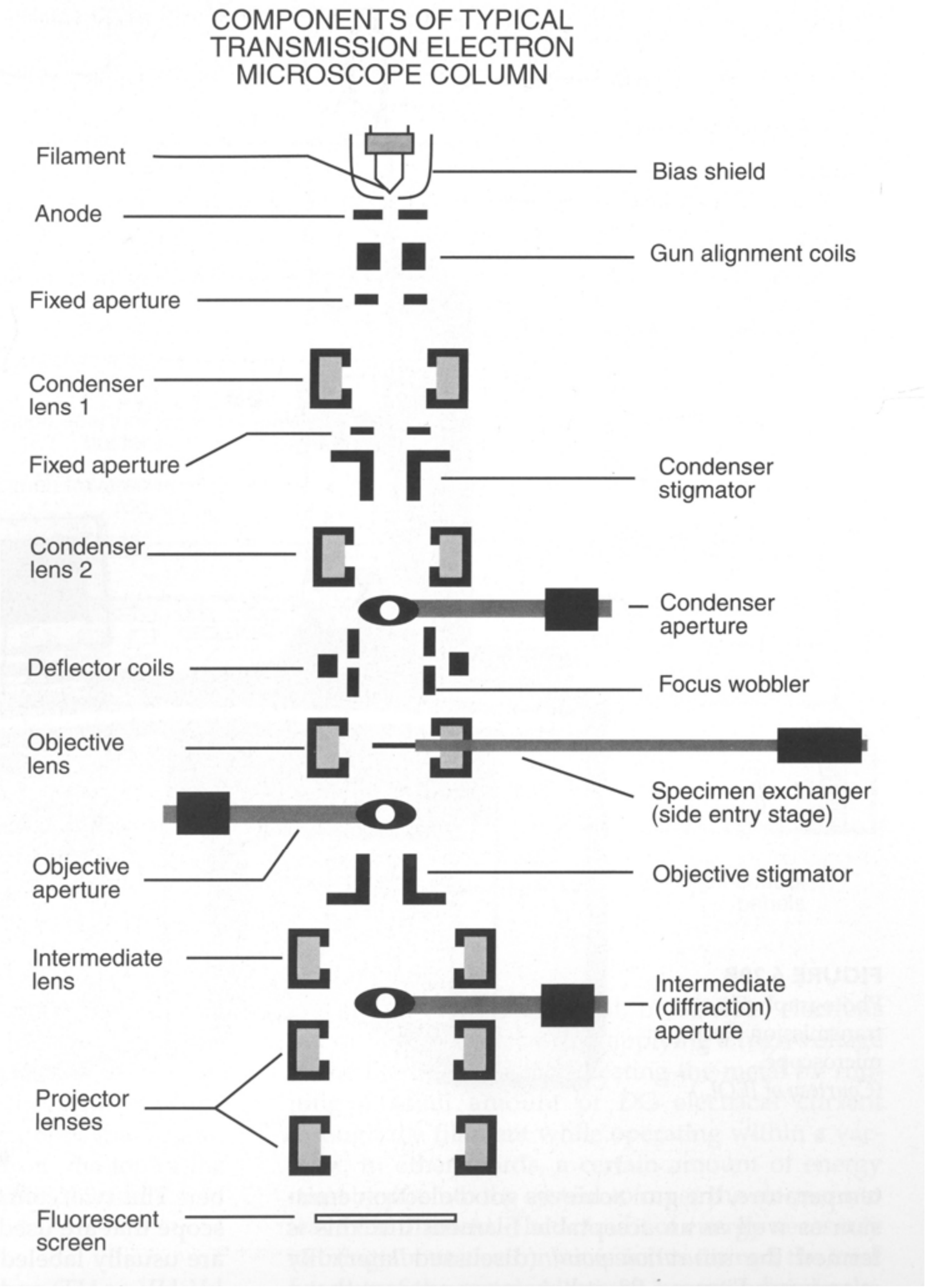

In actuality a modern TEM consists of many more components including a dual condenser system, stigmators, deflector coils, and a combination intermediate and dual projector lens.

Total magnification in the TEM is a combination of the magnification from the objective lens times the magnification of the intermediate lens times the magnification of the projector lens. Each of which is capable of approximately 100X.

$$M_{ob} \times M_{int} \times M_{proj} = \text{Total Mag}$$

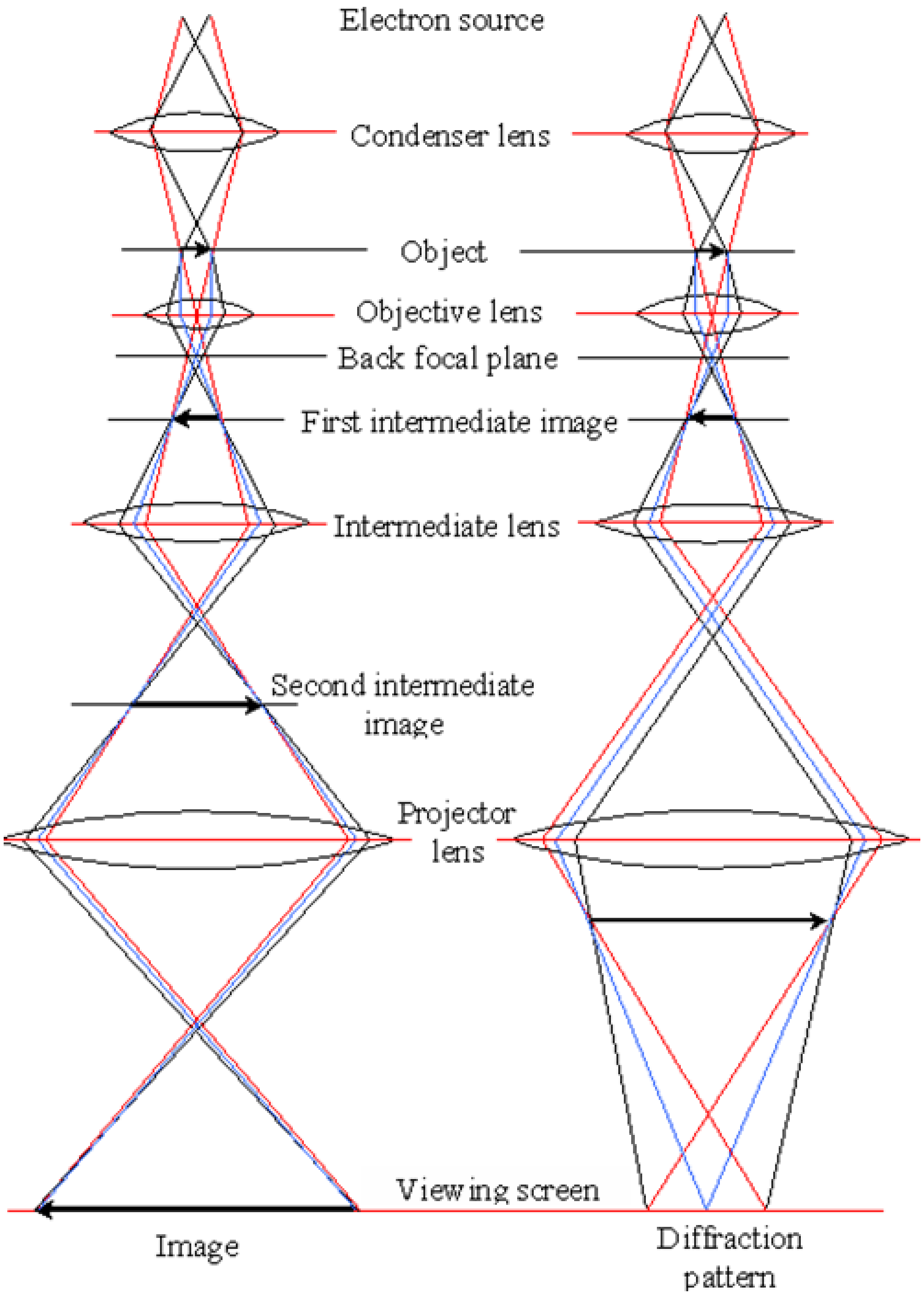

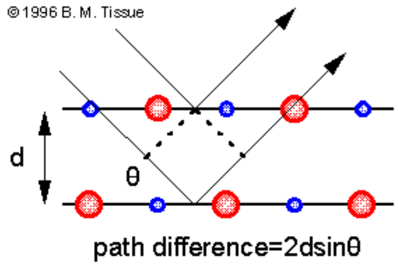
©1996 B. M. Tissue

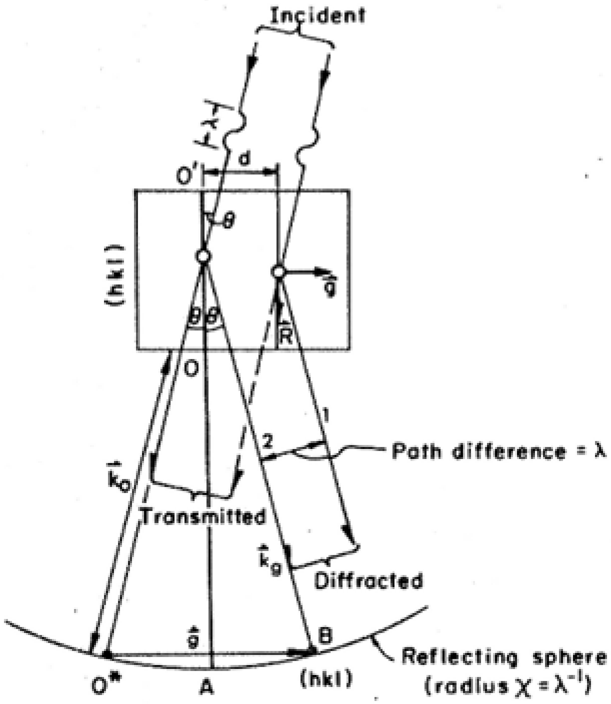

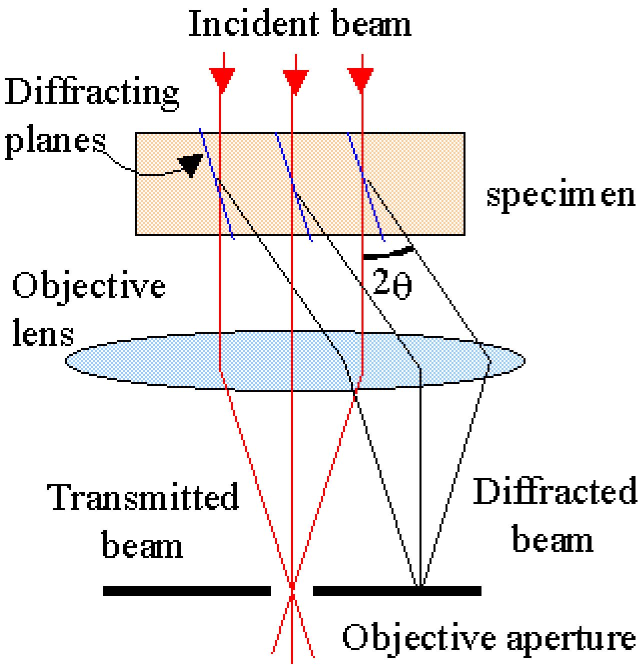

Bright Field Imaging

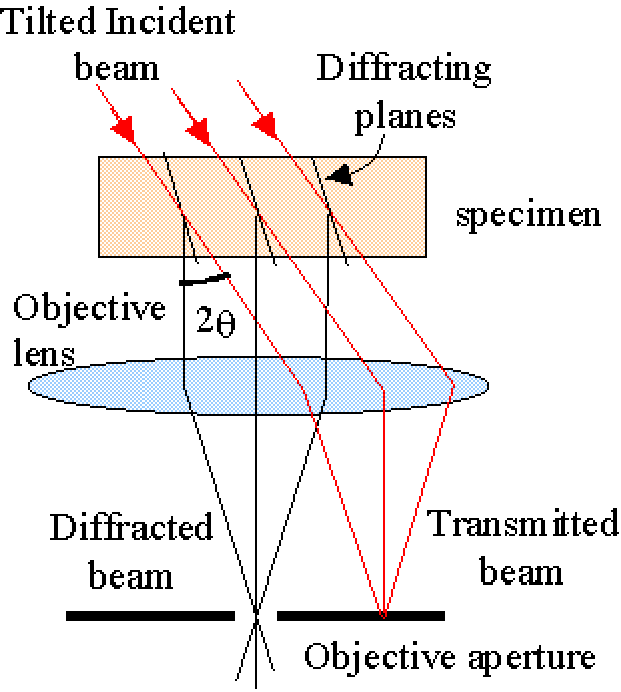

On-axis Dark Field

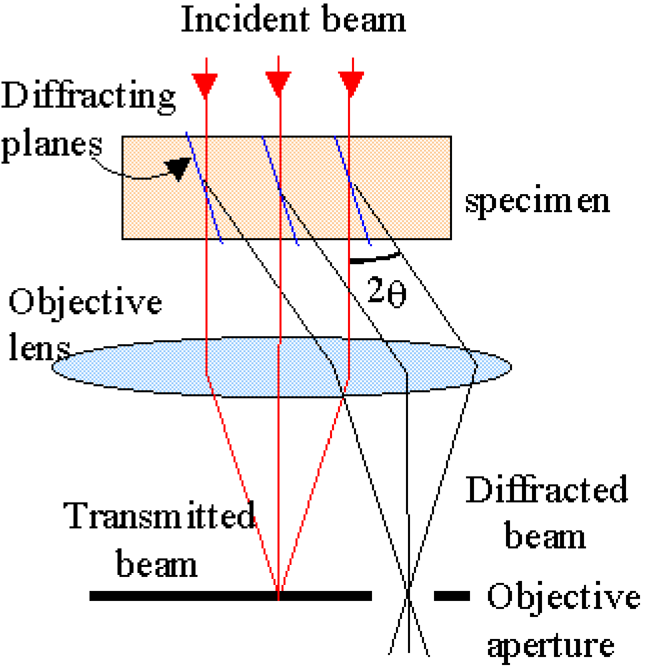

Off-axis Dark Field

Growth of b-FeSi2 films via noble-gas ion-beam mixing of Fe/Si bilayers

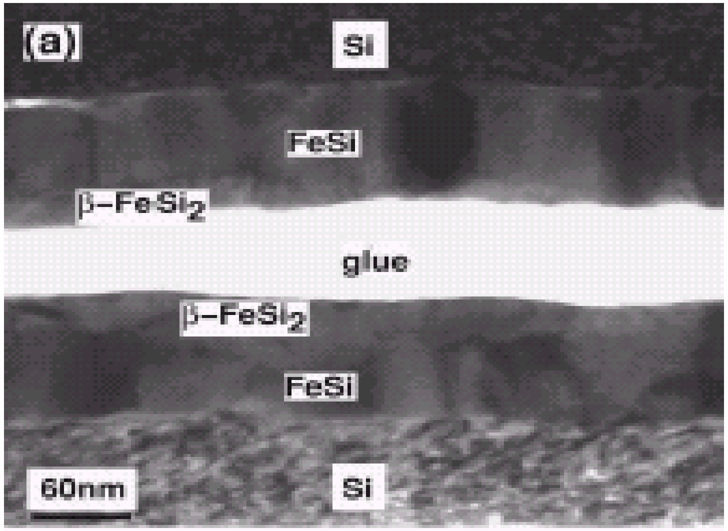

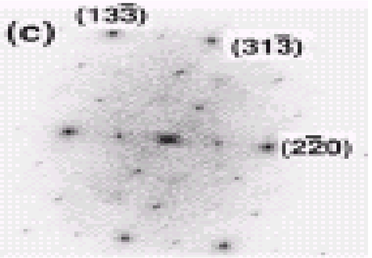

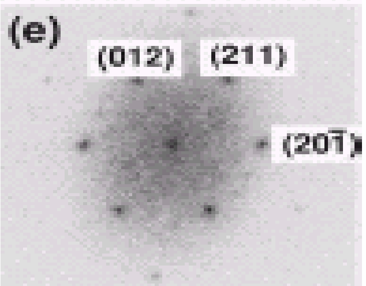

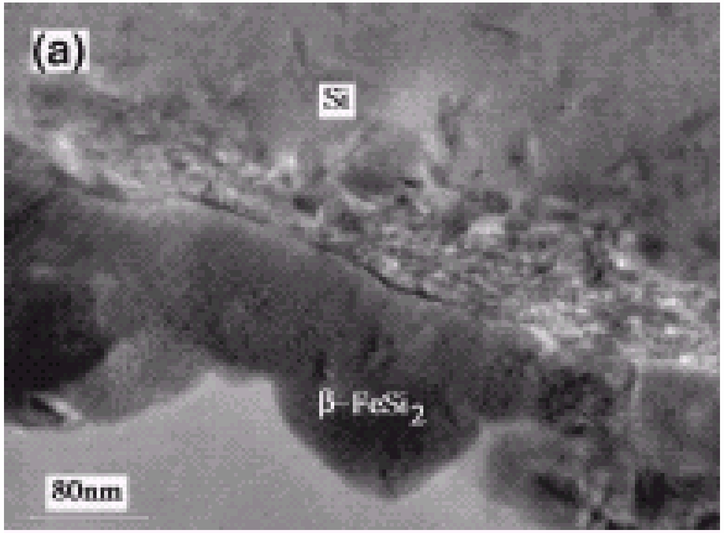

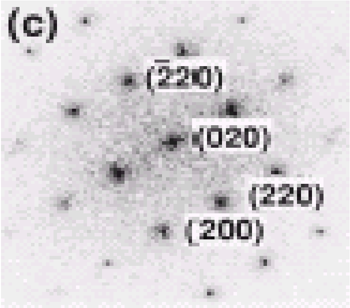

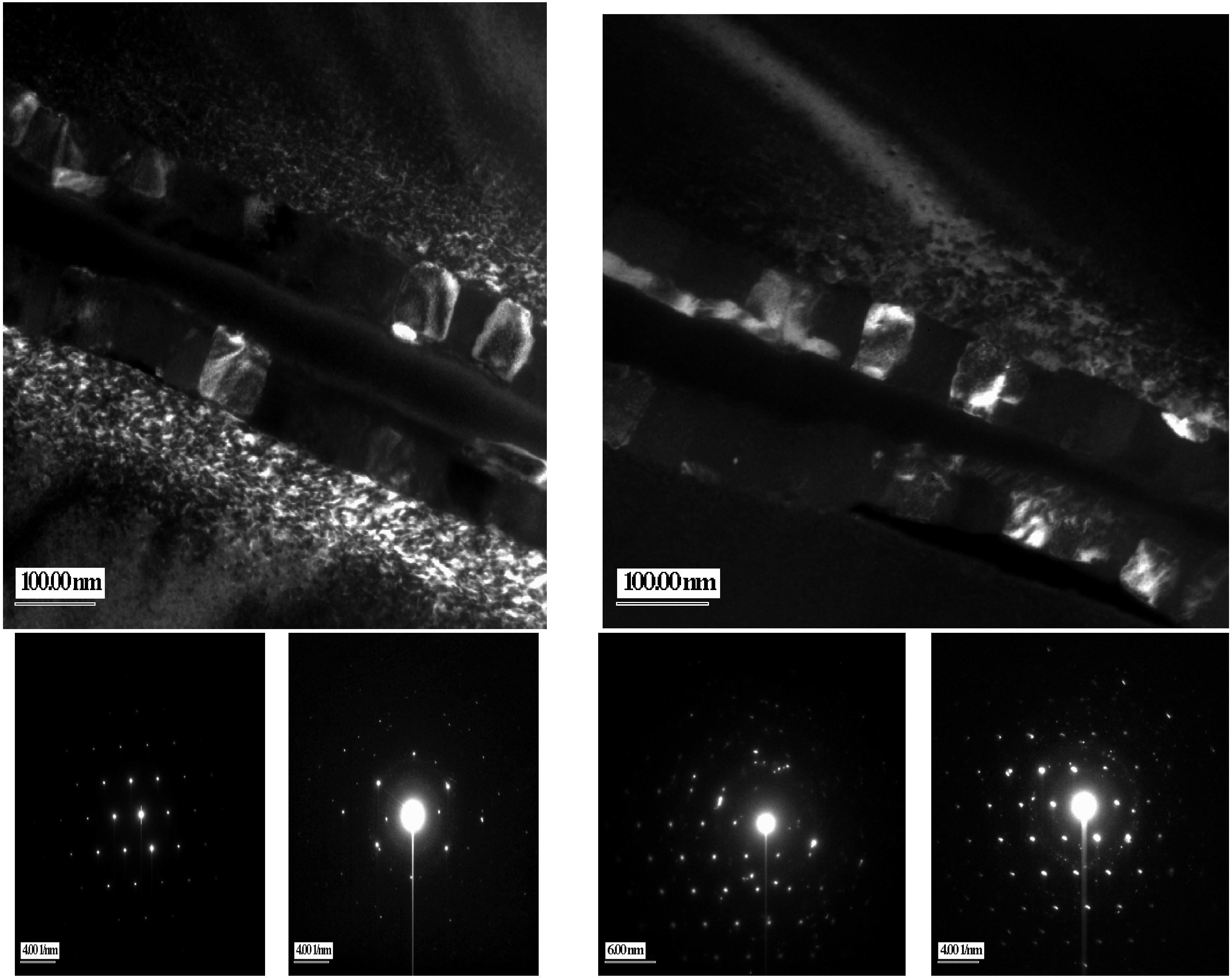
100.00 nm
100.00 nm
4.00 1/nm
4.00 1/nm
6.00 nm
4.00 1/nm

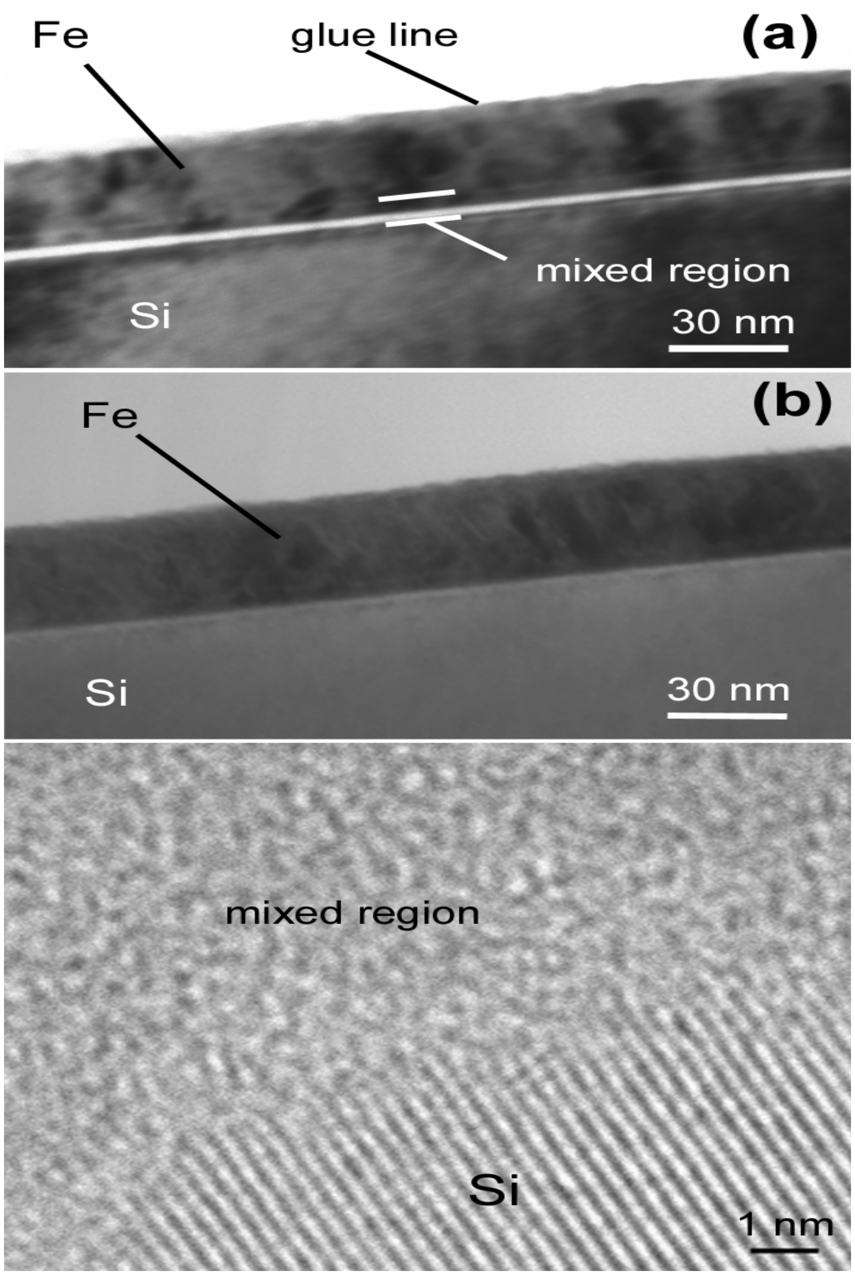
Fe
glue line
(a)
mixed region
Si
30 nm
(b)
Fe
Si
30 nm
mixed region
Si
1 nm

Cu_xSe in $Cu(In,Ga)Se_2$ thin films

EDP

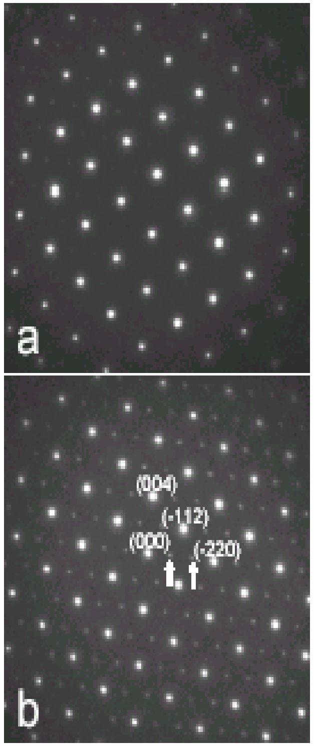

EDS

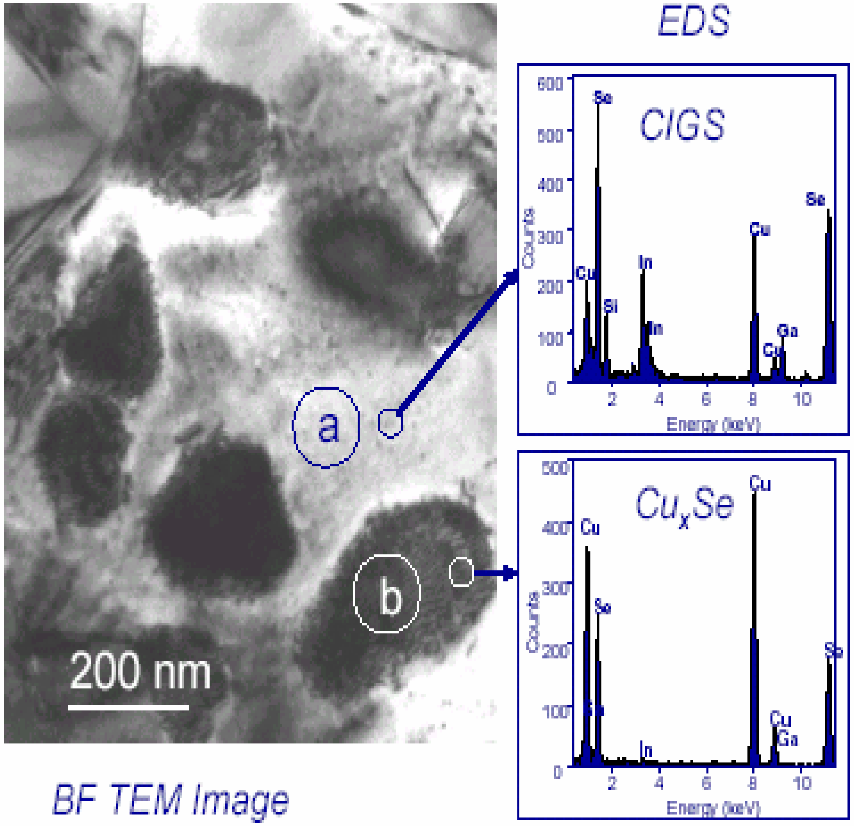

BF TEM Image

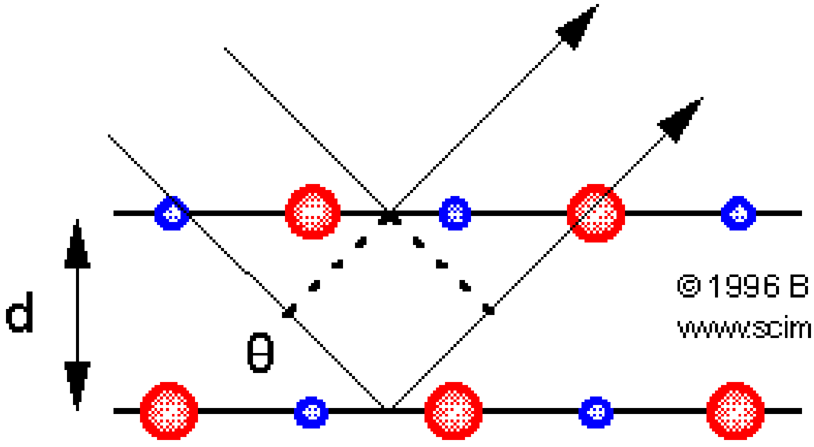

© 1996 B. M. Tissue
www.scimedia.com

path difference=2dsinθ

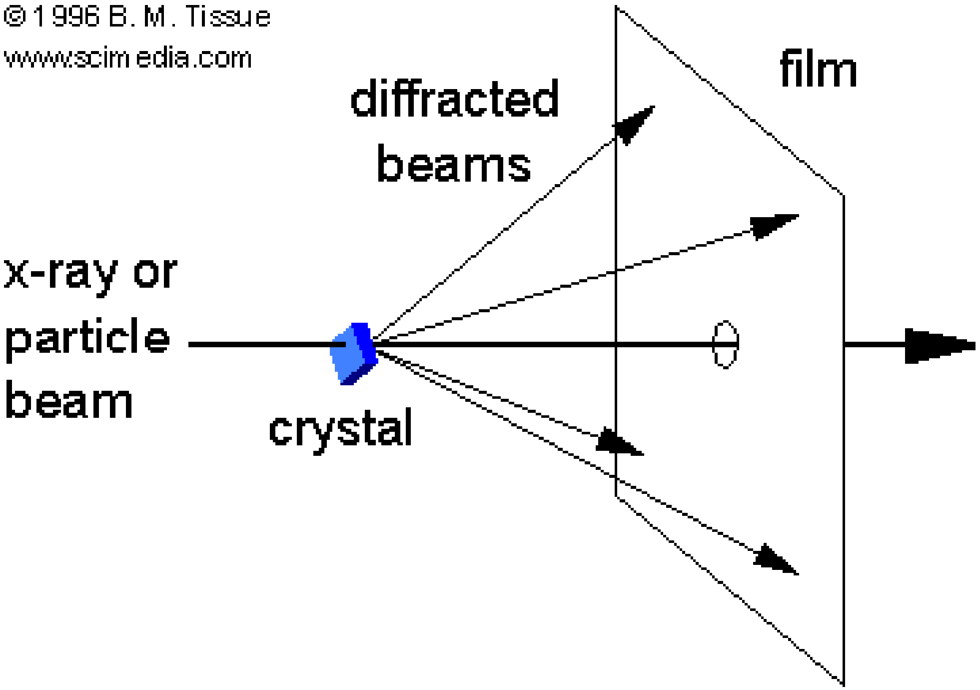

© 1996 B. M. Tissue
www.scimedia.com

***Electron diffraction:* Electrons are diffracted in crystals. Due to the strong interaction (much stronger than with X-rays!) only very thin specimens can be analyzed. The diffraction pattern is characteristic for the crystal structure.**

Table 1. The Characteristics of Light and Various Radiations

Used for Texture Measurement by Diffraction.

	Light	Neutrons	X-rays	Electrons
Wavelength [nm]	400-700	0.05 - 0.3	0.05 - 0.3	0.001 - 0.01
Energy [eV]	1	1.00E-02	1.00E+04	1.00E+05
Charge [C]	0	0	0	-1.60E-19
Rest mass [g]	0	1.67E-24	0	9.11E-28
Penetration depth [mm]	0	10 - 100	0.01 - 0.1	1.00E-03

- ***Electrons are the only radiation in which their penetration depth and interaction volume is small enough to allow diffraction from individual grains (very small volume). Hence, only electrons can be used for MICROTEXTURE***

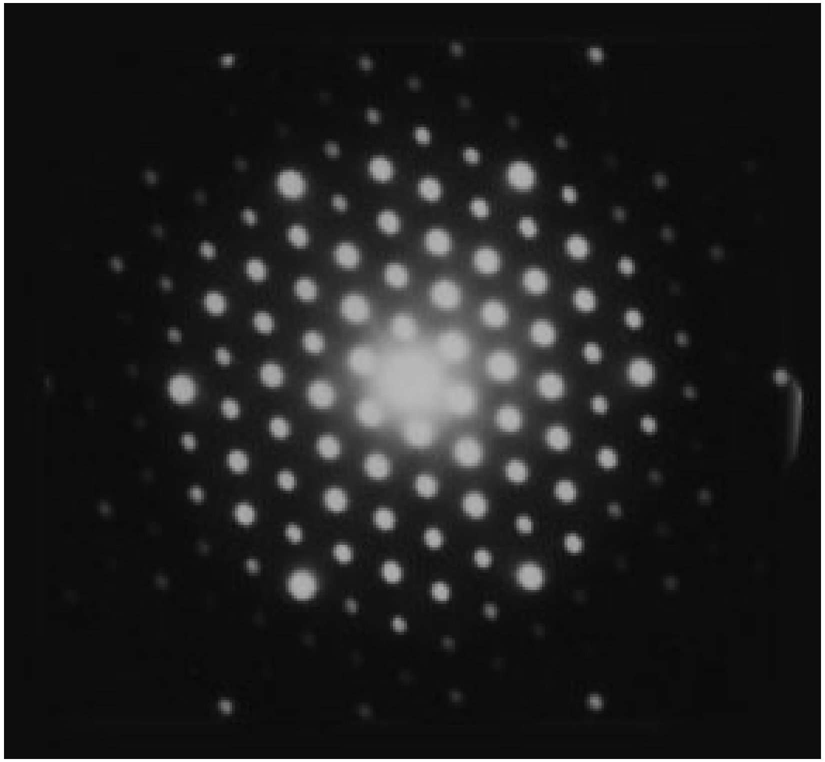

The result is an electron diffraction (ED) pattern. The pattern one obtains is completely dependent on the d-spacing and composition of the crystal that is being analyzed.

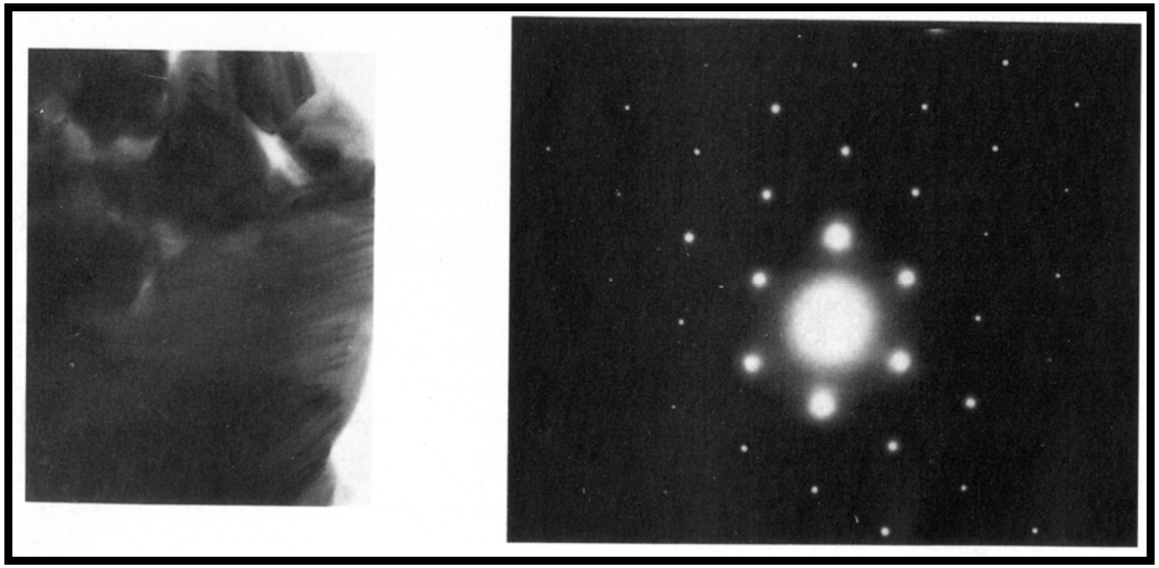

An ED from a single crystal will result in a series of diffraction spots arranged in concentric rings around the central bright spot which is comprised of transmitted electrons.

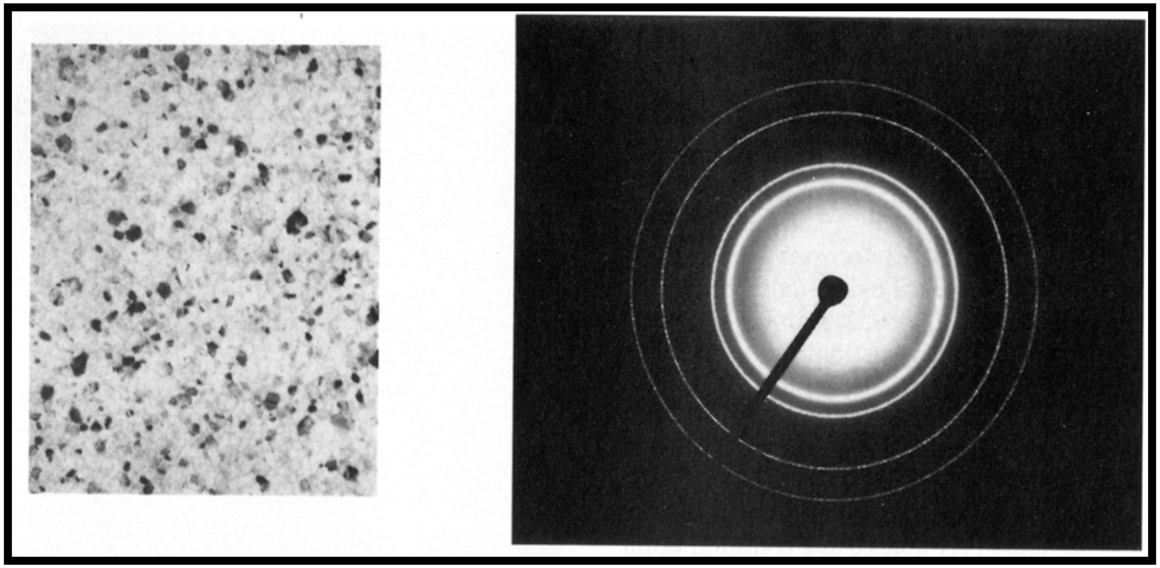

If an ED is made of field of many crystals, some of which are oriented at the Bragg's angle while others are not, a pattern with well defined concentric rings, but not spots, will result.

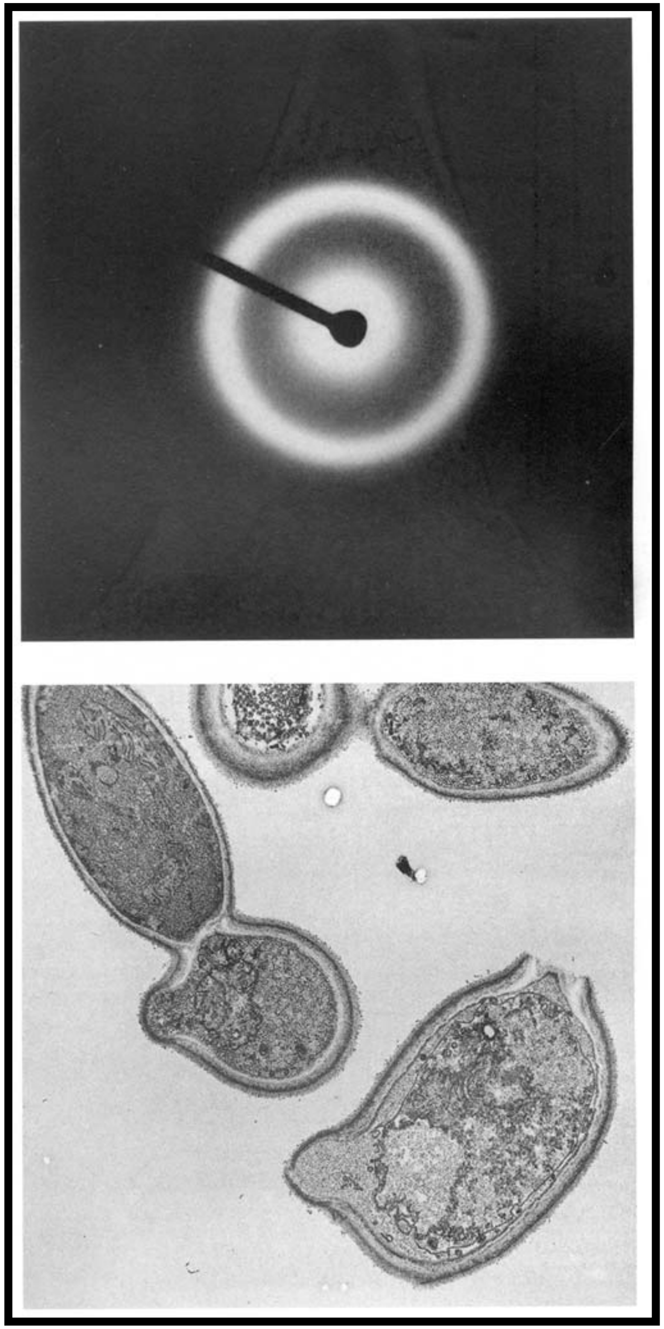

If an ED is made of an amorphous structure (i.e. no crystalline formation) then one simply gets a central bright spot comprised of transmitted electrons and a single ring of randomly forward scattered electrons.

Bright field => image obtained using direct beam

Dark field => image obtained using diffracted beam

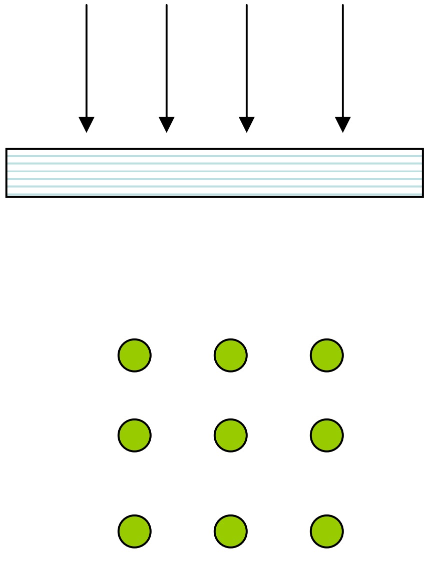

Single Crystal sample

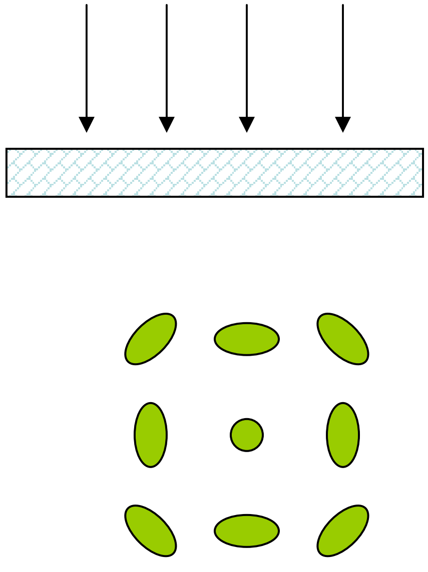

Textured sample

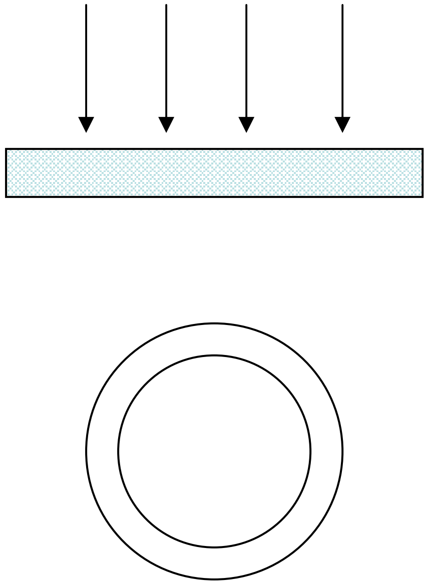

Fine grained sample

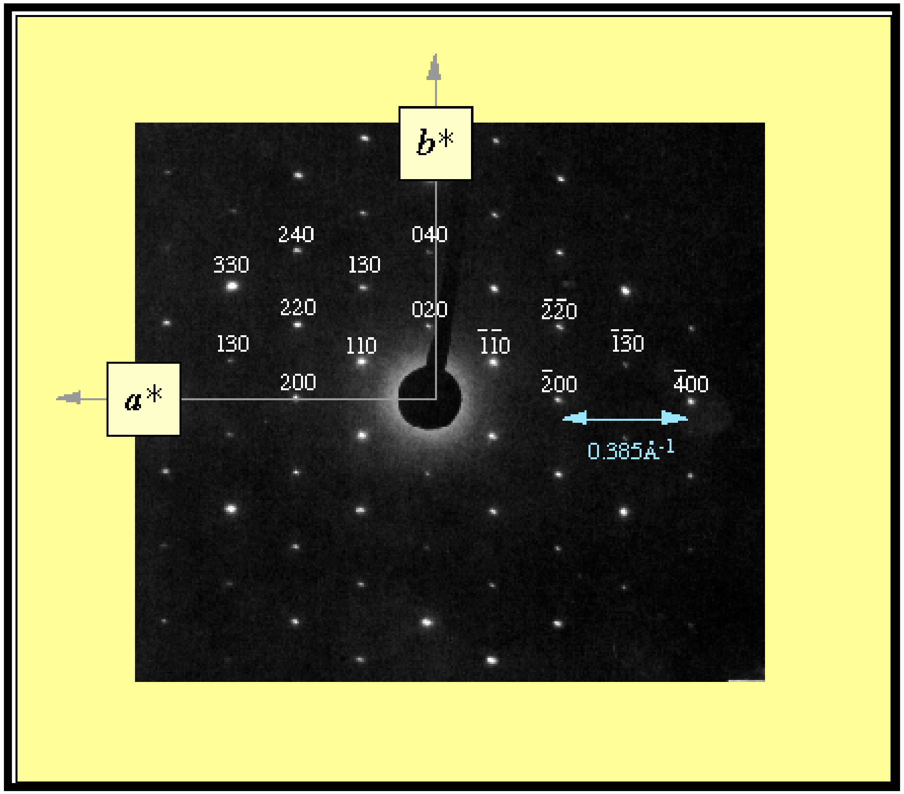

The R values for different order diffraction events can be measured directly from a diffraction pattern but it is crucial that it not be enlarged or reduced. It should always be compared to a pattern of a crystal with a known d-spacing so that the value for the camera length is accurate.

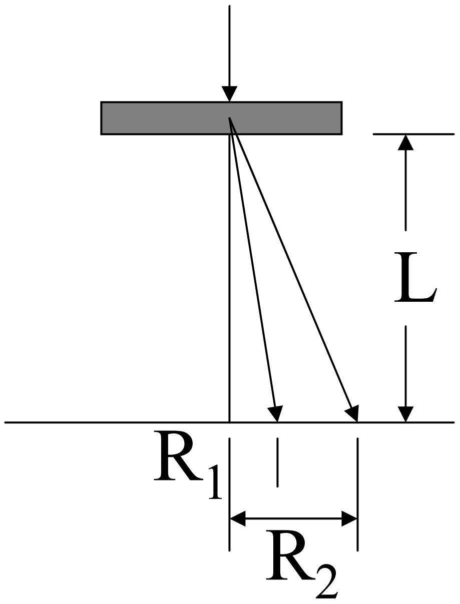

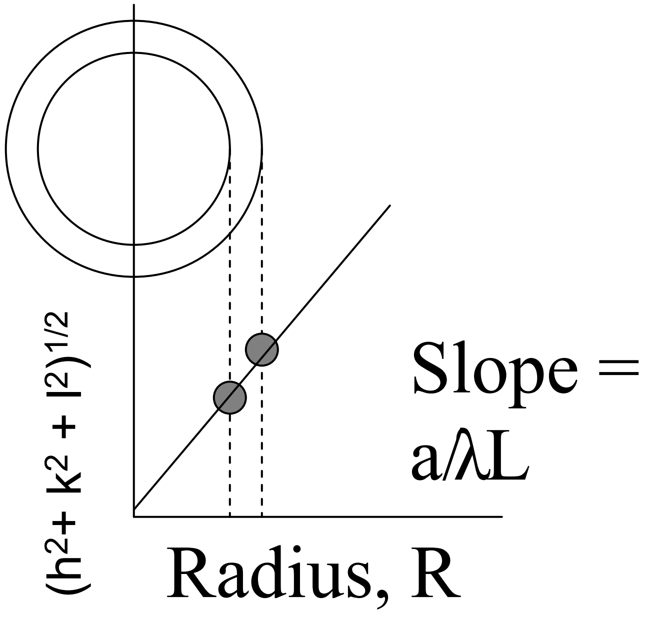

$\tan 2\theta$□2θ □ $2\sin\theta = R/L$

$2d_{hkl}\sin\theta=\lambda$; $d_{hkl}R/L= \lambda$

For cubic: $d_{hkl} = a/(h^2+k^2+l^2)^{1/2}$

$2d_{hkl}\sin\theta=\lambda$; $(a/\lambda L)R = (h^2+k^2+l^2)^{1/2}$

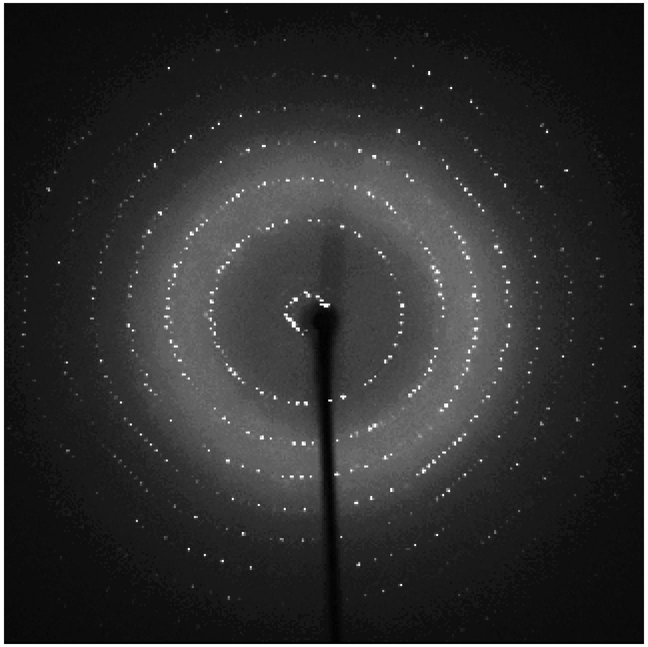

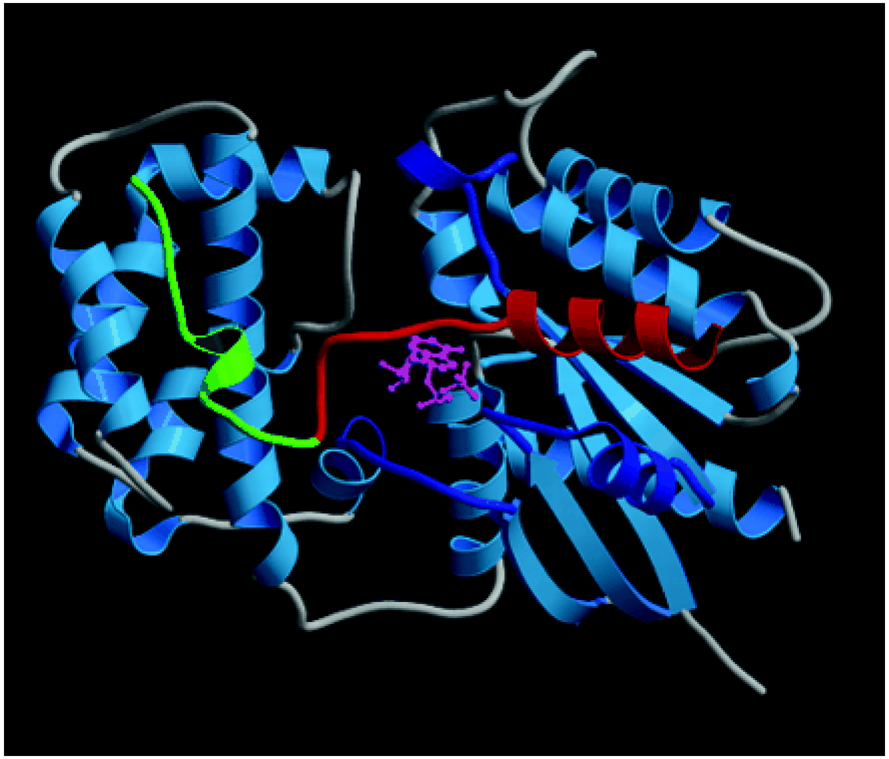

Binding site for Goloco motif on heterotrimeric Galpha protein (Kimple et al., (2002) *Nature* **416**, 878-881)

In this way complex molecular arrangements can be determined

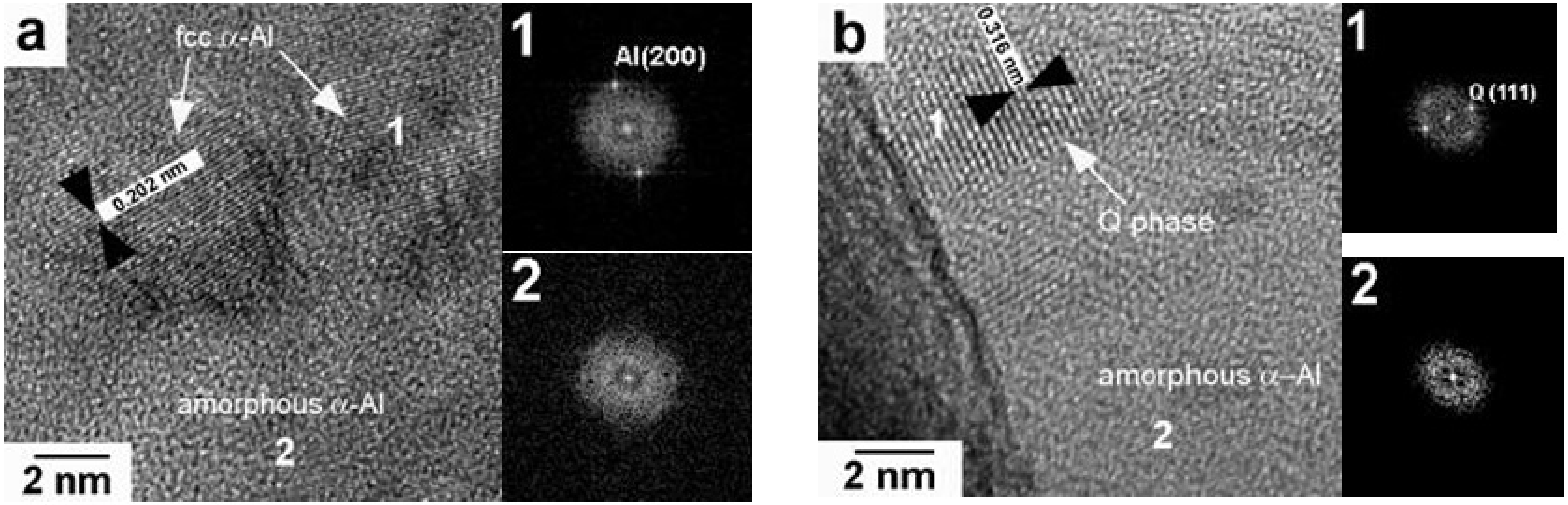

Figure 6. High-resolution images and their respective FFT showing the presence of:
(a)fcc and amorphous a-Al for the alloy with 0.59% Mg and
(b) Q phase and amorphous a-Al for the alloy with 3.80% Mg, for the alloys obtained at 45 ms^{-1}.

Basic Principles: How space is represented by frequency

Basic Principles

Fourier theory states that any signal, in our case visual images, can be expressed as a sum of a series of sinusoids. In the case of imagery, these are sinusoidal variations in brightness across the image. For example the sinusoidal pattern shown below can be captured in a single Fouier term that encodes 1: the spatial frequency, 2: the magnitude (positive or negative), and 3: the phase.

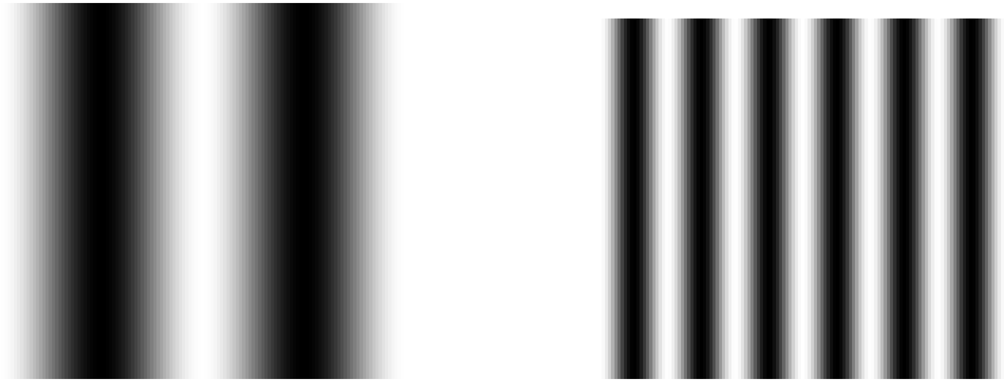

The significant point is that the Fourier image encodes exactly the same information as the brightness image, except expressed in terms of amplitude as a function of spatial frequency, rather than brightness as a function of spatial displacement. An inverse Fourier transform of the Fourier image produces an exact pixel-for-pixel replica of the original brightness image.

The orientation of the sinusoid correlates with the orientation of the peaks in the Fourier image relative to the central DC point. In this case a tilted sinusoidal pattern creates a tilted pair of peaks in the Fourier image.

Brightness Image **Fourier transform**

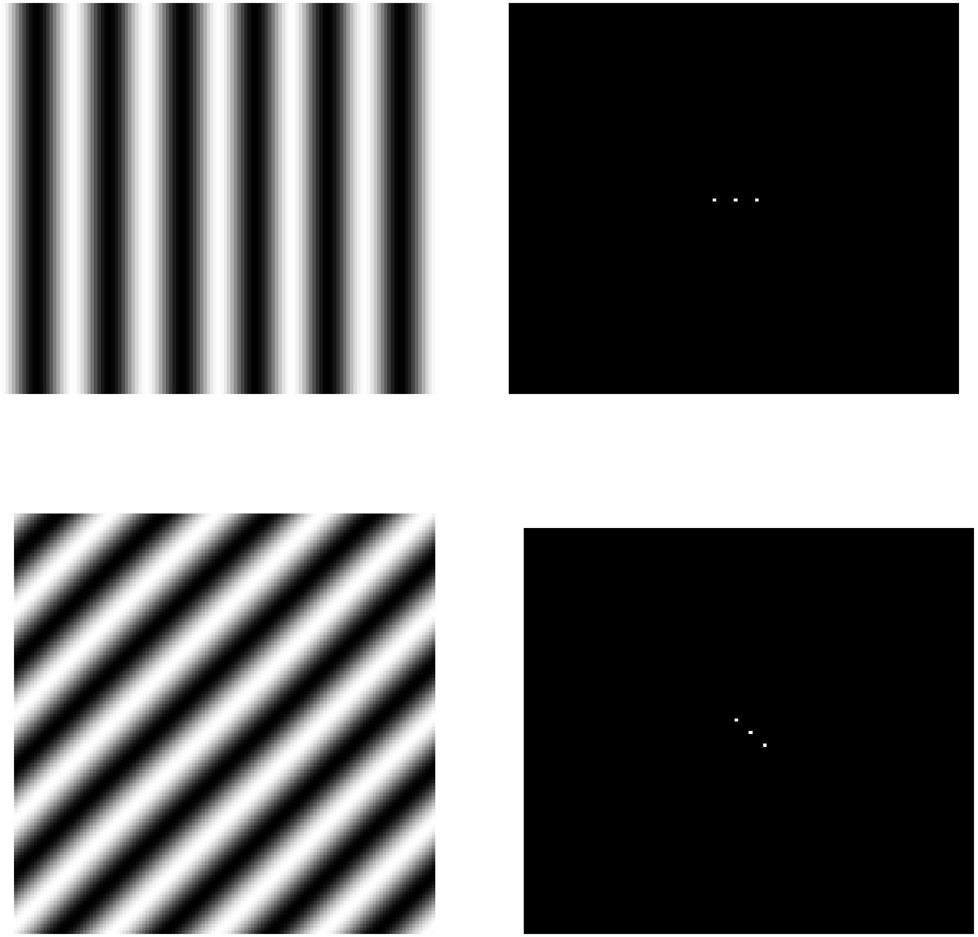

The unique STEM Mode - HAADF imaging

- ***The Super STEM microscopes incorporate computer controlled aberration correction of the objective lens using quadrupole and octupole lenses. This allows the formation of a sub-Angstrom probe for simultaneous ultra-high resolution high angle annular dark field (HAADF) imaging and atomic-column electron energy loss spectroscopy (EELS) analysis of thin specimens.***

- **The High Angle Annular Dark Field image is a unique operational mode of the STEM**
- **Here q - the inner angle of the annular DF detector - is made so large (30 millirads) that no Bragg diffracted electrons are collected**
  - **The outer angle f is made as large as possible**
- **The images comes from elastically scattered electrons which have passed very close to the atomic nucleus. High (single atom column) resolution is possible. There is zero diffraction contrast**

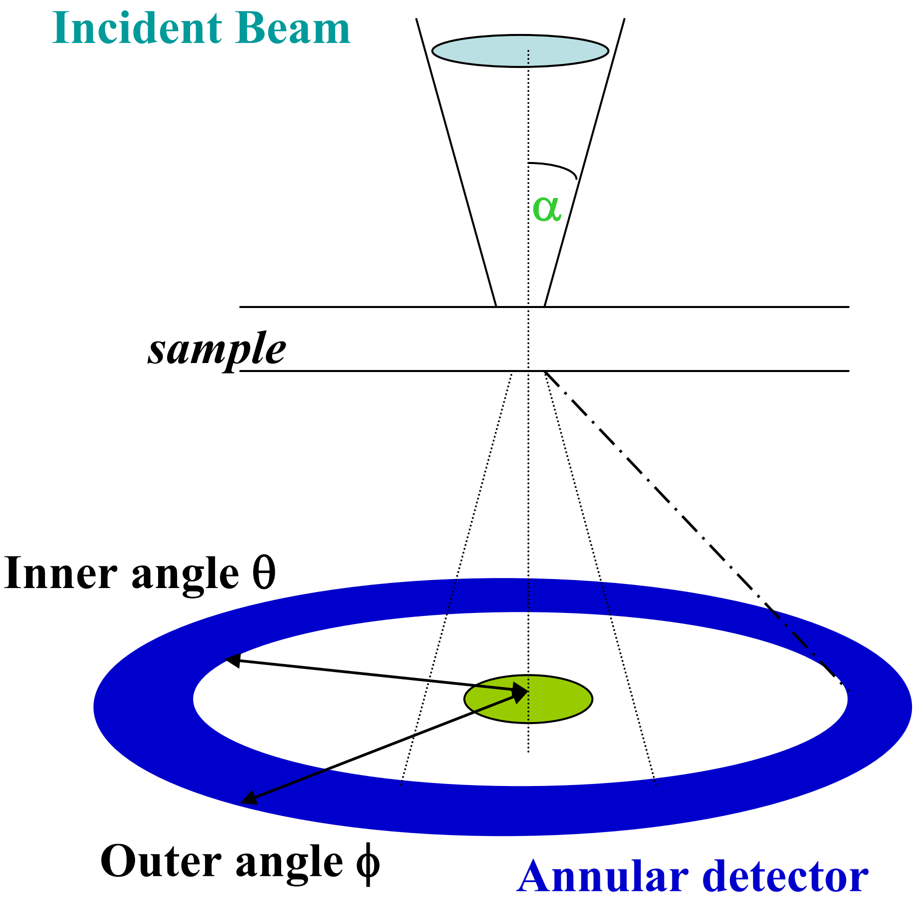

High Angle Angular DF

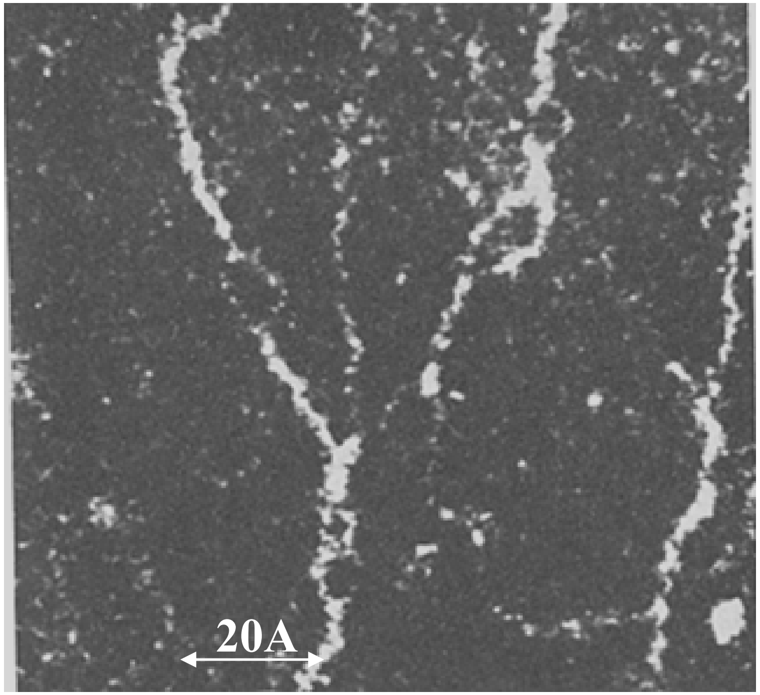

Individual strands of DNA on a carbon substrate (mass thickness contrast) Crewe et al 1971

- *The HAADF signal varies as* **ρT.Z$^{3/2}$** *where T is the specimen thickness, ρ is the density and Z is the atomic number*
- *So we can produce an image which shows pure* **mass - thickness contrast** *(i.e. the signal is proportional to the number of atoms) or* **Z contrast** *images (signal proportional to the atomic number of the atoms)*
- *HAADF works for inorganic and organic samples, and for crystalline and amorphous materials*

Z-contrast imaging of a crystal

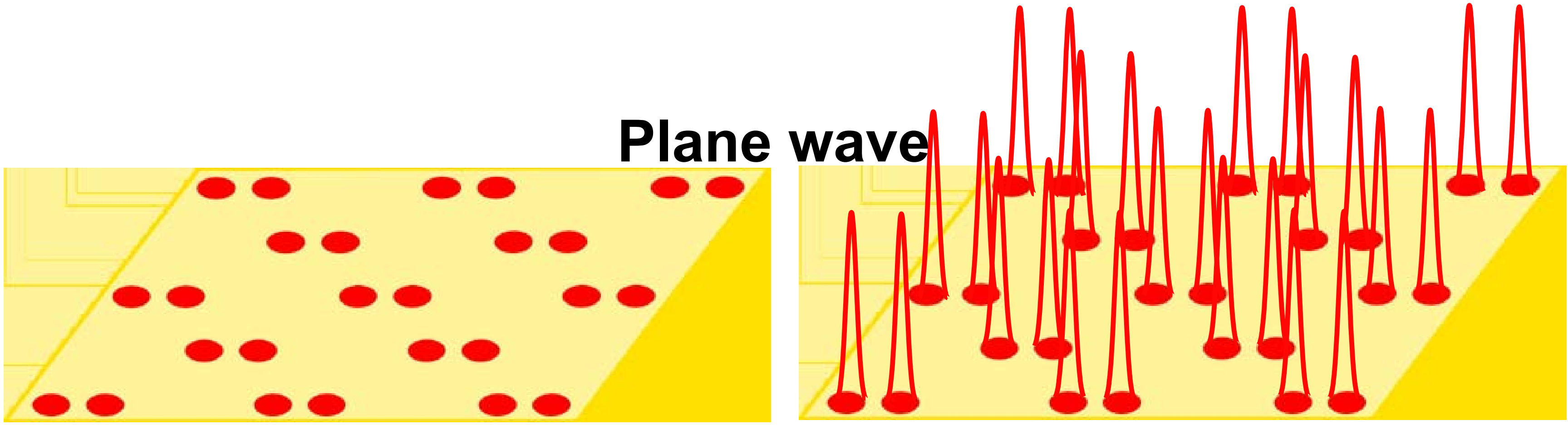

Plane wave

Bloch waves select s-states of the crystal

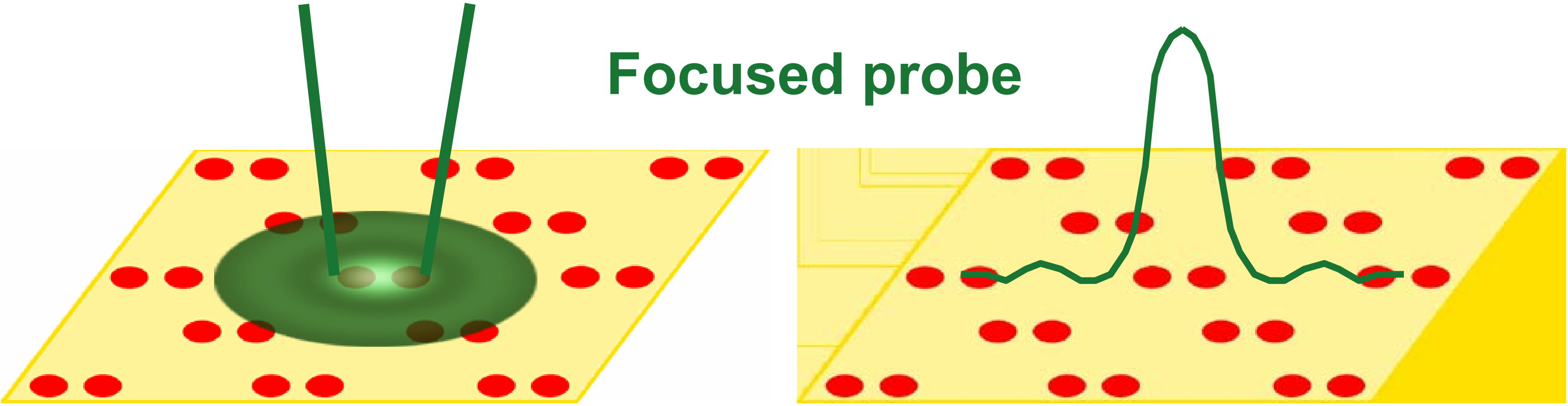

Focused probe

When the crystal lattice is correctly oriented then the beam interaction is localized at the atom column positions ('s' orbitals are selected)

Atomic Level Z-contrast STEM

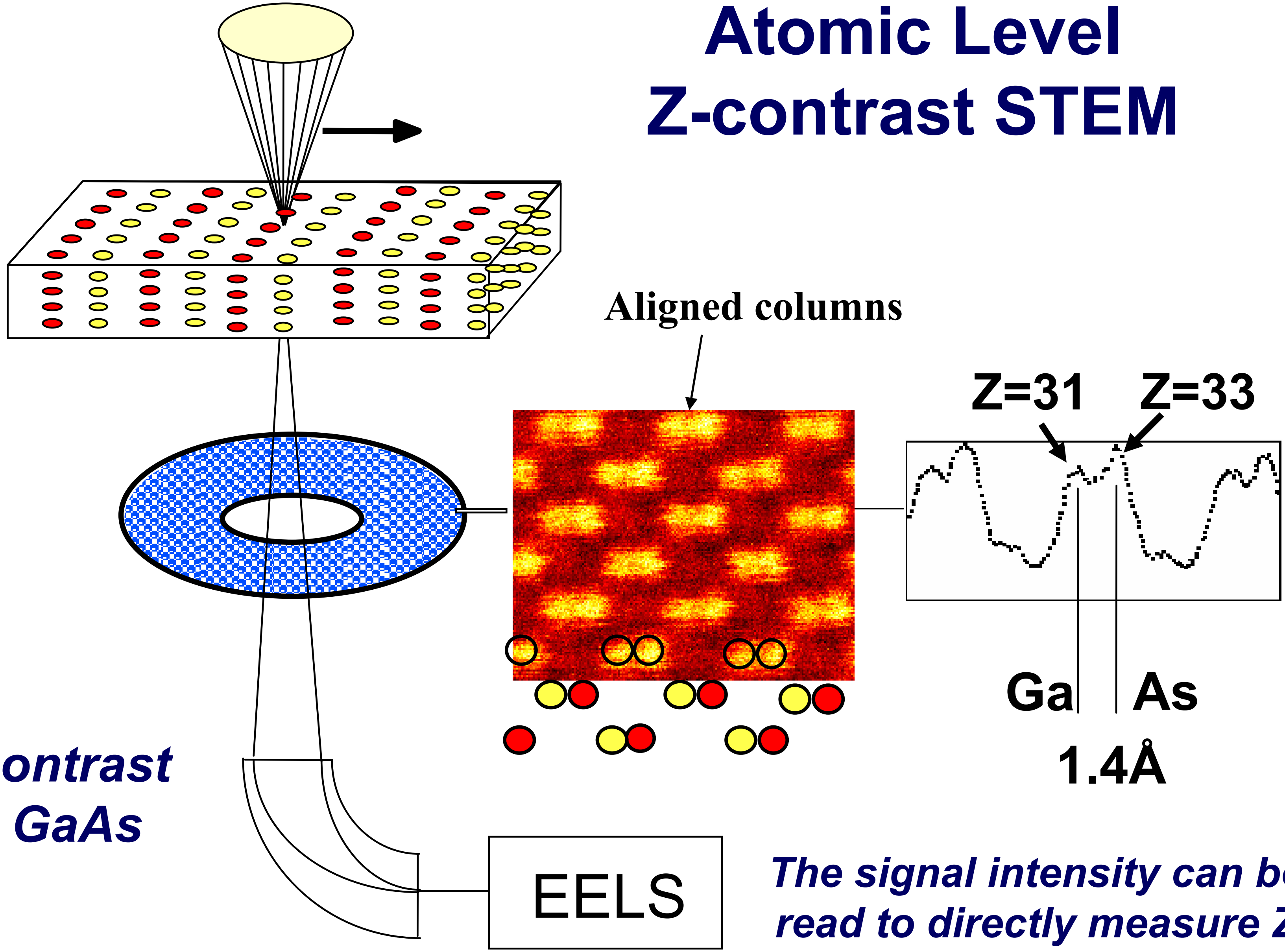

Z-contrast in GaAs

The signal intensity can be read to directly measure Z for each atom column

Why STEM lattice images are better

Z-contrast image showing maximum entropy fit to data. The HAADF Z- mode displays the actual physical positions of the atoms. ***TEM 'lattice images' are only interference effects and there is no correlation between the image positions (which vary with thickness and focus) and atom locations***

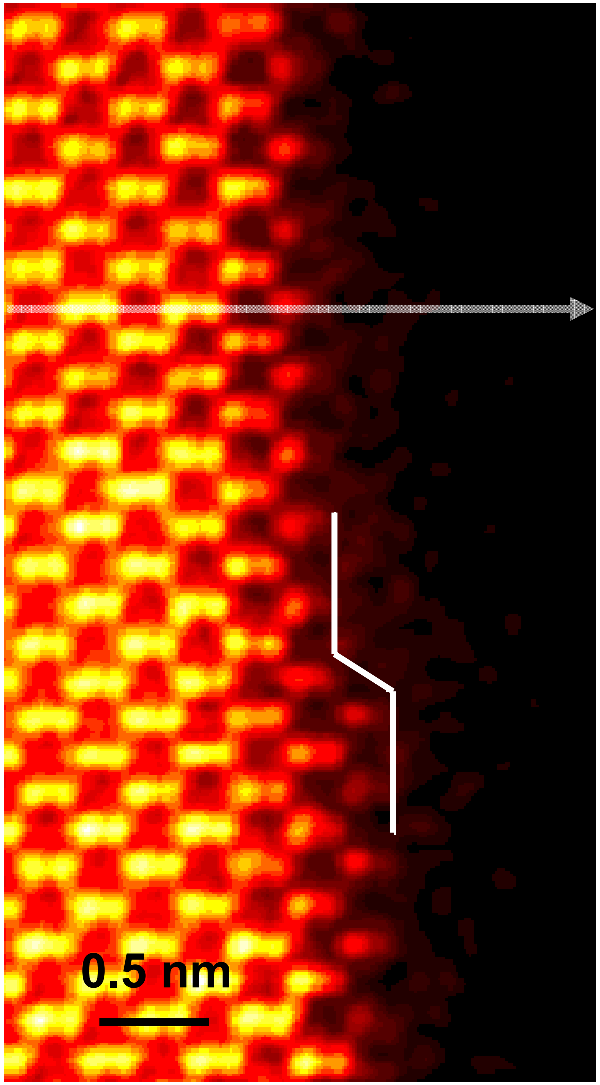

Courtesy Dr. S Pennycook

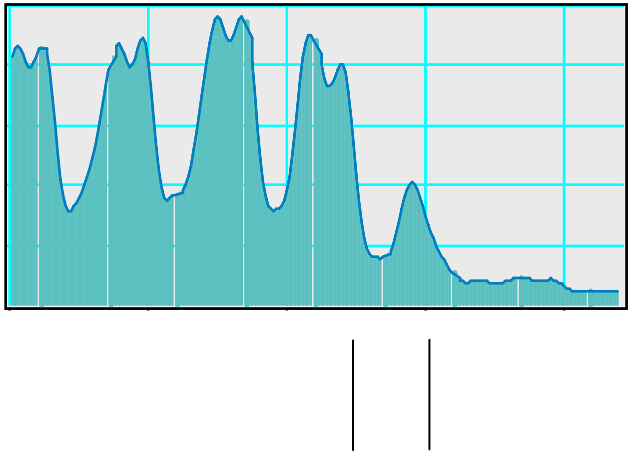

Interface width 3 - 5 Å

The limit - Single atom imaging

CdSe/ZnS core/shell nanocrystals

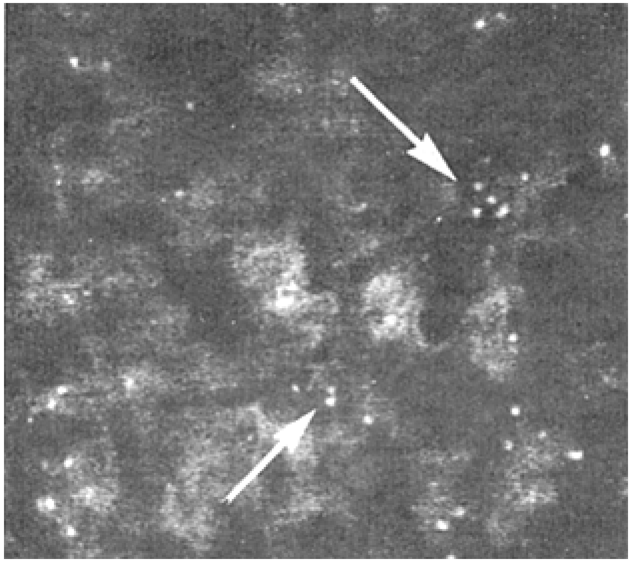

Ag (Z=47) atoms on C (Z=6) foil - Crewe 1970 30keV STEM image

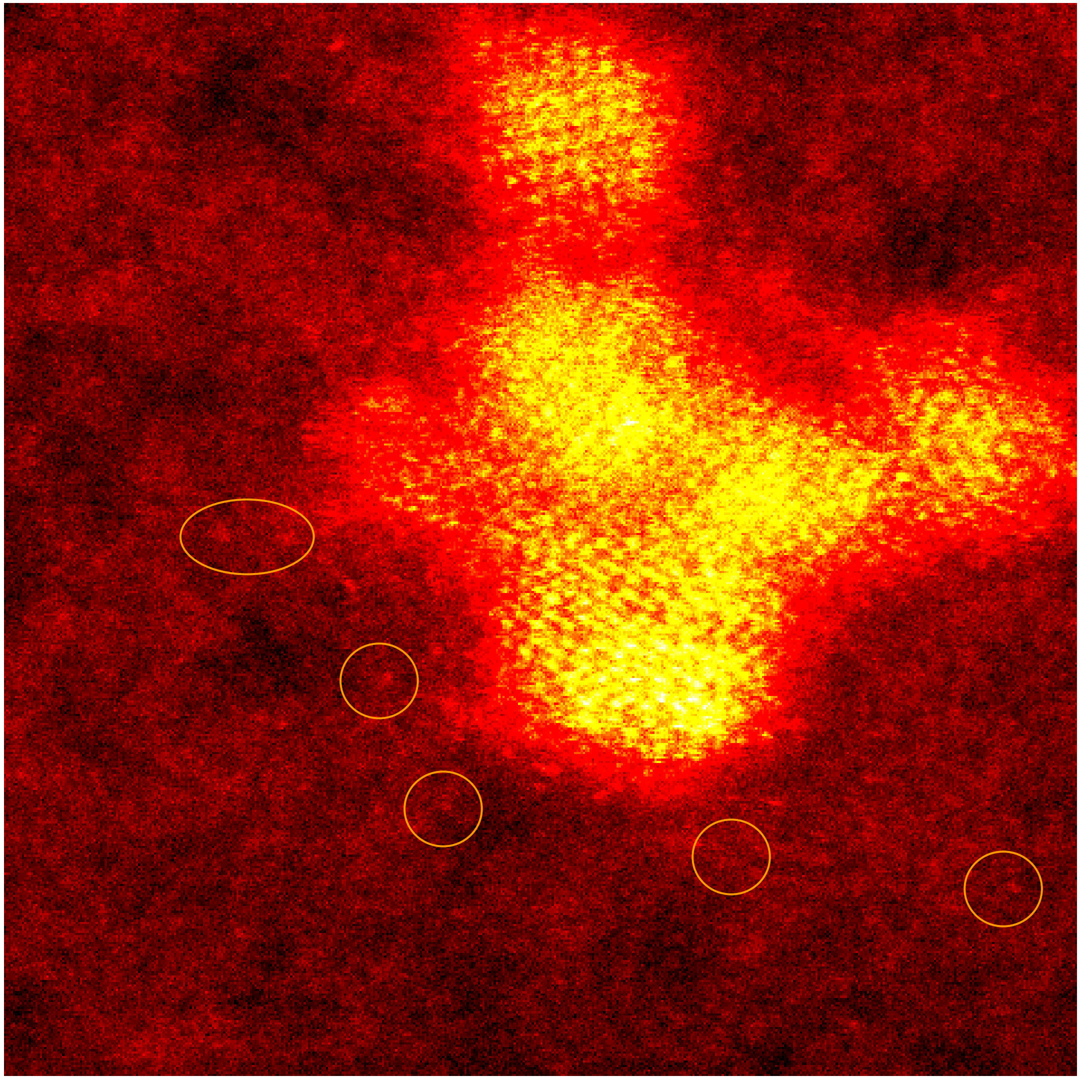

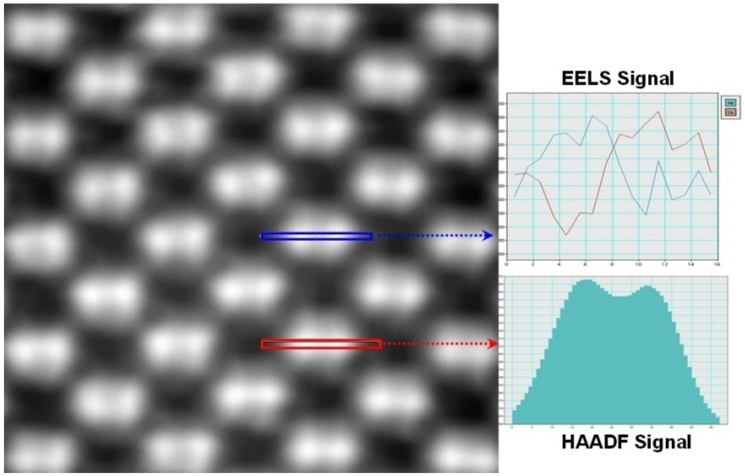

An atomic resolution image of GaAs (courtesy of Glasgow University) in 110 projection showing EELS column contrast along the blue box and dumbbell asymmetry in high angle annular dark field image contrast from the red box. The probe in this case was about 0.14nm; the dumbbell separation between the Ga and As columns is also 0.14nm.

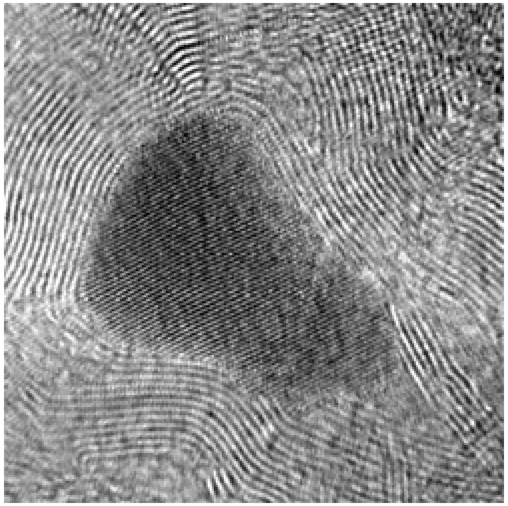

The picture shown above-left is of a catalyst particle enclosed in the tip of a carbon nanotube, and was taken recently at SuperSTEM as part of an investigation being carried out by Dr. Uschi Bangert and colleagues of The University of Manchester. The sample was supplied by Prof. Laszlo Forro (EPFL).

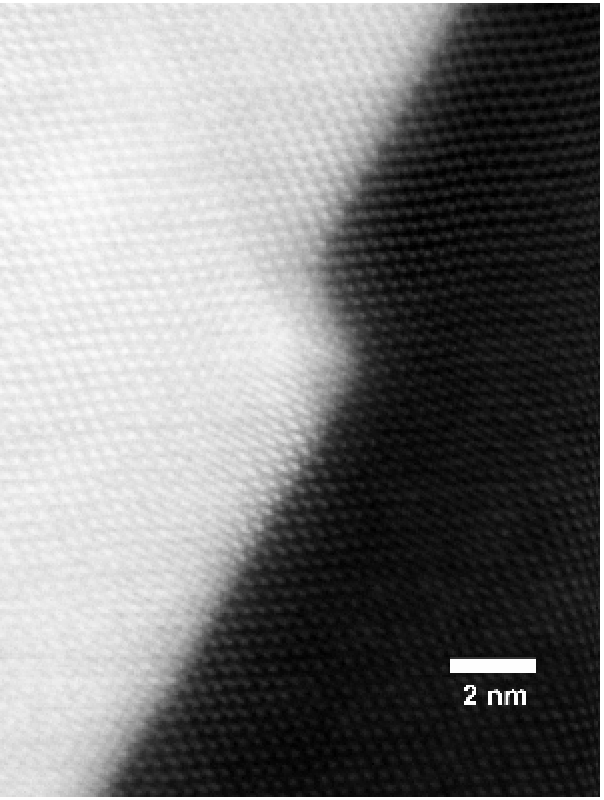

Two different oriented areas of the NiSi_2/Si (100) interface, separated by a surface step with an (111) interface. The structures of the both perspectives are well distinguishable.

Laboratorija za atomsku fiziku

Philips EM 400

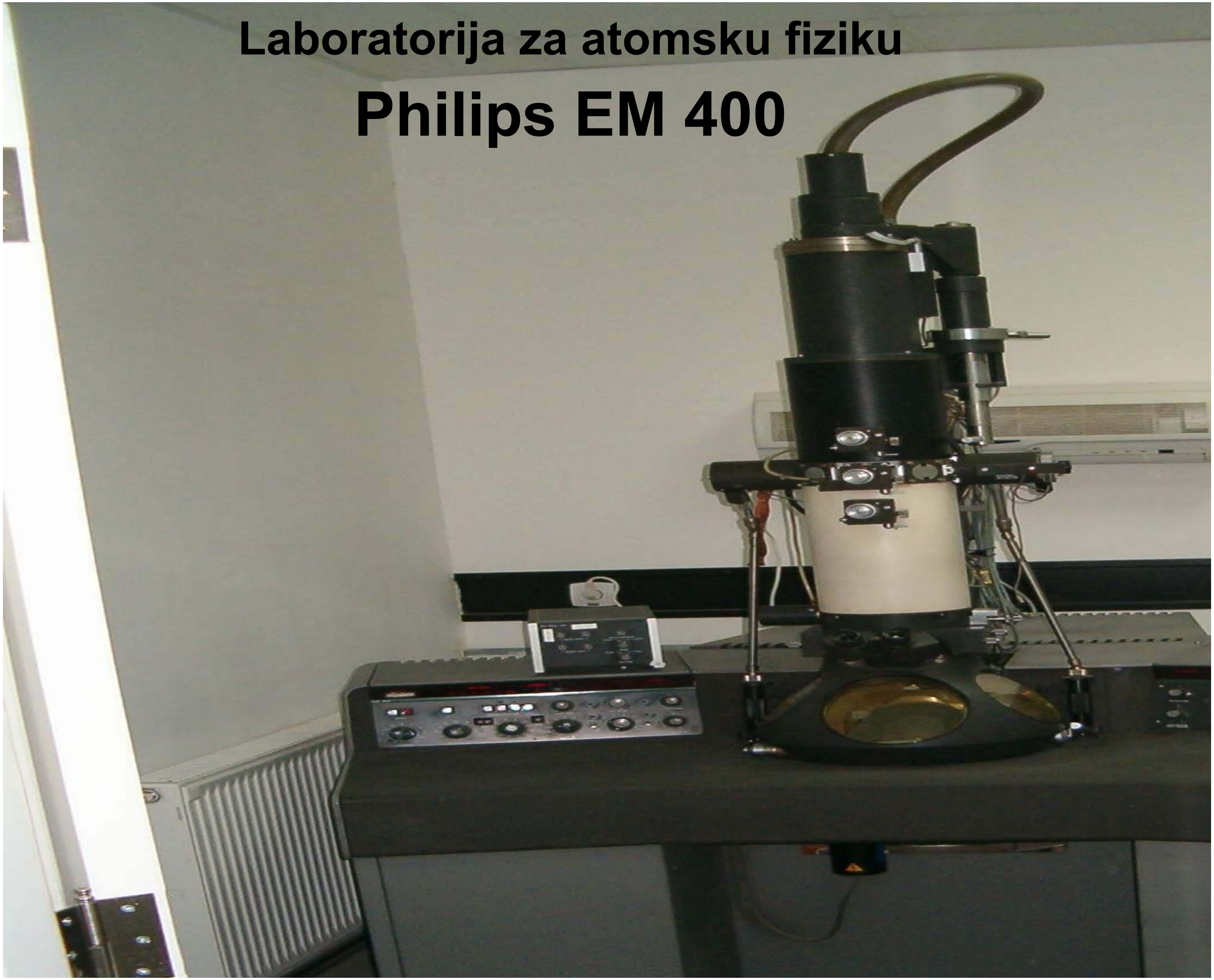

SAMPLE PREPARATION

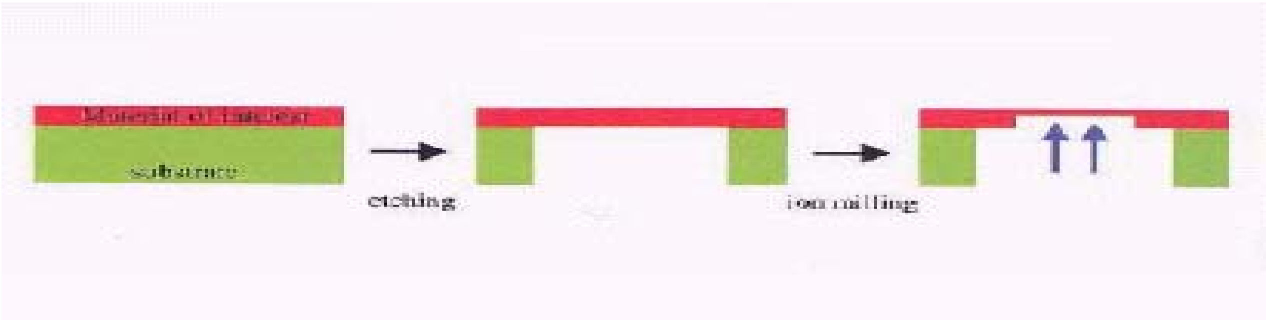

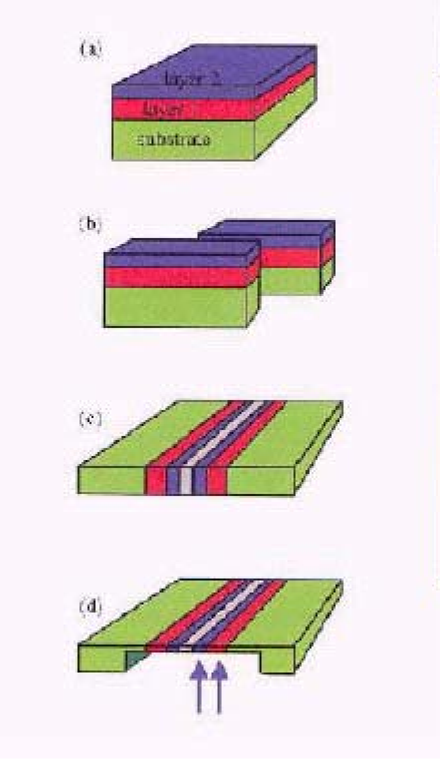

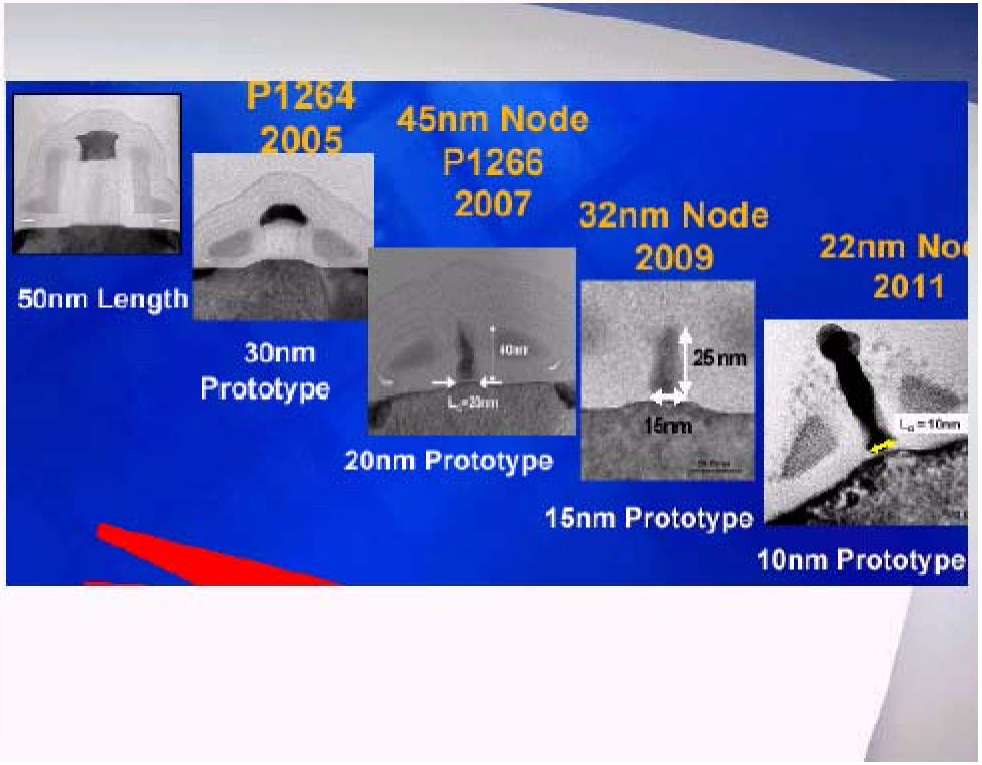

Detection limits of analytical instruments

Evans Analytical Group

Analytical Resolution versus Detection Limit

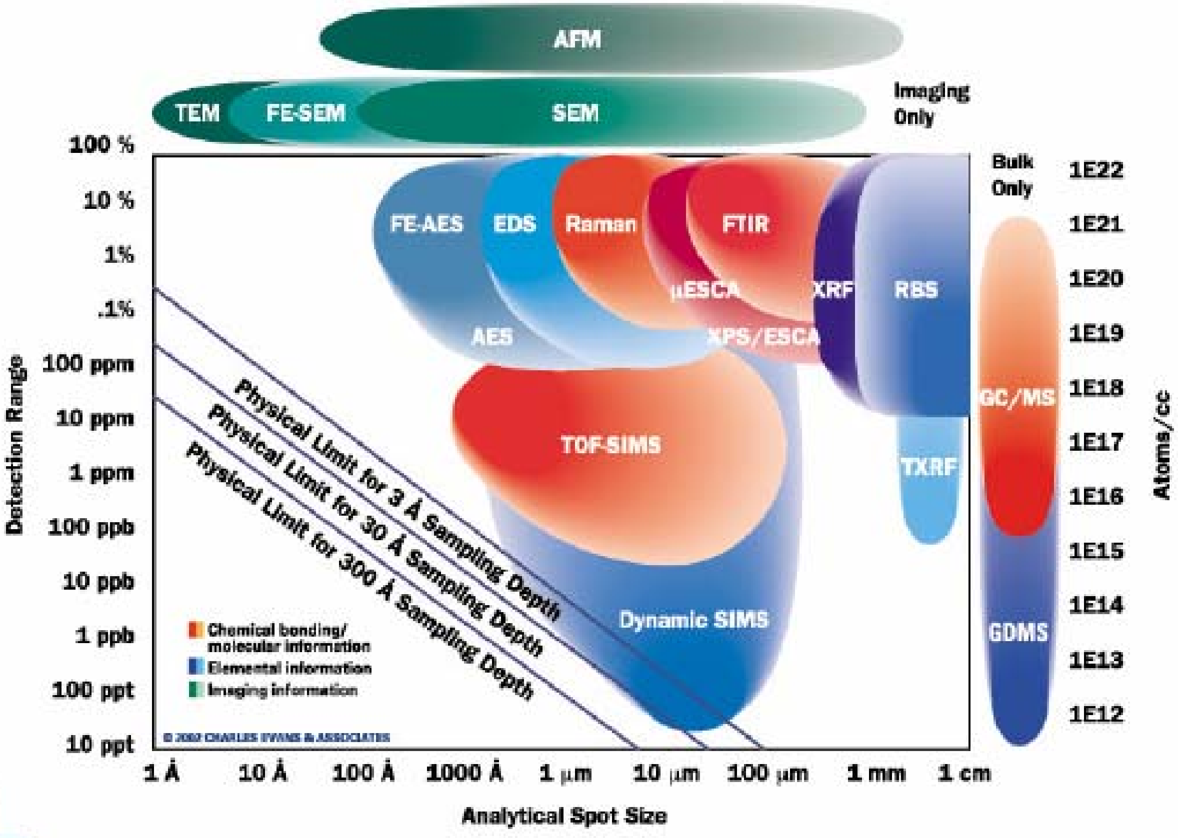

Copyright © 2003, Evans Analytical Group. All rights reserved.

What is an accelerator?

An accelerator produces a beam of a particular type of particle at a specific energy.

Common Uses:

- *Implantation*
- *RBS: Rutherford Back Scattering*
- *PIXE: Particle Induced X-ray Emission*

Accelerator Requires:

- *Source of charged particles*
  - *hot filament emits electrons*
  - *ionized atoms from ion source*
- *Accelerating Voltage (100’s of kV)*
- *Focusing/Steering Apparatus*
  - *Beam tends to diverge like natural light*
- *Target*

Efekti koje jonska implantacija proizvodi na meti se mogu grubo sumirati na sledeći način:

- Kontrolisano unošenje primesa u osnovni materijal, zbog veoma precizno kontrolisanog procesa u odnosu na klasične postupke.
- Promena krstalne strukture na atomskoj skali pri manjim jonskim dozama.
- Narušavanje kristalne strukture i/ili amorfizacija mete na površini pri velikim dozama. Kod poluprovodnika se struktura potpuno regeneriše u toku naknadnog postupka termičke aktivacije primesa, dok se metali amorfizuju samo u slučaju kada se meta hladi na temperaturi tečnog azota ili niže.
- Sinteza jedinjenja u meti implantacijom jona koji reaguju hemijski sa osnovnim materijalom. Za dovoljno velike doze u meti se može ugraditi kontinualan sloj nekog jedinjenja.
- Stvaranje nano-uključaka i formiranje nanostruktura.
- Unošenje materijala u metu u koncentracijama iznad granice rastvorljivosti.
- Formiranje metastabilnih faza zahvaljujući termodinamički neravnotežnom procesu. Zbog velike gustine enrgije, koja se u kratkom vremenu unosi u materijal, mnogi termodinamički parametri za dati sistem mogu biti prevaziđeni pri čemu nastaje mogućnost dobijanja novih faza koje nisu definisane faznim dijagramom za dati sistem. Dakle, na ovaj način se dobijaju nove osobine materijala i novi materijali, koje nije moguće dobiti drugim konvencionalnim postupcima.
- Unošenje nerastvorljivih materijala i stvaranje lokalnog naprezanja u kristalnoj rešetci

Promena morfologije na površini i homogenizacija strukture, što je posebno interesantno za obradu tvrdih i zaštitnih prevlaka, kod kojih se još i višestruko povećava adhezija za podlogu.

Principles of ion beam analysis

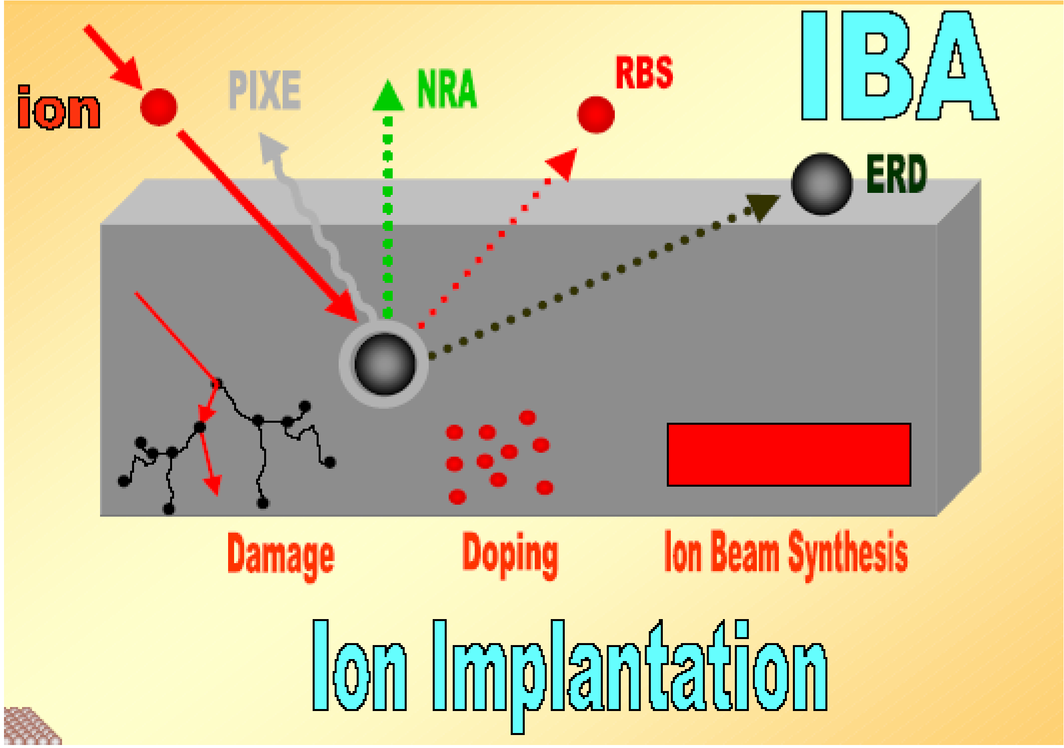

In its passage through matter, an ion may interact with

- ***THE ATOMIC ELECTRONS***

and/or

- ***THE ATOMIC NUCLEI***

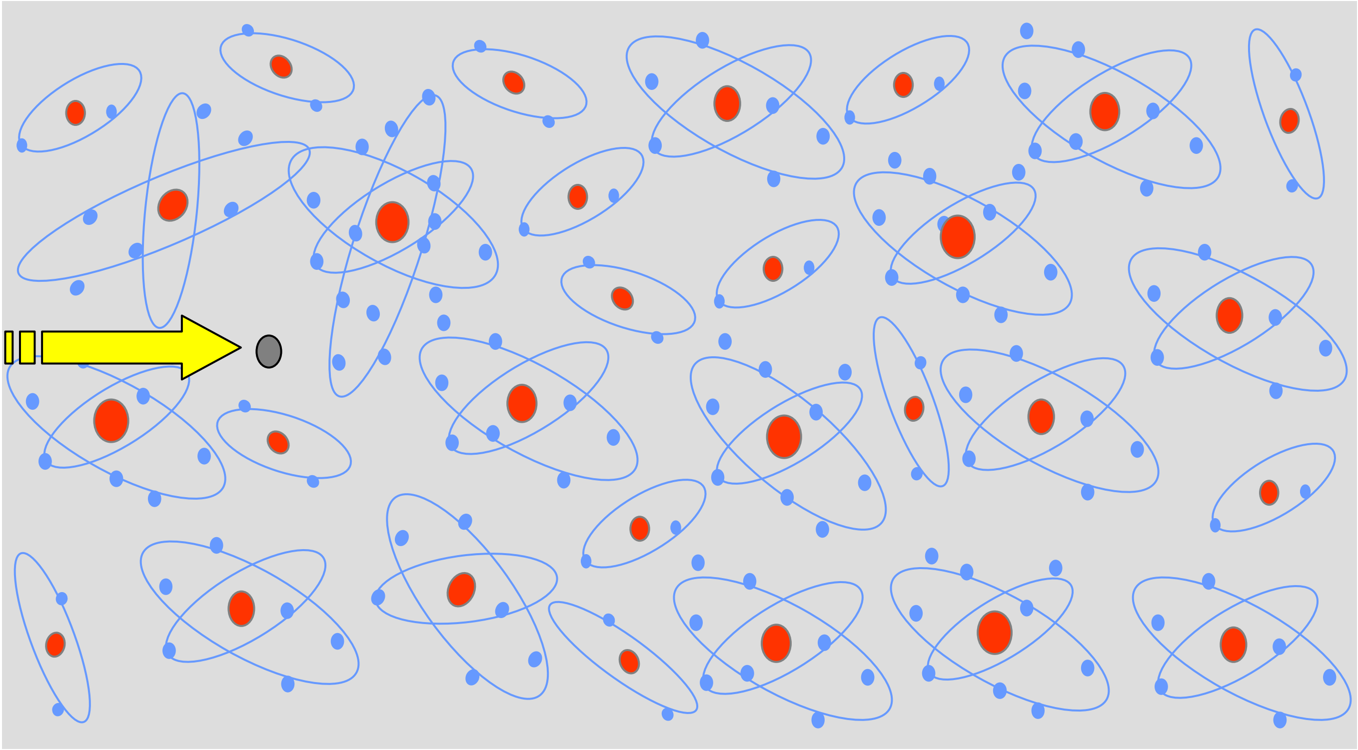

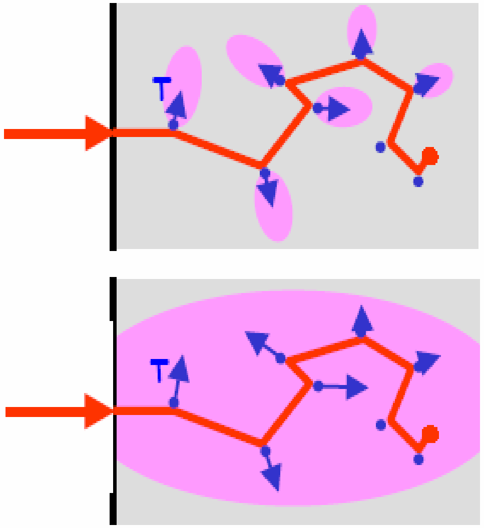

Fig. 9.2

Schematic of the cascade formation for an individual ion trajectory, depending on the average primary initial energy transfer T: Small subscascades for light ions at high energy (top), and one large cascade for heavy ions at sufficiently low energy (bottom).

The density of deposited energy does not only influence the spatial development of the cascade, but also its internal dynamics. Conventionally, three regimes are defined (see Fig. 9.3). In the single-collision regime (Fig. 9.3a), which is typical for light ions at low energy, a cascade does not really develop and the atomic motion is stopped after a few collision events.

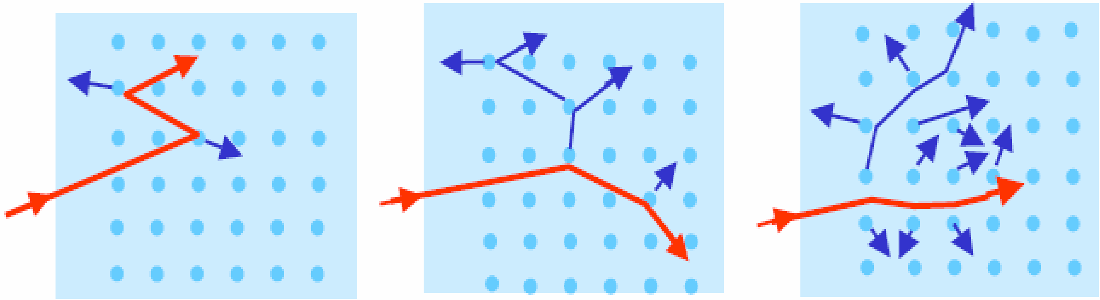

(a) (b) (c)

Fig. 9.3

Cascade regimes (schematically): (a) Single collision regime; (b) Linear cascade; (c) Thermal spike

Schematic View of a Linear Collision Cascade

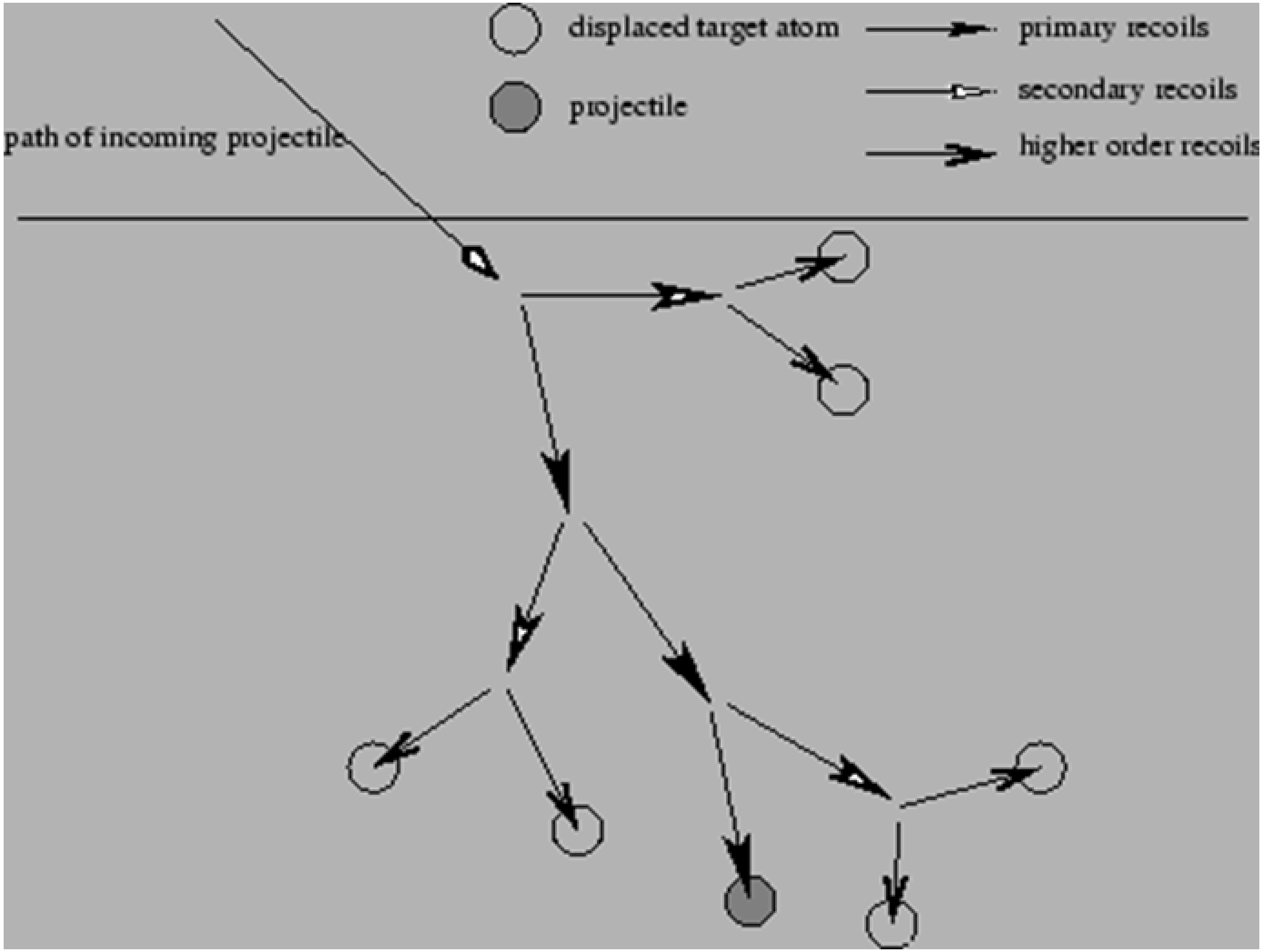

http://www.acclab.helsinki.fi/~koehenri/work/www_gradu/gradu_html/node8.html

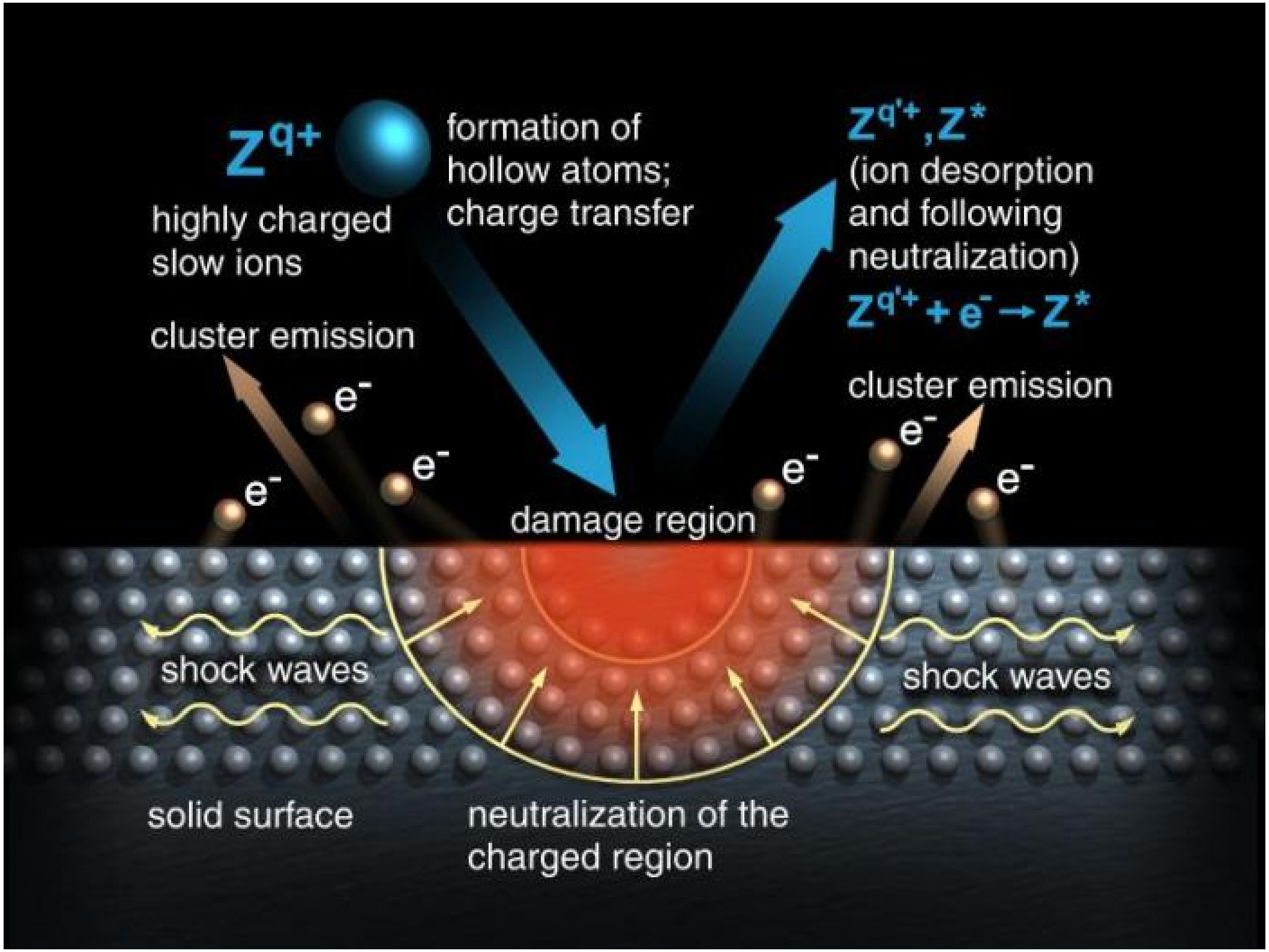

Z^{q+}
highly charged slow ions
formation of hollow atoms; charge transfer
$Z^{q'+}, Z^*$
(ion desorption and following neutralization)
$Z^{q'+} + e^- \rightarrow Z^*$
cluster emission
cluster emission
e^-
e^-
e^-
e^-
e^-
e^-
damage region
shock waves
shock waves
solid surface
neutralization of the charged region

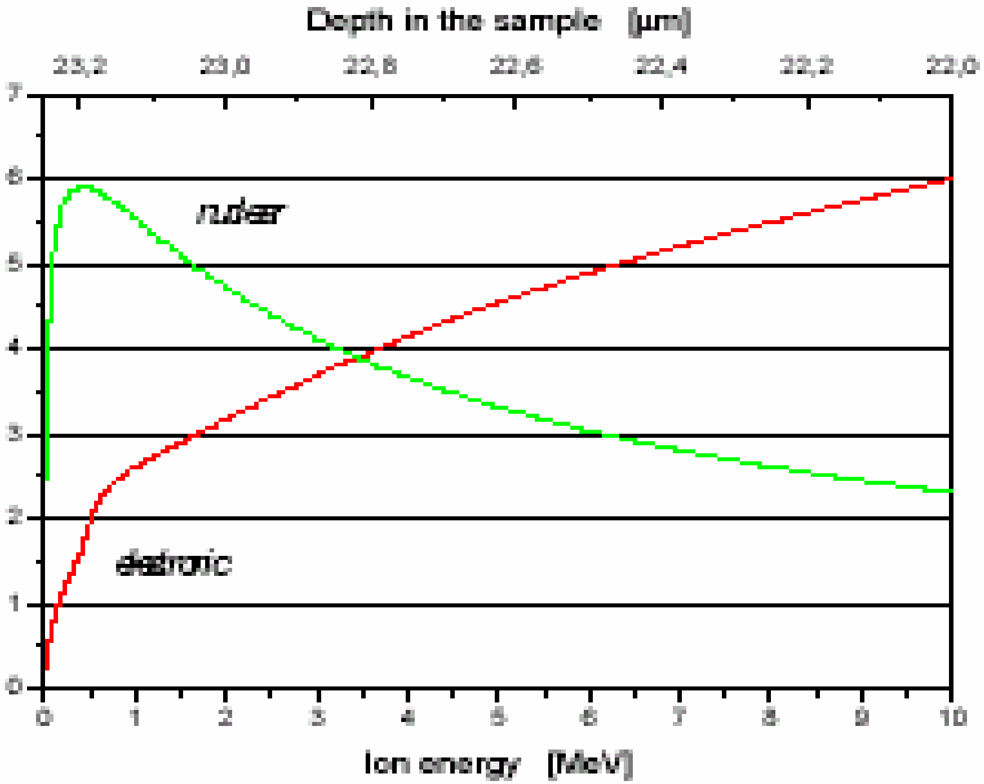
Depth in the sample [µm]
23,2
23,0
22,8
22,6
22,4
22,2
22,0
7
6
5
4
3
2
1
0
nuclear
electronic
0
1
2
3
4
5
6
7
8
9
10
Ion energy [MeV]

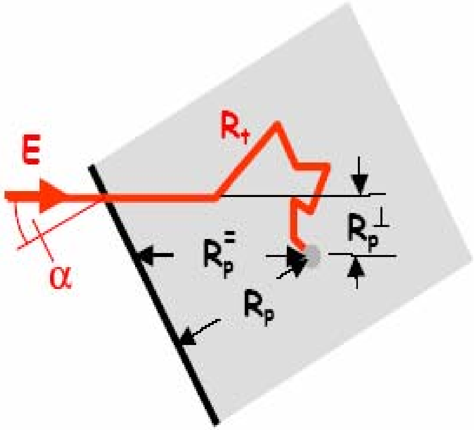

Fig. 8.1

Schematic of an ion track for an ion of incident energy E and angle of incidence α, with range definitions

8. Ion Ranges

As a consequence of stopping and scattering, each individual incident ion forms a random trajectory as shown in Fig. 8.1. Stopping alone defines the total pathlength R_t. From the endpoint of the trajectory projected ranges can be defined (longitudinal, $R_p^{=}$, and lateral, $R_p^{\perp}$). For practical purposes, the (normal) projected range R_p is mostly of interest, since it characterises the implantation depth with respect to the surface. Obviously, R_p is equal to $R_p^{=}$ for normal incidence. As in most implantation processes the extension of the implanted area is very large compared to the ion range, R_p is mostly also the only range quantity which is accessible to measurement.

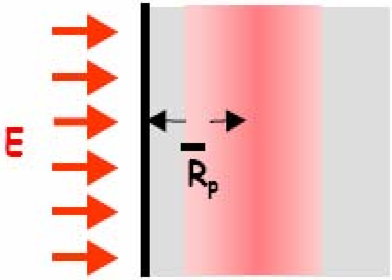

Fig. 8.2

Schematic of range distribution at normal incidence

Stopping of Ions in Matter

- ***Nuclear***

- ***Electronic***

If E is the energy of the ion at any point x along the path, the average rate of energy loss is

$$\frac{dE}{dx} = -n[S_n(E) + S_e(E)]$$

S_n (E) and S_e (E) are, respectively, nuclear and electronic stopping cross-sections.

Average range of ions in the target:

$$R(E) = \int_0^R dx = \int_0^{E_0} \frac{dE}{n[S_n(E) + S_e(E)]}$$

$$S_n(E) = k\ E$$

$$S_e(E) = k_e E^{1/2}$$

Slowing Down due to Electronic Interactions (Inelastic)

According to the model of Lindhardt, Schraff and Schiott (LSS model) the rate of energy loss to electrons by the striking ions per unit depth is:

$$\left(\frac{dE}{dx}\right)_e = -K_e\sqrt{E} = -n\,S_e(E)$$

In dimensionless units:

$$\left(\frac{d\varepsilon}{d\rho}\right)_e = -s_e(\varepsilon) = -k_L\,\varepsilon^{1/2}$$

where

$$k_L = Z_1^{1/6}\,\frac{0.0793\,Z_1^{1/2}\,Z_2^{1/2}\,(m+M)^{3/2}}{(Z_1^{2/3}+Z_2^{2/3})^{3/4}\,m^{3/2}\,M^{1/2}}$$

$$K_e = k_L\left(\frac{E}{\varepsilon}\right)^{1/2}\left(\frac{\rho}{x}\right)$$

Energy Loss or Slowing Down due to Nuclear Interactions

- ***Collisions between the screened nuclear charges of the incident ion and the target atoms;***

- ***Complex interactions at low energies;***

- ***Screened Coulomb scattering at medium energies – energies less than A keV where A is the incident ion atomic weight ;***

- ***Rutherford scattering at high energies.***

$$c(x) = \frac{N_p(x)}{n\Delta x}\frac{\Phi_{tot}}{N_H} \tag{11.15}$$

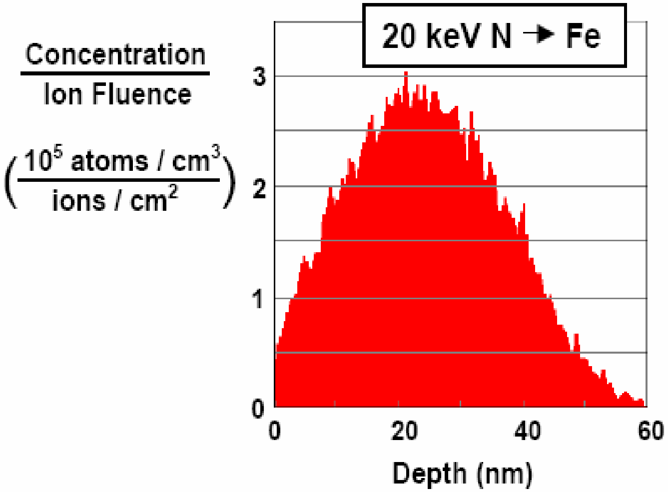

Fig. 11.5

Projected range distribution of 20 keV nitrogen ions implanted into iron, from a TRIM simulation with 20000 pseudoprojectiles (see Fig. 11.3). The mean projected range is $R_p = 24.5$ nm, the standard deviation $\sigma = 12$ nm, the skewness $\Gamma_1 = 0.19$, and the kurtosis $\Gamma_2 = 2.4$.

In this way, the ordinate of Fig. 11.5 is defined by $c(x)/\Phi_{tot}$. Nevertheless, it should be pointed out that standard TRIM computer simulations are only valid for the low-fluence limit, so that the results cannot readily be extrapolated to high fluences with, e.g., resulting implant concentrations close to stoichiometry or even above, which would be meaningless. In the BCA simulations discussed here, each incident projectile finds the same, unmodified substance that any effects of, e.g., ion deposition or surface erosion (see ch. 13) are neglected.

In a similar way, distribution functions of deposited energy can be obtained (Fig. 11.6). The electronic energy dissipation is sometimes called "ionisation" (such as in SRIM-2000), although the latter contributes only a fraction (see ch. 5). Also in SRIM-2000, the nuclear energy dissipation is called "energy to recoils". Note that the definition of nuclear energy dissipation is only meaningful for

Ion Beam Analysis Methods

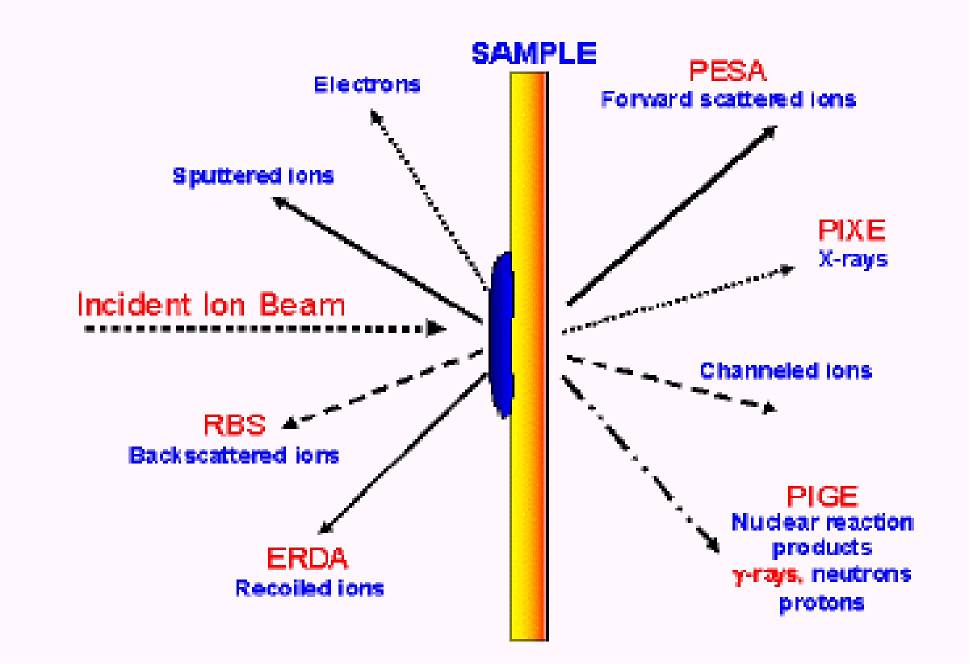

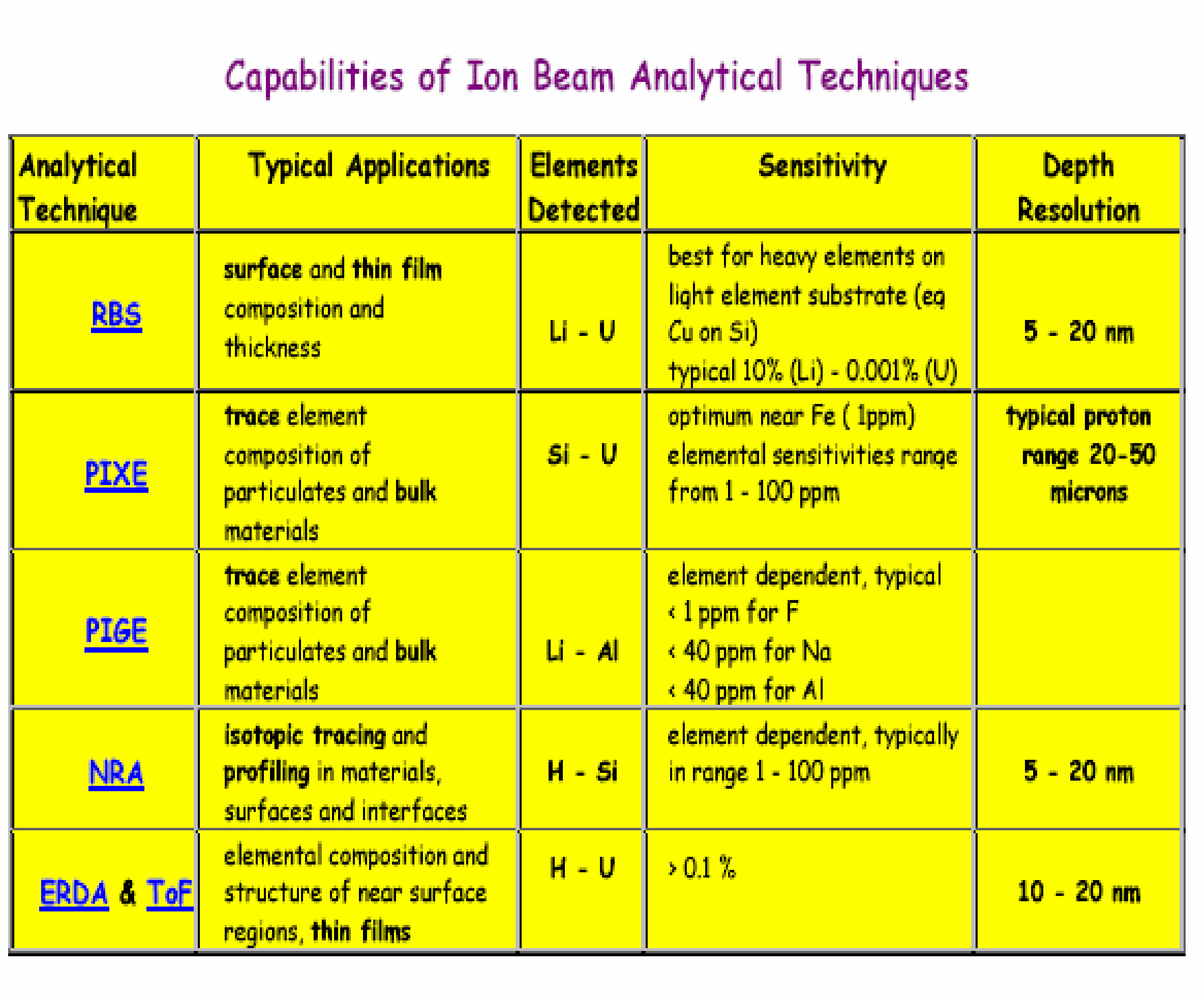

Capabilities of Ion Beam Analytical Techniques

Analytical Technique	Typical Applications	Elements Detected	Sensitivity	Depth Resolution
RBS	**surface** and **thin film** composition and thickness	Li - U	best for heavy elements on light element substrate (eg Cu on Si) typical 10% (Li) - 0.001% (U)	5 - 20 nm
PIXE	**trace** element composition of particulates and **bulk** materials	Si - U	optimum near Fe (1ppm) elemental sensitivities range from 1 - 100 ppm	typical proton range 20-50 microns
PIGE	**trace** element composition of particulates and **bulk** materials	Li - Al	element dependent, typical < 1 ppm for F < 40 ppm for Na < 40 ppm for Al	
NRA	**isotopic tracing** and **profiling** in materials, surfaces and interfaces	H - Si	element dependent, typically in range 1 - 100 ppm	5 - 20 nm
ERDA & ToF	elemental composition and structure of near surface regions, **thin films**	H - U	> 0.1 %	10 - 20 nm

TYPICAL ION BEAMS AND INCIDENT ENERGIES USED IN VARIOUS IBA TECHNQUES:

TECHNIQUE	ION BEAM	ENERGY (MeV)	REMARK
PIXE	H+	1 - 4	Maximum sensitivity in atomic ranges 10<Z<35 and 75<Z<85
RBS	^{4}He+, H+	≤ 2	Non-Rutherford scattering becomes significant for energy >2 MeV
PESA FAST	H+ ^{4}HE+	3 - 30	High incident energy is required for good mass separation, but the classical elastic scattering cross-section formula is not valid for high incident energy.
ERDA	^{35}Cl+, ^{20}Ne+ ^{3}He+, ^{4}He+	2 - 40	Mass of incident ion must be greater than that of target nucleus. ^{3}He+ and ^{4}He+ are used only for the measurement of H.
NRA	H+, D+	0.4 - 3	Reactions used include (p,γ) (p,p'γ), (p,$\alpha\gamma$), (d,p), (d,pγ)

RBS

- ***Rutherford Back Scattering***
- ***Positive charges directed towards a sample.***
- ***Energy of back scattered particle determines the mass of the target nucleus.***
- ***If the target is not of uniform composition, the distribution of back scattered energies determines relative compositions.***

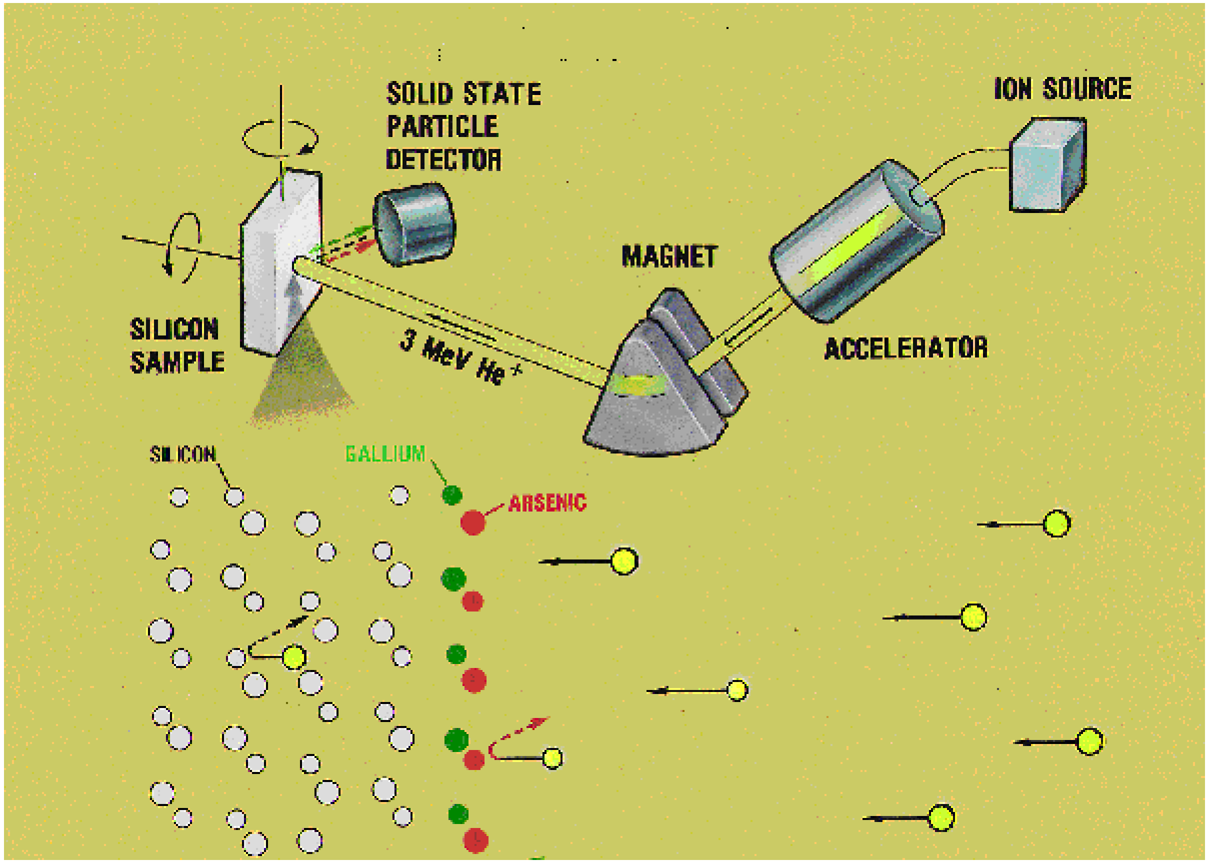
SOLID STATE PARTICLE DETECTOR
ION SOURCE
MAGNET
ACCELERATOR
SILICON SAMPLE
3 MeV He⁺
SILICON
GALLIUM
ARSENIC

RBS metoda omogućava sledeće analize materijala:

- Odredjuvanje koncentracionih profila komponenenata (elemenata), do debljina od nekoliko μm, sa rezolucijom do nekoliko nm.
- Precizno odredjivanje odnosa koncentracije komponenata u kompozitnim materijalima, a time i njihovog hemijskog sastava.
- Precizno merenje debljina višeslojnih struktura i odredjivanje stepena interakcije komponenata u ovakvim strukturama.
- Odredjivanje vrste i raspodele primesa u osnovnom materijalu, prisustva teških elemenata u tragovima, a u kombinaciji sa EBS, ERDA ili PIXE takodje i lakih elemnata.
- Analiza kristalne strukture monokristalnih materijala, stepena uredjenosti kristalne rešetke, kao i stepena i dubine oštećenja ili narušavanja kristalne strukture – metodom *ion channeling*.
- Odredjivanje substitucionog, odnosno intersticijalnog položaja primesa u monokristalima, takodje metodom *ion channeling*.

RBS Principle

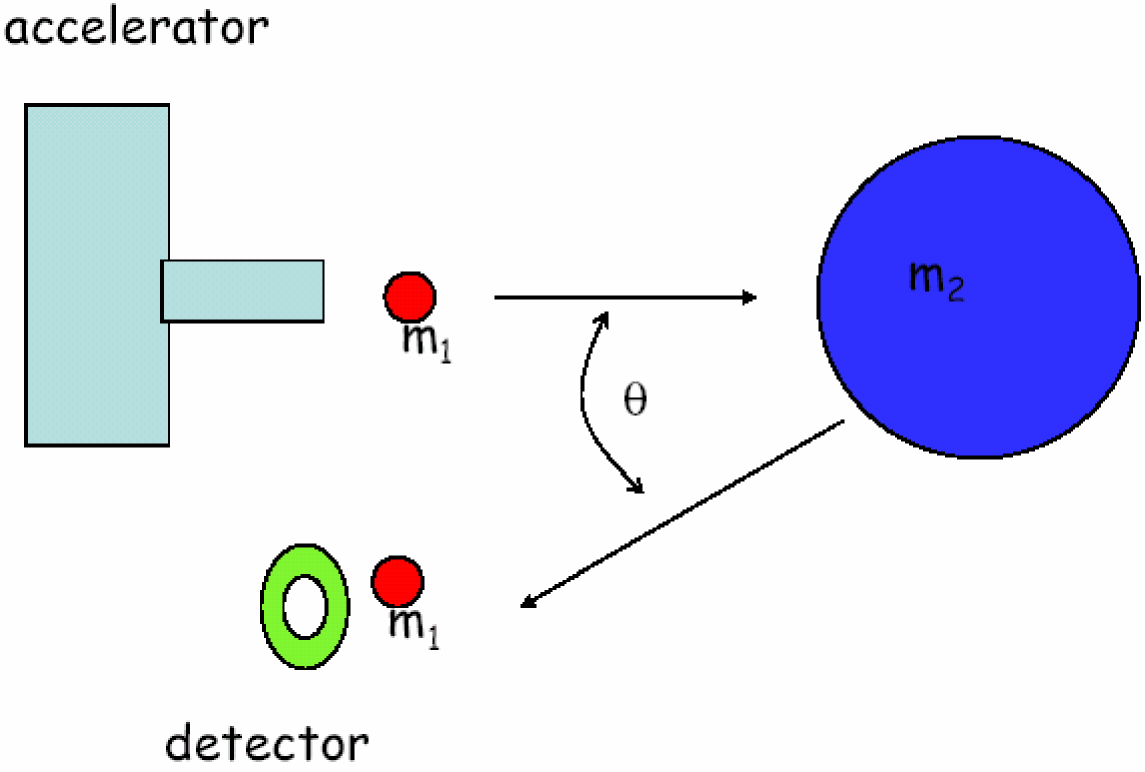

Rutherford Backscattering

- ***Shoot a beam of α particles (helium nuclei) having known energy E_i into a sample of unknown composition. Measure the energy E_f of the α particles that bounce back out at ~180° with respect to the incoming beam.***

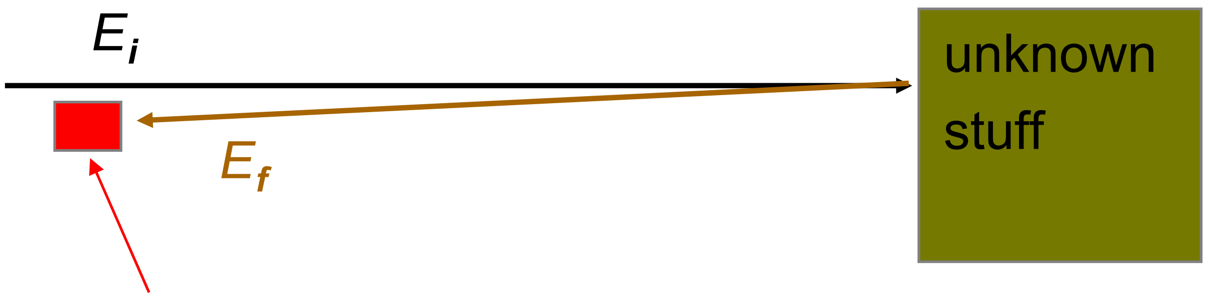

$$M = \frac{m\left(1+\sqrt{E_f/E_i}\right)}{\left(1-\sqrt{E_f/E_i}\right)}$$

So we learn about the mass of the nuclei in the unknown stuff. (We learn what the stuff is).

Rutherford Backscattering

- ***For example: Suppose we are shooting α particles that have an initial energy of E_i = 2 MeV at a target made of an unknown material. The α particles return with final energy E_f = 1.1 MeV. What is the weight of the unknown material?***
  - **m(α) = 4 (2 protons, 2 neutrons)**

$$M = \frac{m\left(1+\sqrt{E_f / E_i}\right)}{\left(1-\sqrt{E_f / E_i}\right)} = \frac{4\left(1+\sqrt{1.1/2}\right)}{\left(1-\sqrt{1.1/2}\right)}$$

Aluminum!! (13 protons, 14 neutrons)

RBS

Kinematic factor,
Mass identification

Energy loss,
Depth scale

Scattering cross sections,
Composition, (quantitative)

KINEMATIC FACTOR

E can be derived from the principle of conservation of energy and momentum, and is given by (in laboratory frame of reference):

$$\boxed{E=\left[\left(\frac{1}{1+\frac{M}{m}}\right)\times\left(\cos\theta+\sqrt{\left(\frac{M}{m}\right)^{2}-\sin^{2}\theta}\right)\right]^{2}E_{o}=kE_{o}}$$

The multiplication factor of E_o on the right hand side of the equation is often referred to as the kinematic factor and is denoted by k. For M/m > 1, k is a slow-varying function of θ, having the maximum value of 1 at $\theta = 0$ and the minimum value at $\theta = 180^o$. For M/m = 1, the value of k is zero beyond 90^o.

$$k = \frac{E_1}{E_0} = \left[\frac{\left(M_2^2 - M_1^2 \sin^2\theta\right)^{\frac{1}{2}} + M_1 \cos\theta}{M_2 + M_1} \right]^2$$

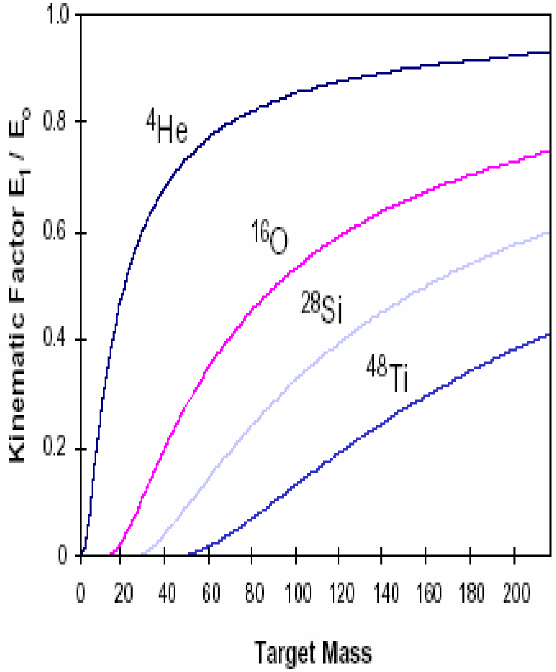

Kinematic factor (at θ = 180°) as a function of target mass for a number of projectile types.

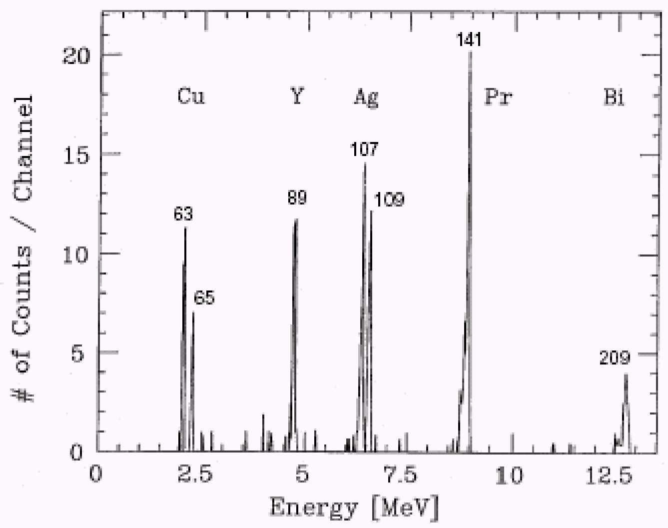

kinematic factor

mass scale!

RBS example demonstrating mass discrimination. Projectile: 25 MeV ^{35}Cl; target: thin layers of Cu, Y, Ag, Pr, Bi. Isotopes of Cu and Ag are resolved.

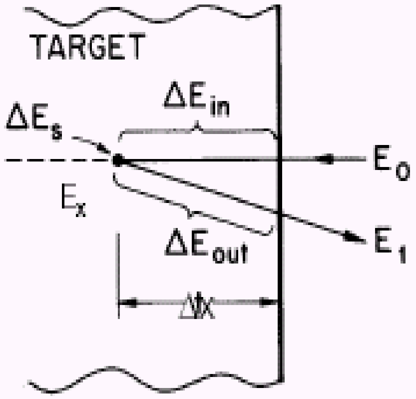

E_x = energy before scattering

$$\Delta E_{in} = \left(\frac{dE}{dx}\right)_{in} \cdot \Delta x$$

$$\Delta E_s = (1-k)\cdot E_x \qquad (\text{kinem. loss})$$

$$\Delta E_{out} = \left(\frac{dE}{dx}\right)_{out} \cdot \frac{\Delta x}{\cos\theta}$$

Detected energy $E_1 = E_o - \Delta E_{in} - \Delta E_s - \Delta E_{out}$

$$\approx kE_o - \underbrace{\left[\left(\frac{dE}{dx}\right)_{in} \cdot k + \left(\frac{dE}{dx}\right)_{out} \cdot \frac{1}{\cos\theta}\right]}_{S} \cdot x$$

Stopping power and depth resolution

-the rate of energy loss dE/dx depends on mass of projectiles, traget, and incident energy

-for 0.5~2.0 MeV, dE/dx is independent of energy

-Depth resolution: 30~100 Å

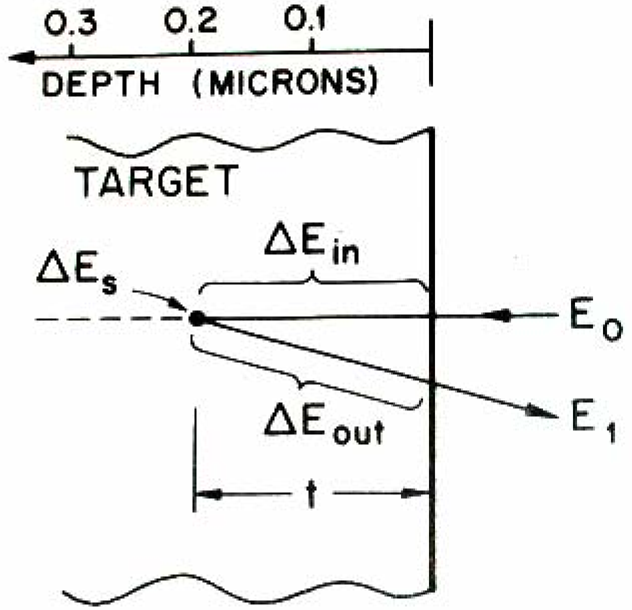

ENERGY LOSS:

$$\Delta E_{in} \simeq \left.\frac{dE}{dx}\right|_{E_0} \cdot t$$

Electronic stopping during going in

$$E_t = E_0 - \Delta E_{in}$$

$$\Delta E_s = (1-K)\,E_t$$

Elastic scattering

$$\Delta E_{out} \simeq \left.\frac{dE}{dx}\right|_{E_1} \cdot \frac{t}{\cos\theta}$$

Electronic stopping during going out

Final Energy of a particle at normal incidence

$$E_1 = E_o - \Delta E_{in} - E_s - \Delta E_{out}$$

Energy spectrum

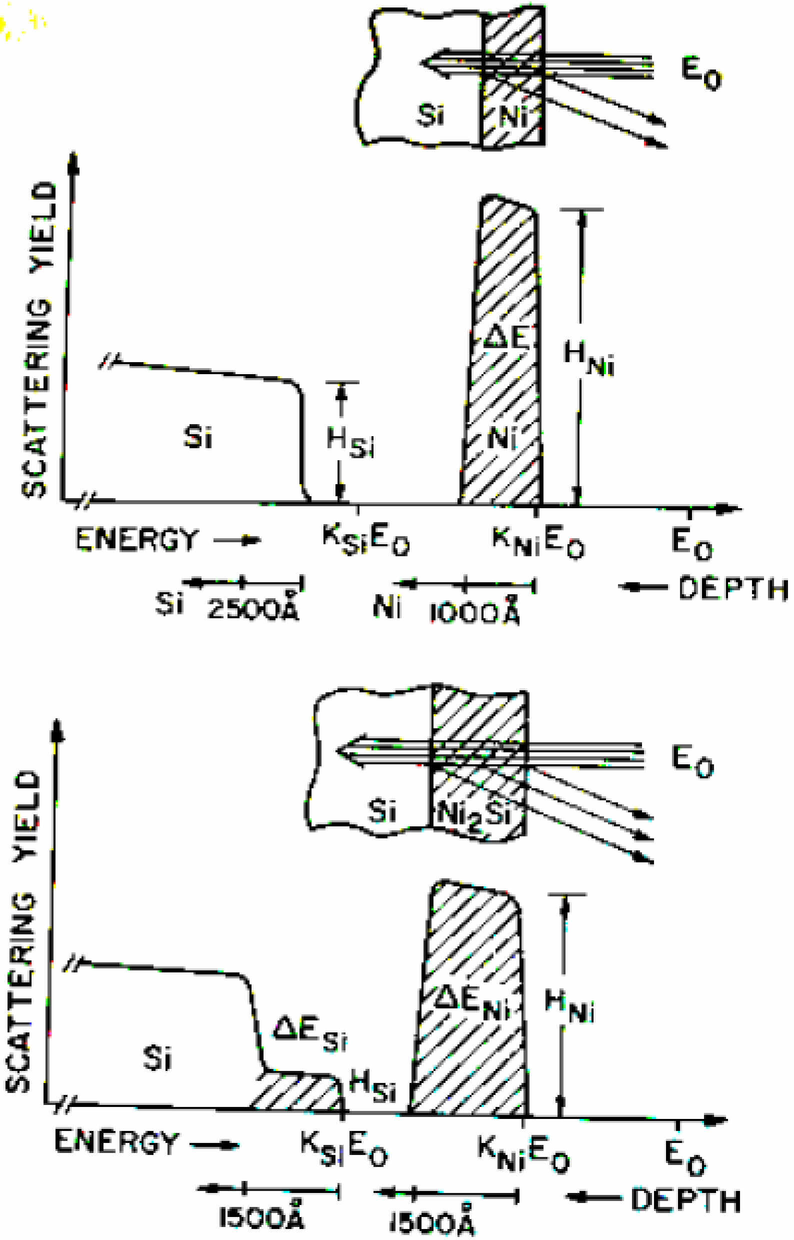

Figure 3.10 Schematic backscattering spectra for MeV ^{4}He ions incident on 1000 Å Ni film on Si (top) and after reaction to form Ni_2Si (bottom). Depth scales are indicated below the energy axes.

$$E_1(x) = kE_o - S \cdot x$$

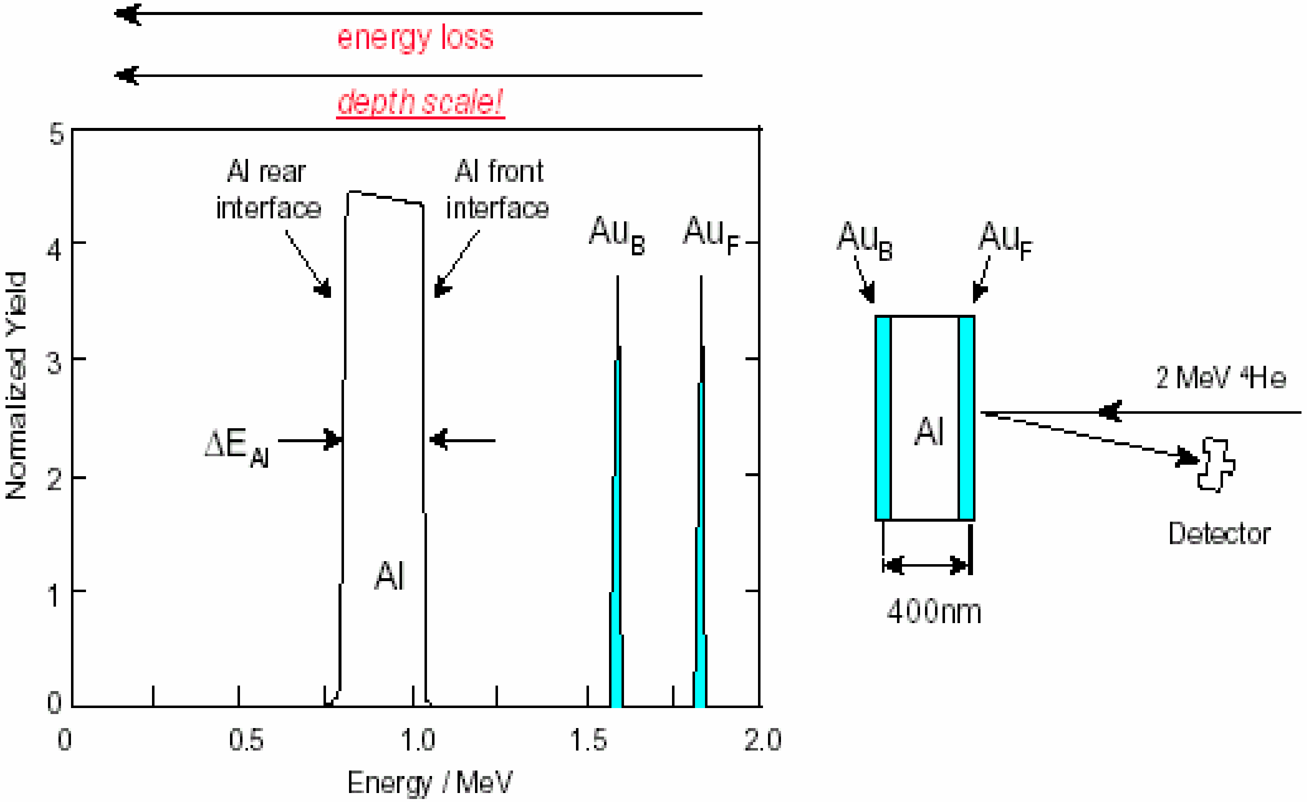

Fig. 6 Interpretation of the depth scale in RBS spectra.

1.2 Cross Section

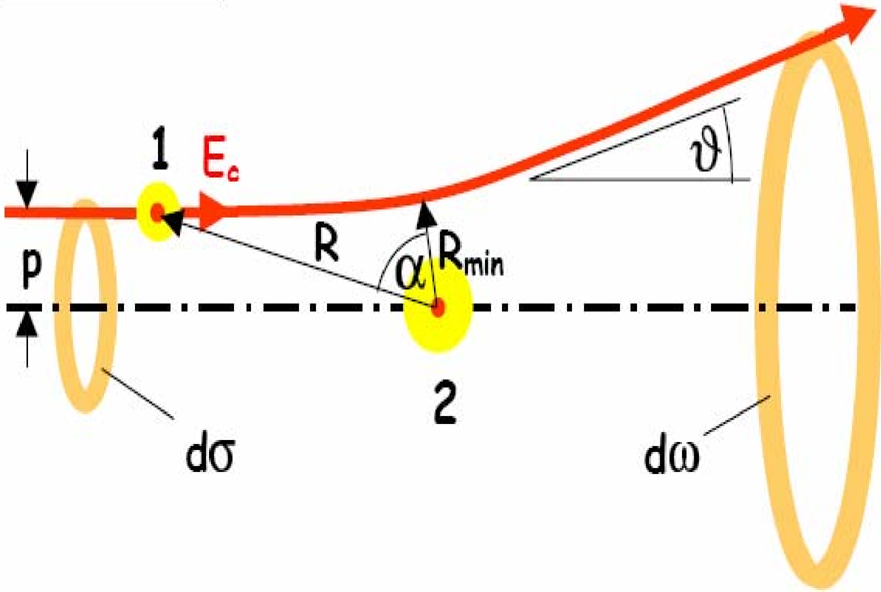

Fig. 1.3:

Scattering trajectory. Incidence within a differential ring at a given impact parameter results in a scattering into a differential solid angle

In cylindrical coordinates, the CMS trajectory is described by the distance R and the angle α (see Fig. 1.3). Energy and angular momentum conservation, and integration yield for the asymptotic scattering angle at a given impact parameter p the so-called "classical trajectory integral"

$$\vartheta = \pi - 2p \int_{0}^{R_{min}^{-1}} \frac{d\left(\frac{1}{R}\right)}{\sqrt{1 - \frac{V(R)}{E_c} - \frac{p^2}{R^2}}} \tag{1.12}$$

Scattering cross section

$2\pi b db = s(\theta)\ 2\pi \sin\theta d\theta$

$\sigma(\theta) = b(db/d\ \theta)/\sin\ \theta$

= # of scattered paricles into $d\Omega$/total # of incident particles

Rutherford formula

$d\sigma\ /d\Omega = [Z_1\ Z_2 e^2/4E_c \sin\theta_c/2]^2\ E_c = [M_2/(M_1+M_2)]E_o$

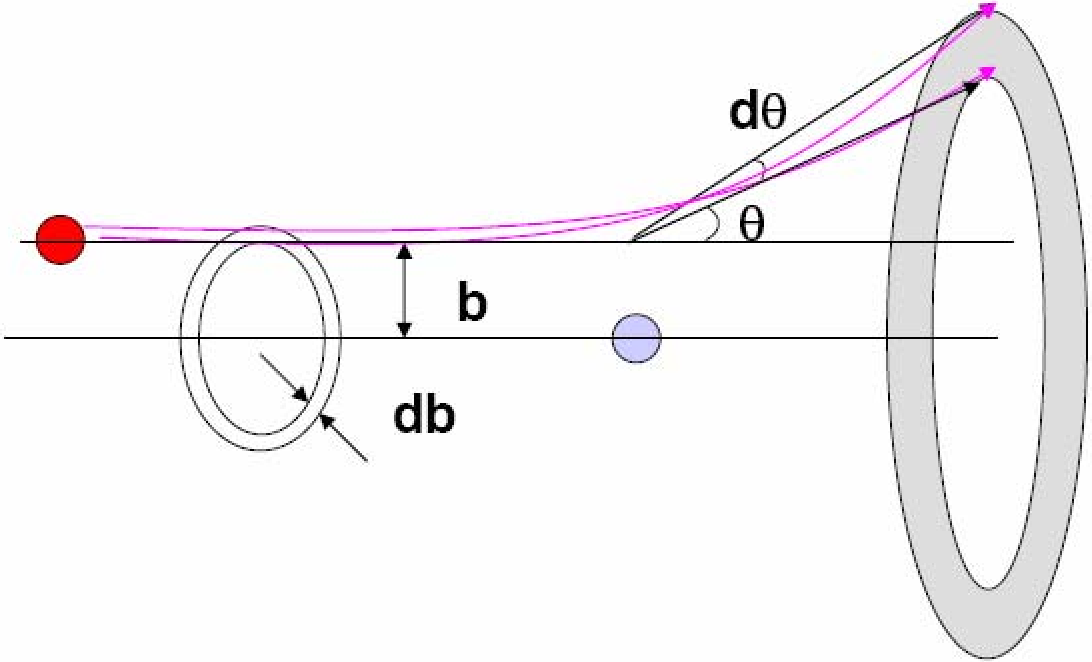

DIFFERENTIAL SCATTERING CROSS SECTION

The theoretical differential cross section for a given scattering angle is given by:

$$\frac{d\sigma}{d\Omega} = \left(\frac{zZe^2}{4E_0}\right)^2 \times \left[\sin^{-4}\frac{\theta}{2} - 2\left(\frac{m}{M}\right)^2 + \ldots\ldots\right]$$

The higher order terms are usually negligible for M>m and the differential cross section can be expressed in the following form, which has the unit of mb/sr (millibarn per steradian) when MeV is used as the unit for E_o:

$$\frac{d\sigma}{d\Omega} = 1.296 \times \left(\frac{zZ}{E_0}\right)^2 \times \left[\sin^{-4}\frac{\theta}{2} - 2\left(\frac{m}{M}\right)^2\right]$$

Cross section: If the projectile energy is chosen properly (above electronic screening, below Coulomb-barrier) the scattering yield follows the well known Rutherford cross-section which is basically inverse proportional to the projectile energy and proportional to the square of the atomic number of the target atom (Fig. 7).

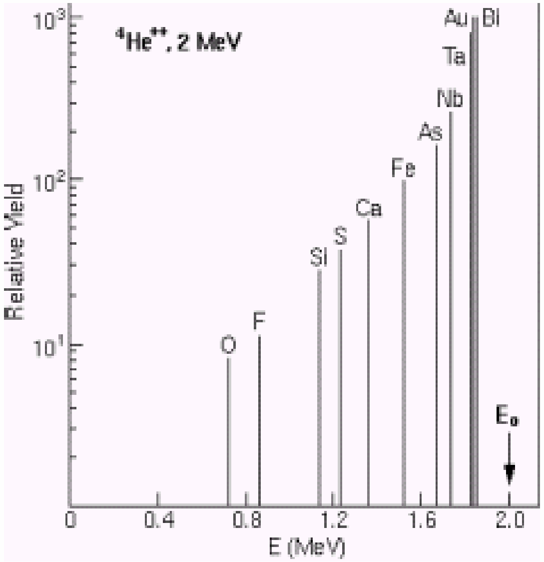

Fig. 7 Comparison of scattering yields as a function of the target atomic number.

$$A = \sigma \Omega Q N t$$

Ion Channelling

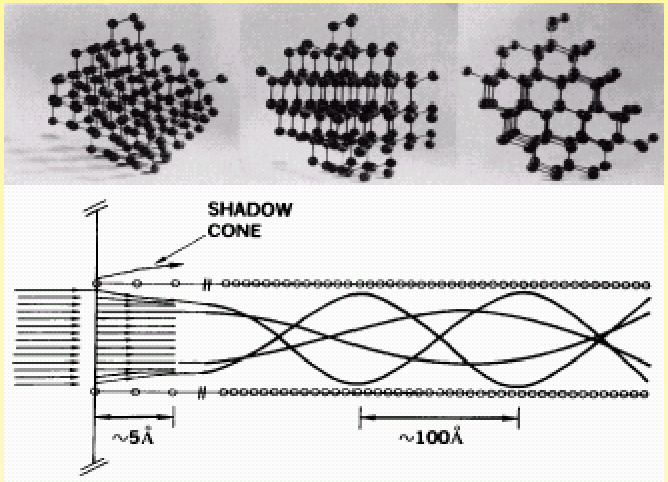

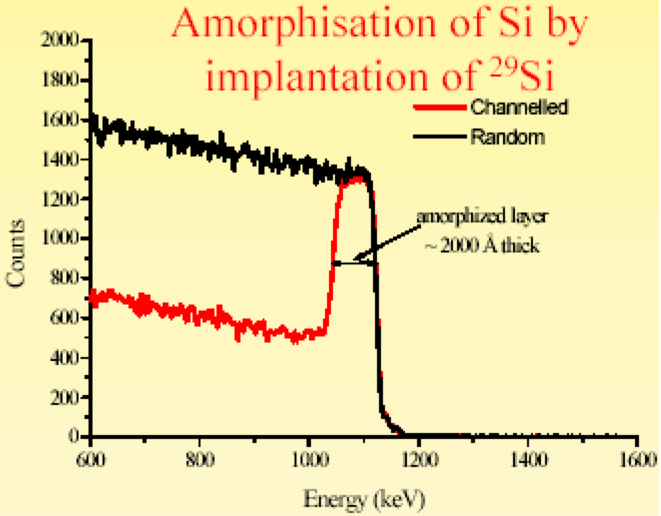
Amorphisation of Si by implantation of ^{29}Si

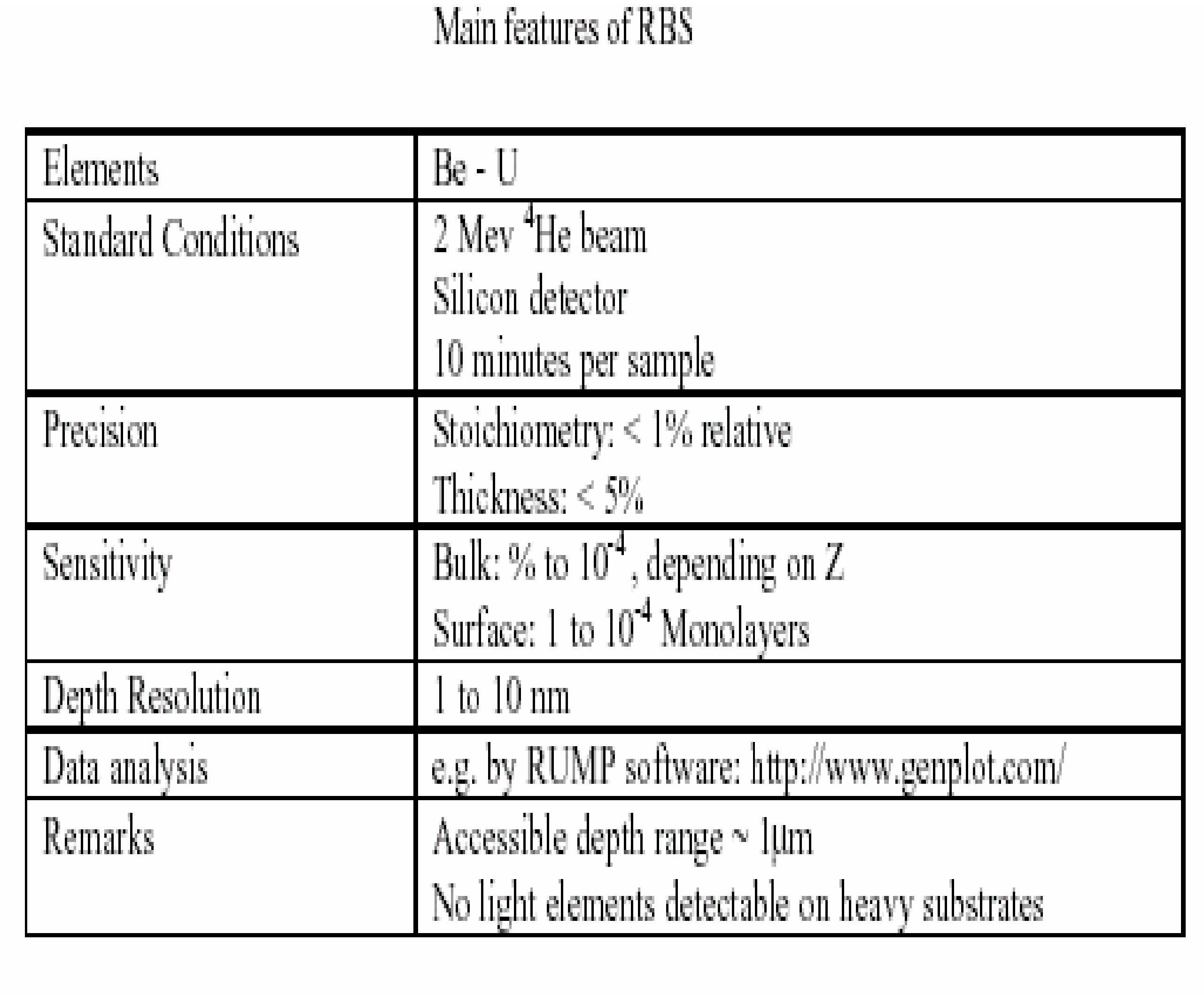

Main features of RBS

Elements	Be - U
Standard Conditions	2 Mev ^{4}He beam Silicon detector 10 minutes per sample
Precision	Stoichiometry: < 1% relative Thickness: < 5%
Sensitivity	Bulk: % to 10^{-4} , depending on Z Surface: 1 to 10^{-4} Monolayers
Depth Resolution	1 to 10 nm
Data analysis	e.g. by RUMP software: http://www.genplot.com/
Remarks	Accessible depth range ~ 1μm No light elements detectable on heavy substrates

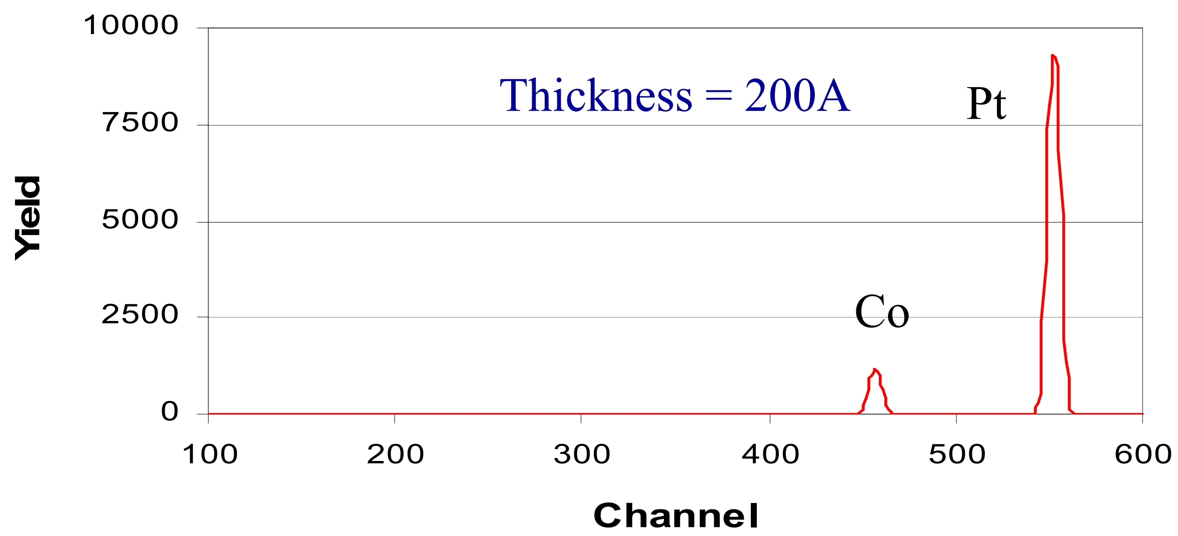

10000
7500
5000
2500
0
Yield
100
200
300
400
500
600
Channel
Thickness = 200A
Pt
Co

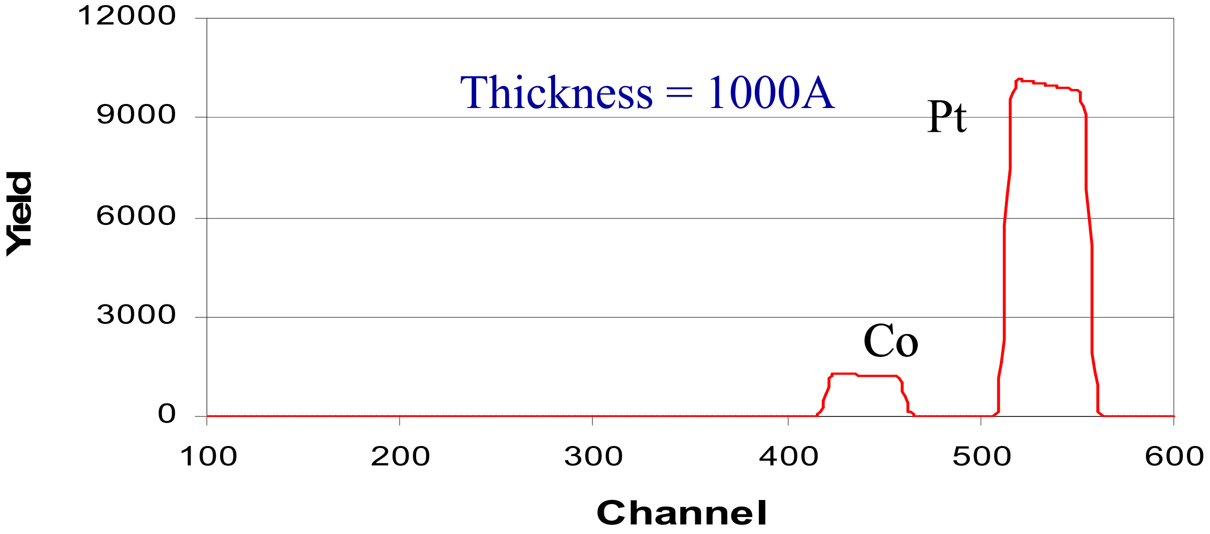

12000
9000
6000
3000
0
Yield
100
200
300
400
500
600
Channel
Thickness = 1000A
Pt
Co

SIMULATED RBS SPECTRUM

Target : Pt-Co (1:1) alloy of thickness 6000A
Incident ion: 2 MeV ^{4}He+
Scatter angle: 160°

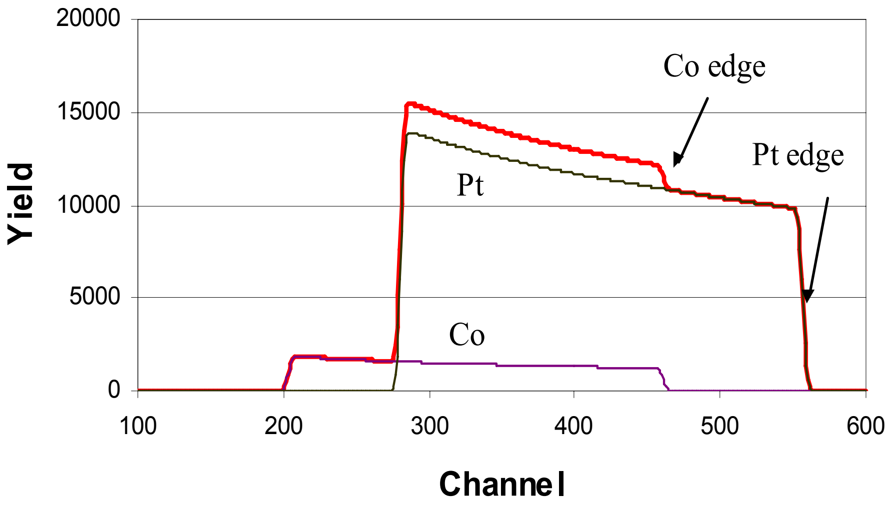

Example : RBS spectrum of hard-disk

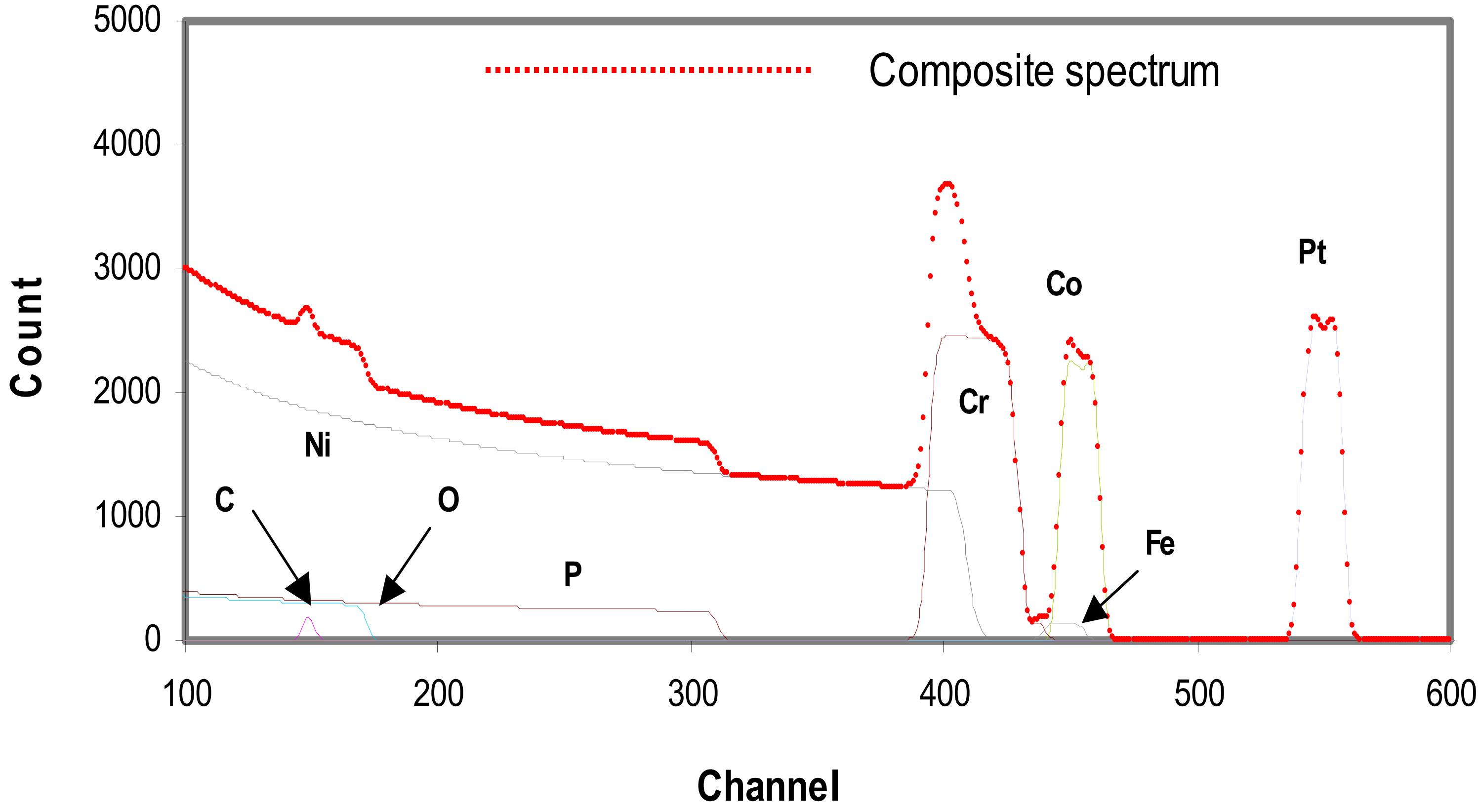

Layer structure:		
	Protective polymeric material	(~200A)
	Co-Pt-Fe alloy	(~200A)
	Cr	(~10A)
	Co-Pt.Fe alloy	(~200A)
	Cr	(~1000A)
	$Ni_3(PO_4)_2$	(~100,000A)
	Al substrate	

2000 keV ^{4}He, θ = 165° backscattered from Au on Si substrate

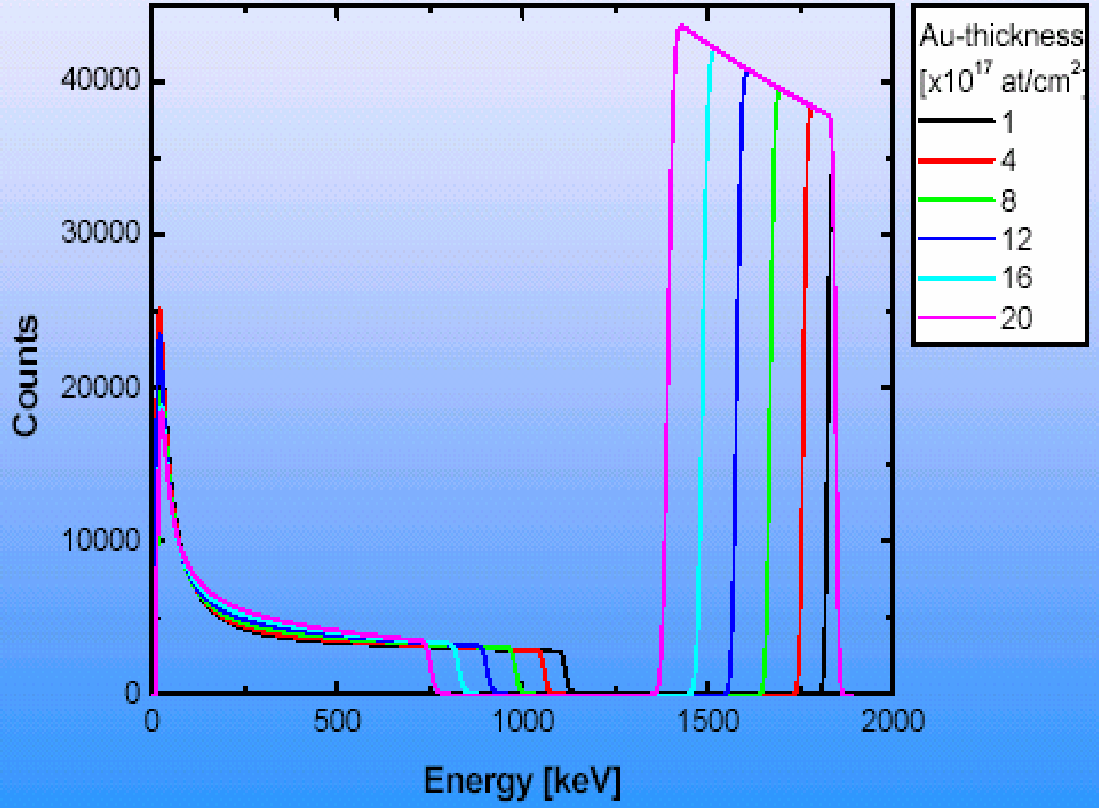

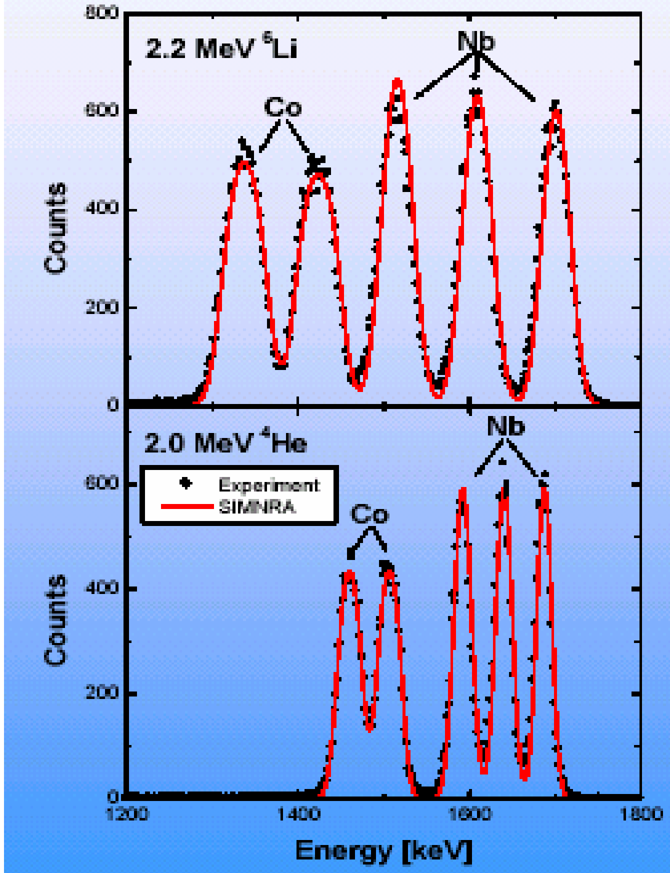

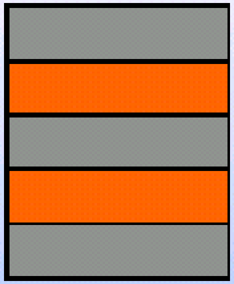
Nb

Co

Nb

Co

Nb

Nb: 1.0×10^{17} at/cm^2
Co: 2.2×10^{17} at/cm^2

M. Mayer et al., Nucl. Instr. Meth. B190 (2002) 405

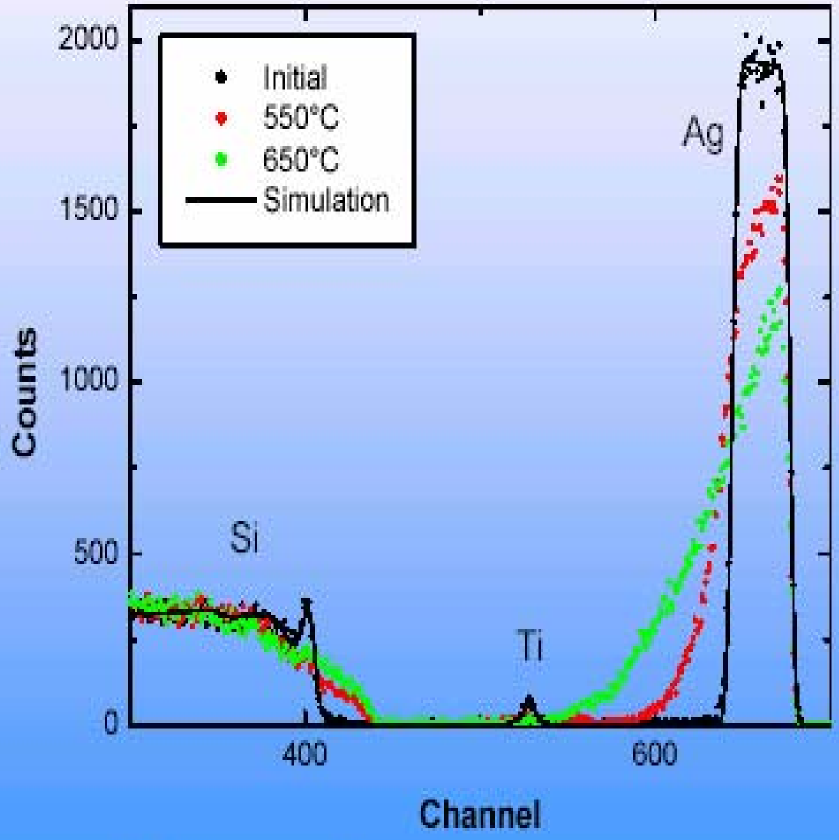

3980 keV ^{4}He, θ = 165°

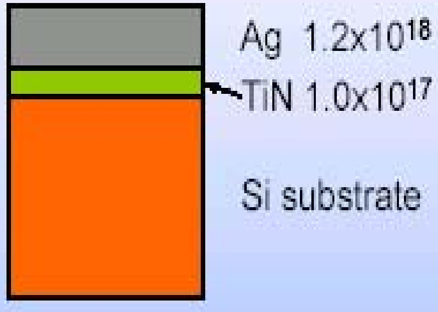

M. Balden, unpublished

1.9 MeV ^{4}He, 170° backscattered from ceramic glass

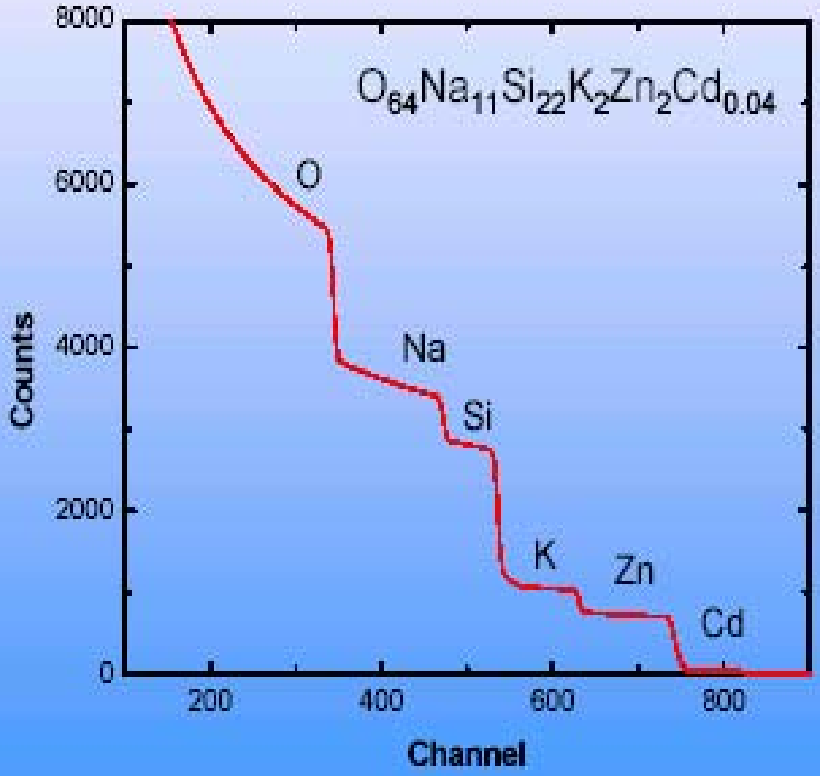

Blok sema jonskog implantera

VN - visoki napon
JI - jonski izvor
VP - vakuumske pumpe
PV - preklopni ventil
FE - fokusirajuci elementi
AM - analizirajuci magnet
SE - skanirajuce elektrode
DB - dijagnostika snopa
IK - interakciona komora

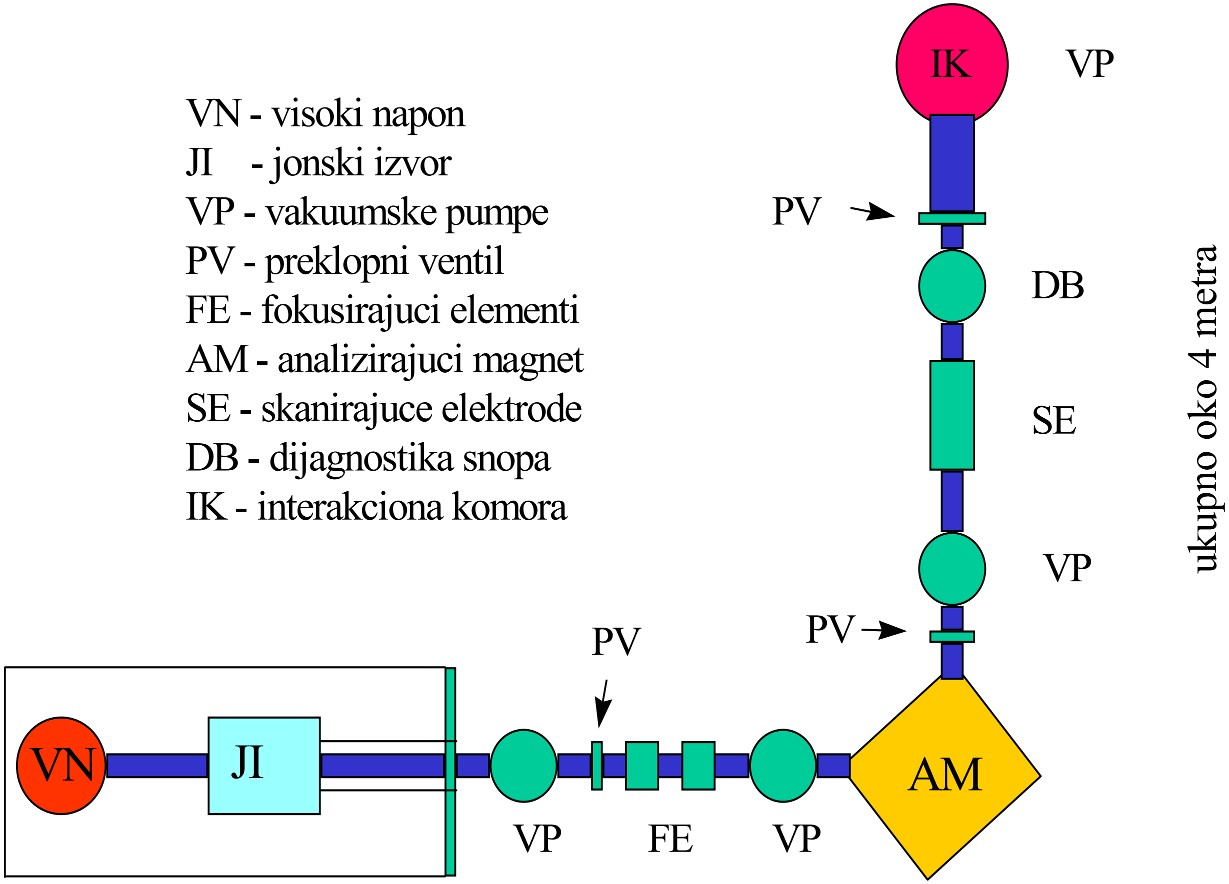

Skretni magnet VdG

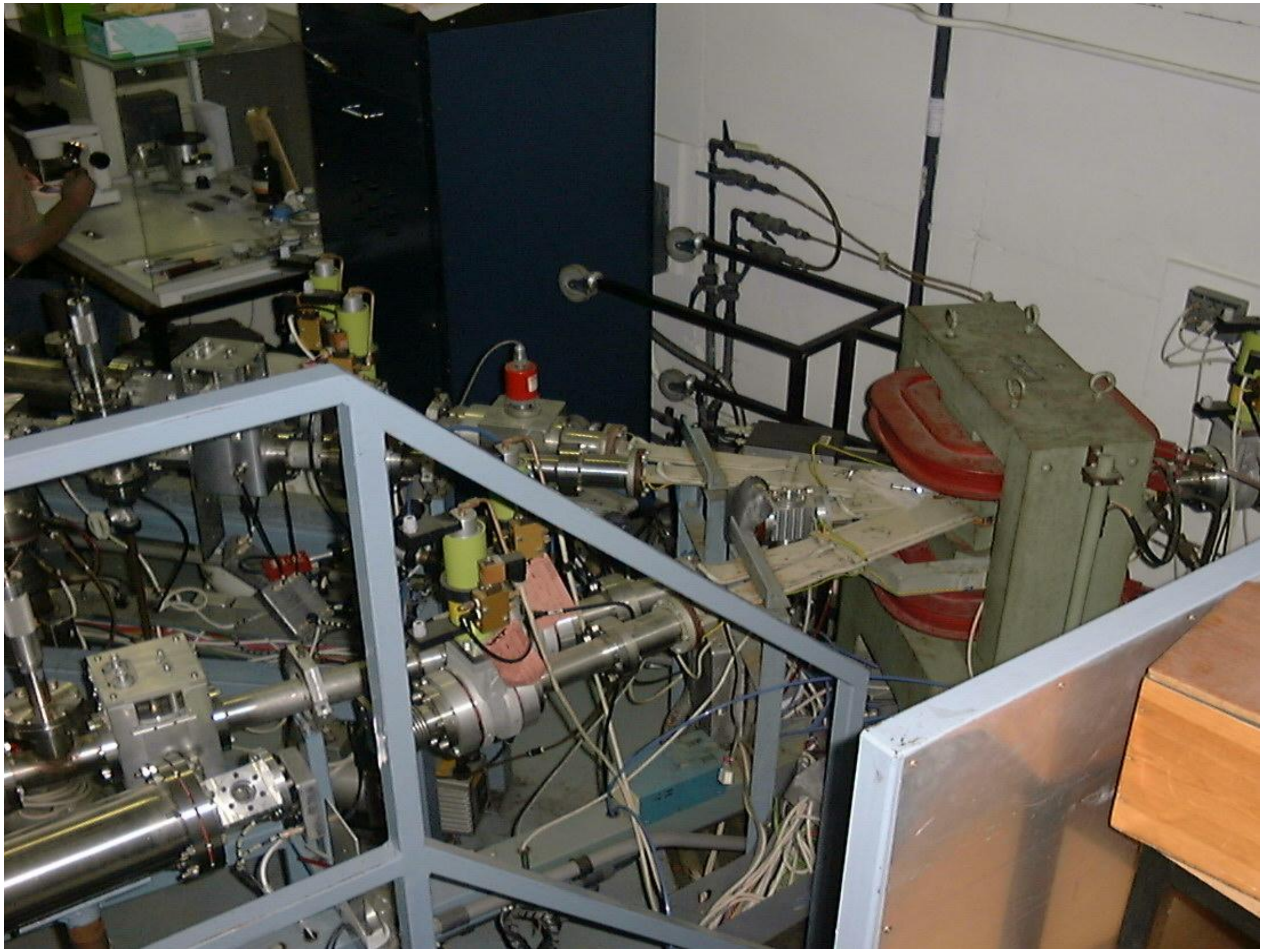

RBS linija

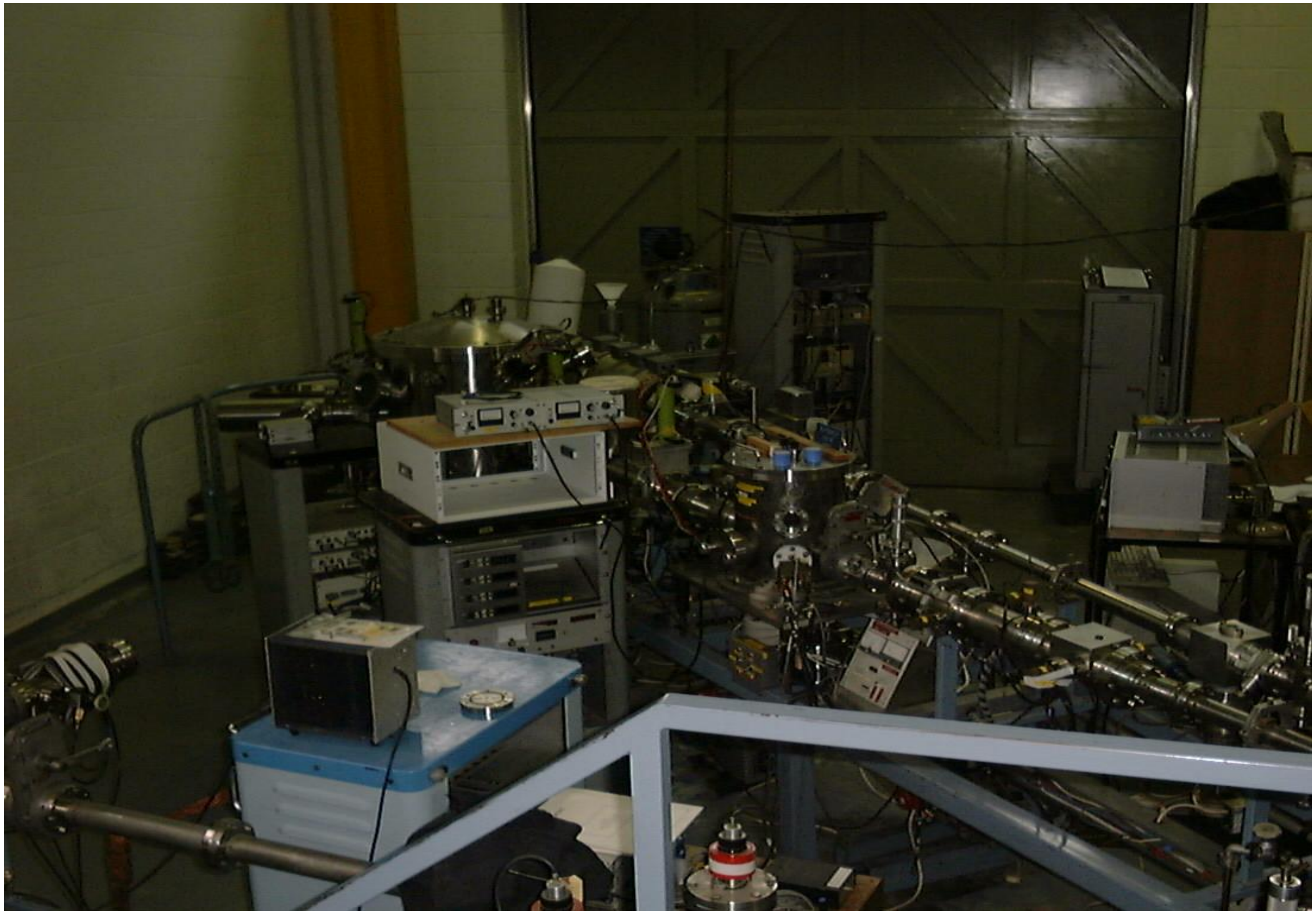

Van de Graaff

Van de Graaff akceleratorska cev

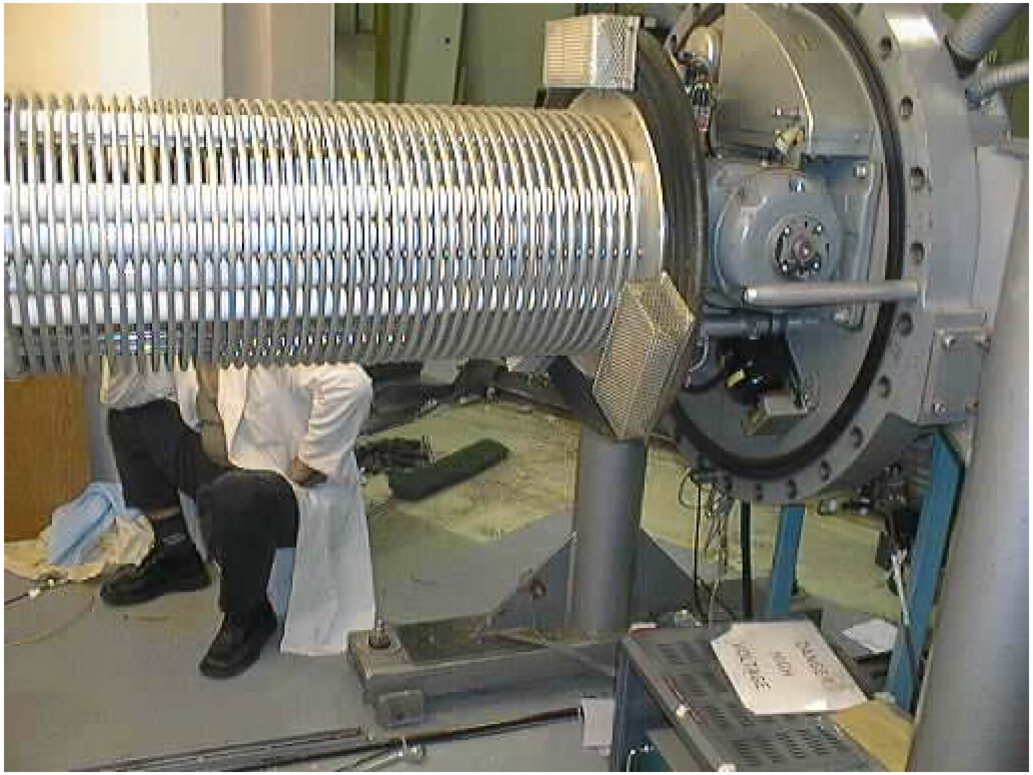

Analizatorski magnet, 500kV implanter

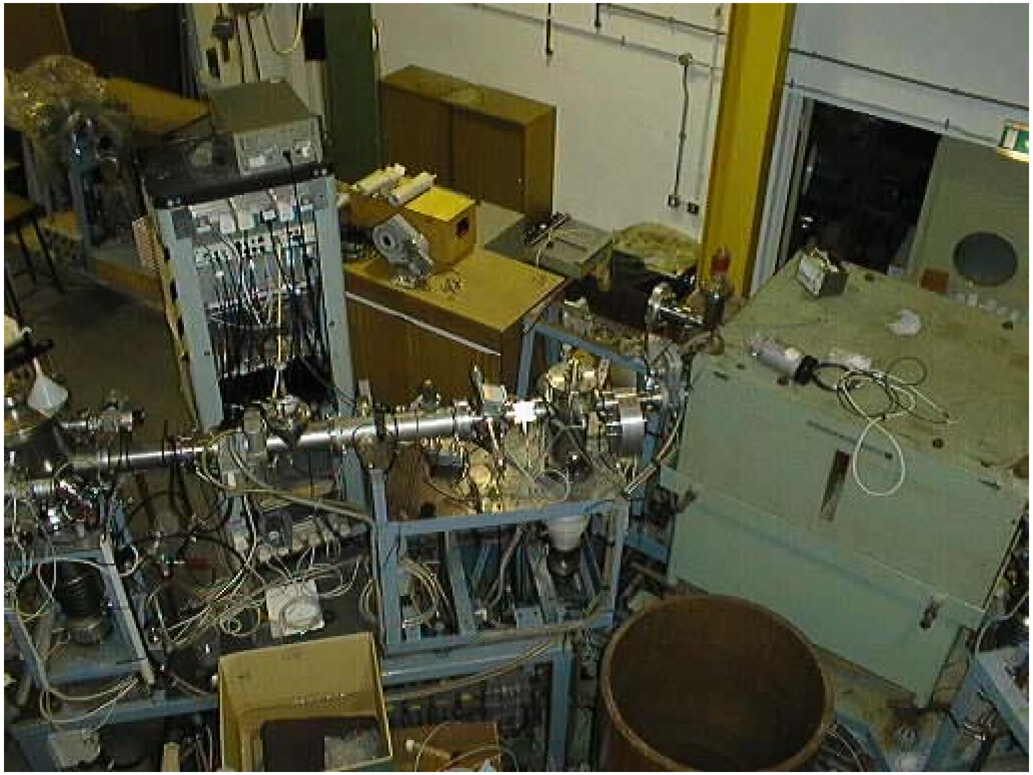

Van de Graaff

Schematic view of the ion beam mixing experiments

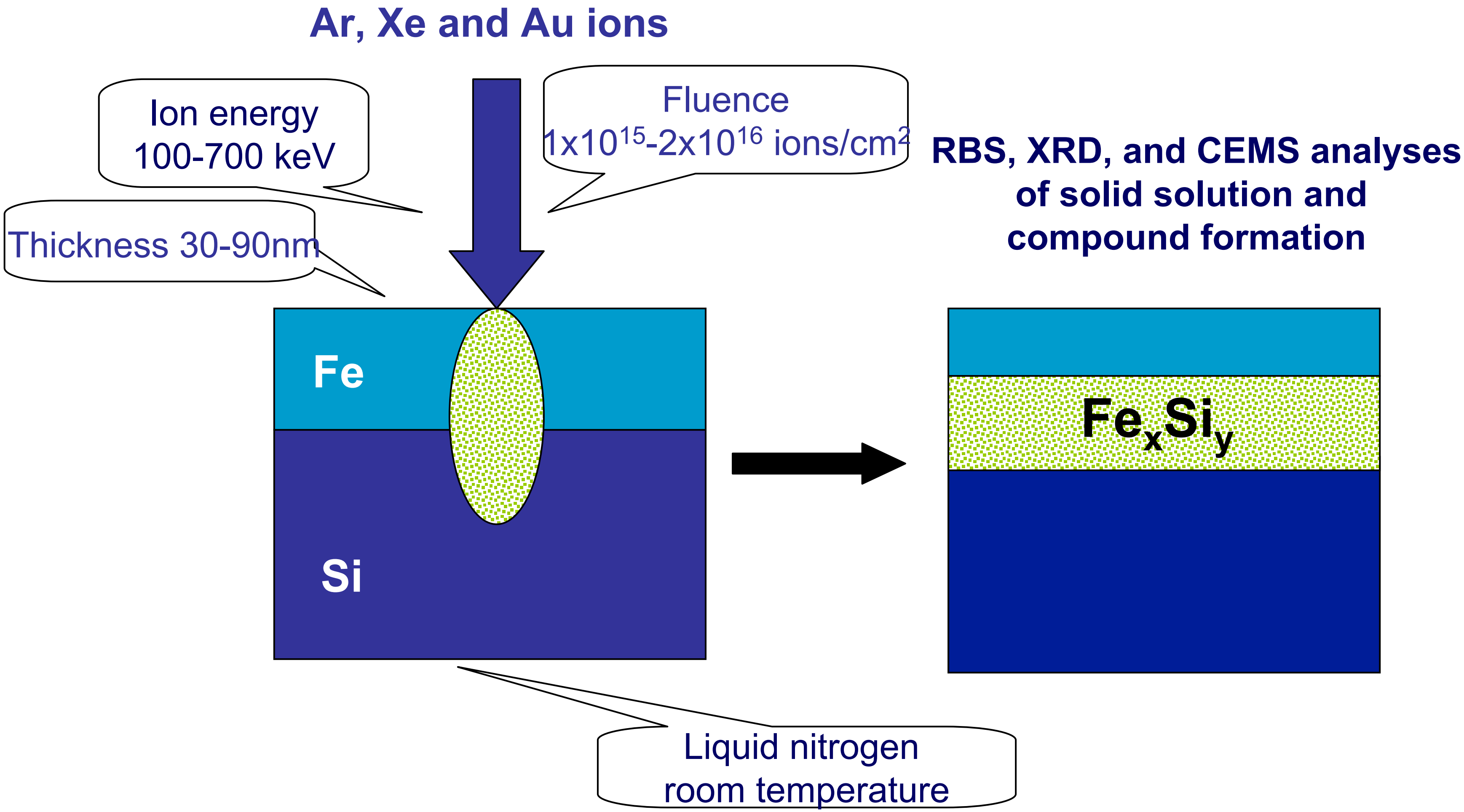

Ar, Xe and Au ions

Ion energy
100-700 keV

Fluence
1×10^{15}-2×10^{16} ions/cm^2

Thickness 30-90nm

RBS, XRD, and CEMS analyses of solid solution and compound formation

Liquid nitrogen
room temperature

RBS spectra (a); Fe and Si concentration profiles (b) of Fe/Si bilayers irradiated with 1×10^{15} - 2×10^{16} Xe$^+$ ions/cm^2 at 250 keV

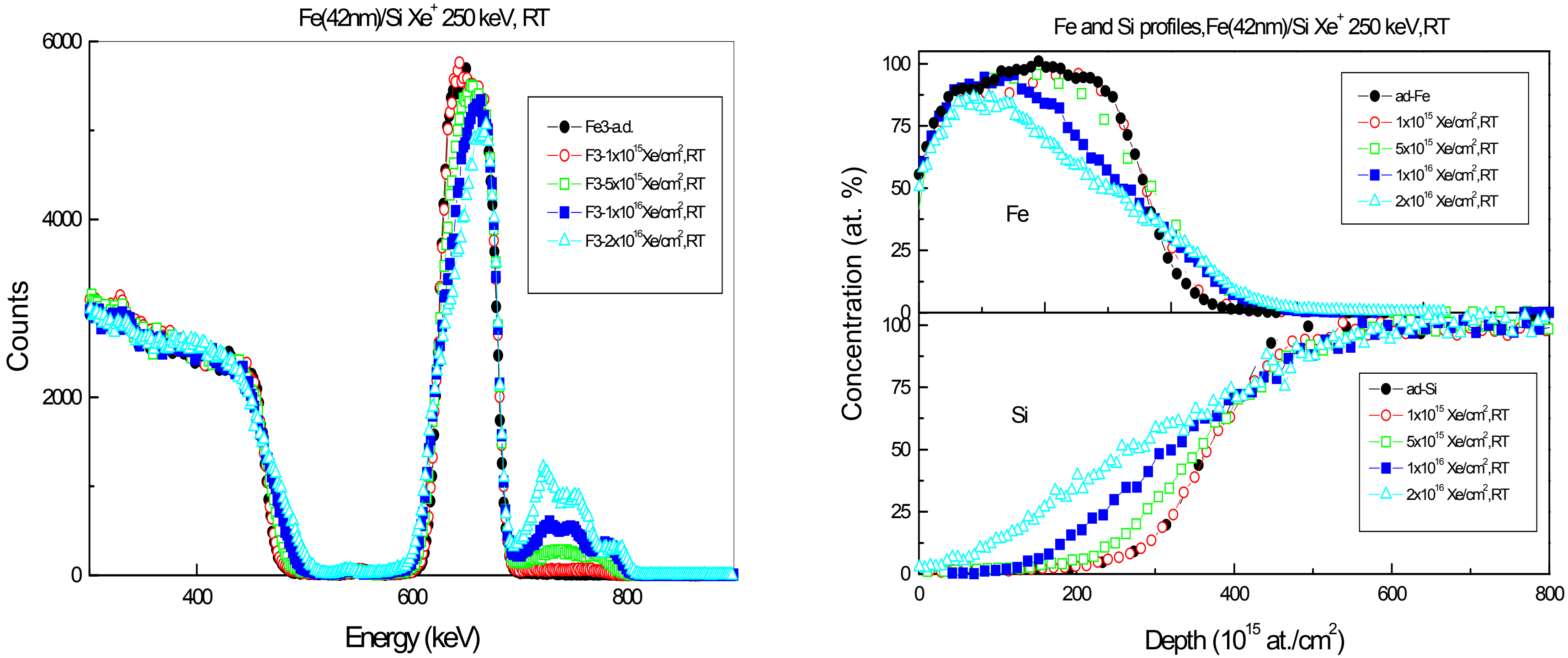

Amorphous-iron disilicide: A promising semiconductor

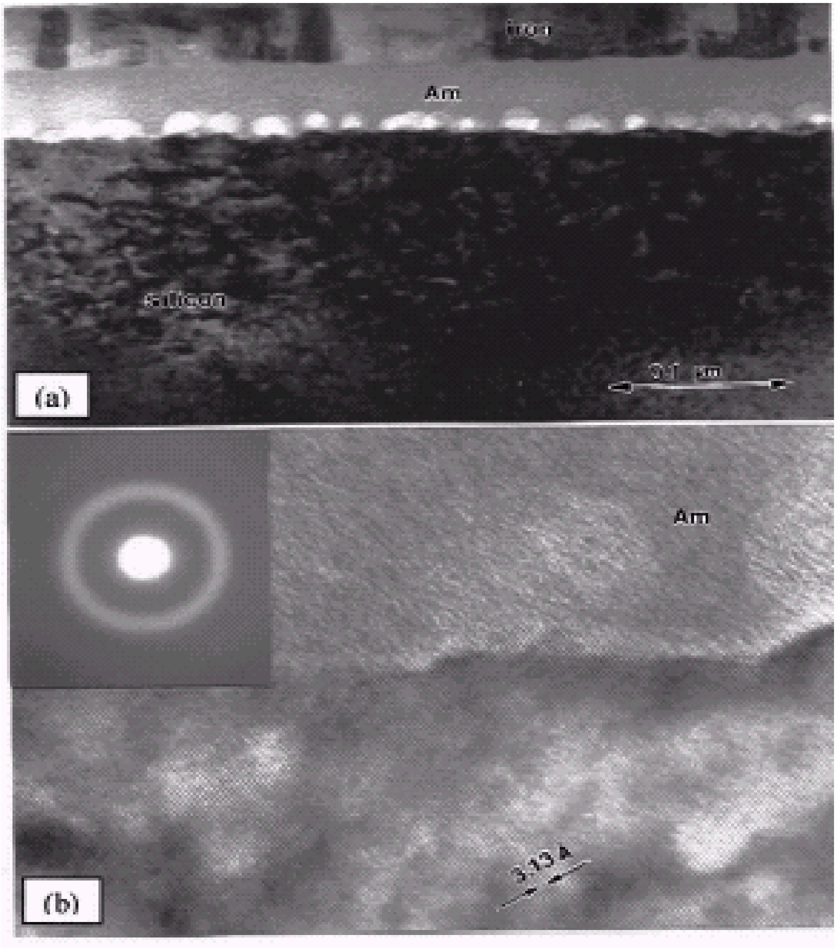

CEMS spectra of ^{57}Fe/Si bilayers irradiated to a fluence of 2×10^{16} ions/cm^2 with 250 keV Xe^{1+} at RT (a) and LN$_2$ (b) and for 100 keV Ar^{1+} ions at RT (c) and LN$_2$ (d)

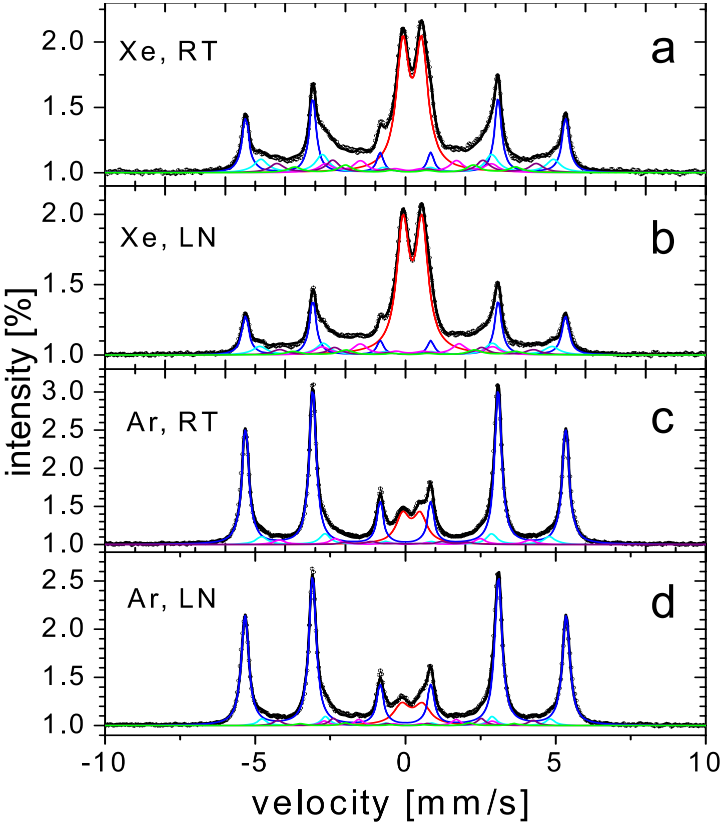

The sextets are attributed to the ferromagnetic solid solution of Si in the bcc Fe → bcc-Fe(Si) phase

One broad doublet (IS=0.22829 mm/s, QS= 0.63(3) mm/s, Γ =0.50(2) mm/s) and up to five sextets with hyperifine fields ranging from 33 T down to 17T

Methods

Mössbauer spectrometry

Transmission geometry: γ

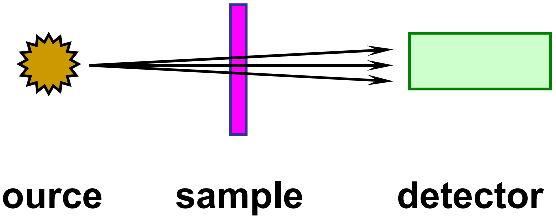

De-excitation:

- γ photons
- X-rays
- conversion electrons (e$^-$)

Conversion electrons (CEMS): e$^-$

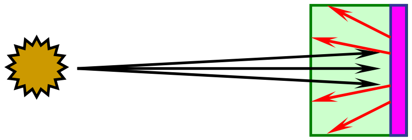

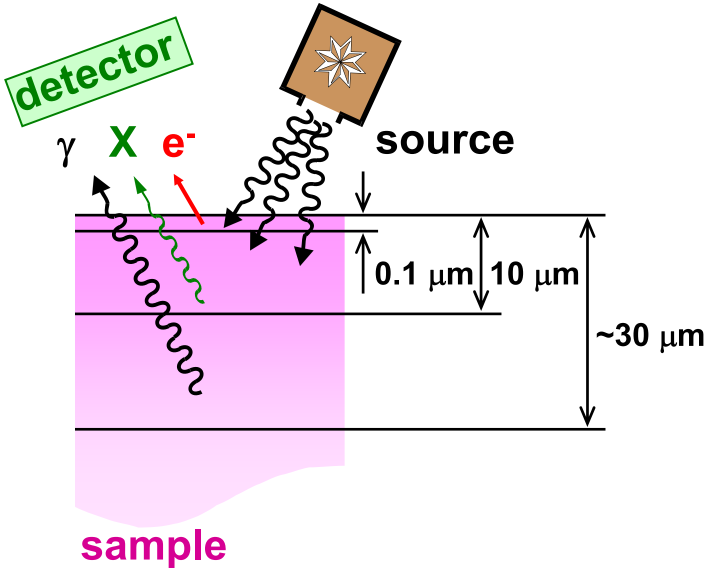

CEMS spectra of Xe ion beam mixed ^{57}Fe/Si bilayers in the smaller velocity range

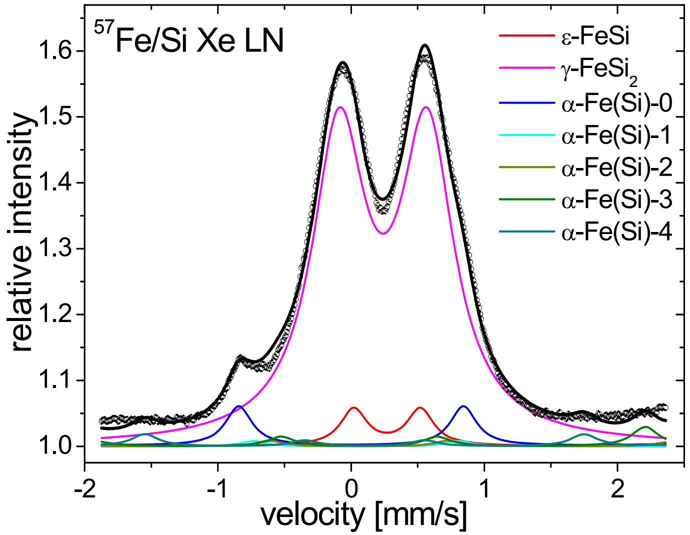

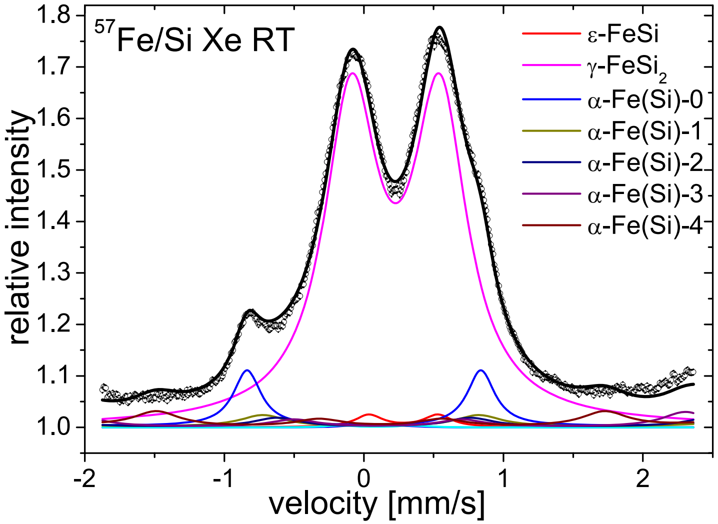

The doublet represents a mixture of paramagentic phases, mainly to γ-FeSi$_2$and small farction of ε-FeSi
After mixing with Xe ions a fraction of 39% at RT and 47% at LN.
For mixing with Ar ions the corresponding fraction resulted as 12% at RT and 10% at LN

The quantitative information of the redistribution of the components across the interface Interface variance of the mixed Fe/Si bilayer $\Delta\sigma^2$, after RT irradiation, as a function of ion fluence Φ (a) Ar and (b) Xe

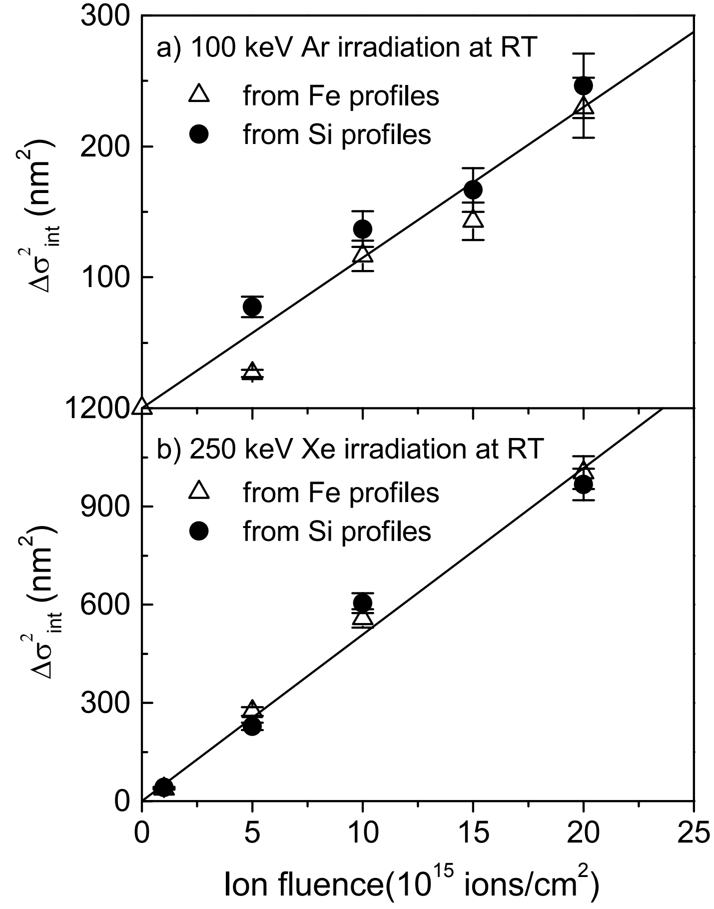

← $\Delta\sigma^2/\Phi$= 1.3 ± 0.2 nm^4

k (mixing rates)

← $\Delta\sigma^2/\Phi$ = 4.8 ± 0.5 nm^4

RBS spectra taken from Fe/Si bilayers irradiated with 400 keV Au^{+} ions

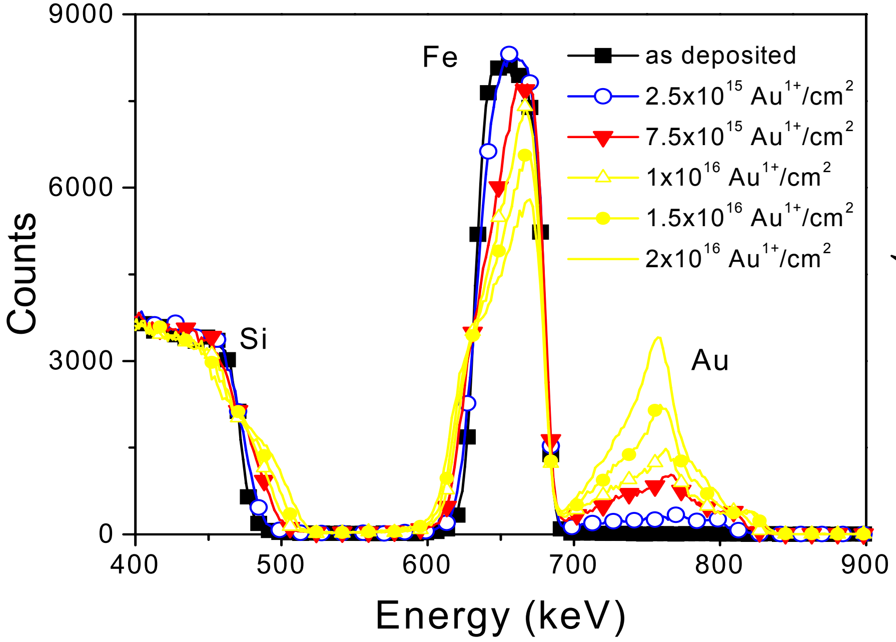

The similar effects are observed after irradiation with **700 keV Xe^{2+}** ions

Interface broadening variance $\Delta\sigma^2$ versus ion fluence Φ for Fe/Si bilayers irradiated with a 100 keV Ar^+ ions, 250 keV Xe^+ and 700 keV Xe^{2+}, and 400 keV Au^+

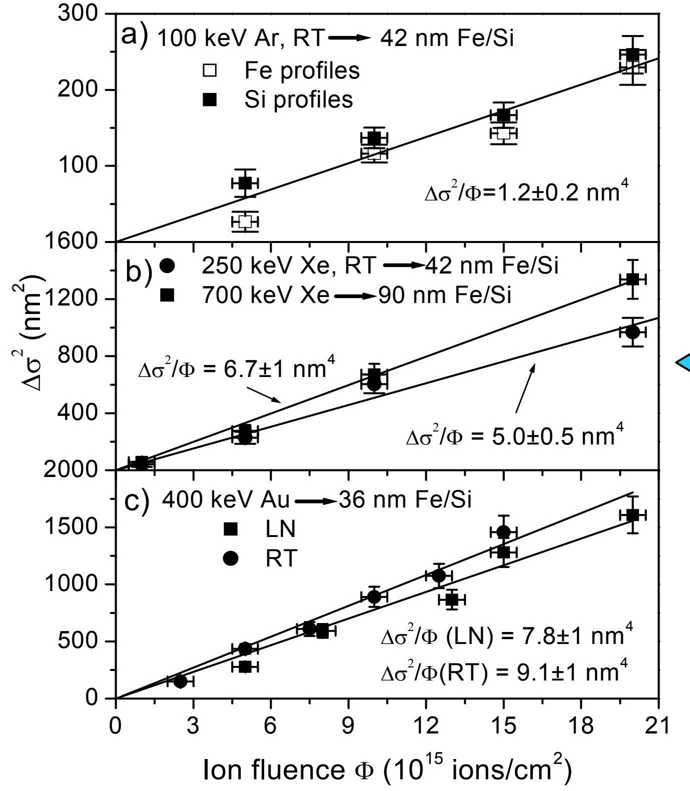

a) linear dependece

b) athermal regime

c) influence of ion mass

The deduced mixing rates are inserted

BALLISTIC MODEL

Under ballistic model mixing rate k_{ball} is given as:

$$k_{ball} = \frac{1}{3}\Gamma_0 \xi \frac{R_d^2}{NE_d} F_D \quad \ldots\ldots\ldots \quad (1)$$

Γ_0= 0.608, N = average atomic density
ξ = kinematic factor involving the masses of the colliding atoms
F_D= deposited energy density , E_d= displacement energy
R_d ˜ 1 nm, the minimum separation distance for the production of a stable Frankel pair

THERMAL SPIKE MODEL

If the mixed region consists of both solid solution and compounds, mixing rate is given as:

$k = k_{spike}\,[p_{comp}\,.f_{comp} + (1 - p_{comp})\,f_{sol}]$ ………. (2)

where p_{comp} is the fraction of the compound phase in the mixed region. By considering A_aB_b compound via chemical reaction $A+B \rightarrow A_aB_b$, the compound enhancement factor f_{comp} can be expressed as:

$$f_{comp} = 2\left[\frac{C_A}{aC/(a+b)} + \frac{C_B}{bC/(a+b)}\right] \qquad \text{……..} \ (3)$$

C_A and C_B are the atomic densities of the A and B layers, C is the atomic density of the compound.

Under solution approximation, the factor f_{sol} due to formation of A-B solution is given by:

$$f_{sol} = 1 + K_2 \frac{\Delta H_{mix}}{\Delta H_{coh}} \qquad \text{…….. ……..} \qquad (4)$$

Factor for k_{spike}, the expression derived for either local spikes

$$k_{spike} = \frac{K_S Z_{ave}^{1.77}}{C^{2/3} \Delta H_{coh}^{2}} F_D \qquad \text{.................} \; \textbf{(5)}$$

or global spike

$$k_{spike} = \frac{K_1}{C^{5/3} \Delta H_{coh}^{2}} F_D^{2} \qquad \text{.................} \; \textbf{(6)}$$

$K_S = 0.9 \times 10^{-6}$ keV-nm^3, $K_1 = 0.0035$ nm, $K_2 = 50$ are constants

ΔH_{mix} and ΔH_{coh} are the average heat of mixing and cohesive energy of the bilayer elements, respectively.

$Z_{ave} = 20$, C_A = the atomic density of Fe = 85 atoms/nm^3, C_B = 50 atoms/nm^3(Si),

C = 61.7 atoms/nm ($FeSi_2$). $\Delta H_{mix} = 0.14$ eV/atom and $\Delta H_{coh} = 4.45$ eV/atom

Si is the dominant mobile species under the present irradiation conditions

The second term within the bracket in Eq. 3 should be considered in the calculation.

Comparison of experimental and calculated mixing rates in Fe/Si bilayers

Ion	Sample Temp.	Phase	F_D (keV/ nm)	Exper. mixing rate (nm^4)	Ion-beam mixing model (nm^4)		
					Ballistic[b]	Local spike[c]	Global spike[d]
Au	RT, LN	$FeSi_2$ [a] compound & Fe-Si solid solution	5.1	8.5 ± 1.5	0.9	7.4	10
Xe			3.3	6.7 ± 1	0.6	4.8	4.1
			2.8	4.8 ± 0.5	0.5	4	3.5
Ar			0.9	1.3 ± 0.2	0.16	1.3	0.4

[a] $FeSi_2$ phase assumed for Au irradiation

[b] Ballistic model

[c] Local spike model

[d] Global spike model

Ion-beam mixing in Fe/Si bilayers

Summary

- The growth variance $\Delta\sigma^2$ in the mixed Fe/Si layer depends linerly on the fluence Φ

- The mixing rates are very well reproduced by the local thermal spike model

- The enhancement factor is due to a Darken-type term for the presence of a solid solution and/or the fact that the a compound phase is formed

Formation of nitrides by irradiation of ^{57}Fe/Si bilayers

The synthesis of specific iron nitride phases during irradiation of ^{57}Fe/Si bilayer structures with 22 keV N^{2+} ions

Iron nitrogen phase diagram consists

interstitial solutions
($\alpha,\gamma,\varepsilon$)

chemical compounds
(γ'-Fe_4N and ζ-Fe_2N)

metastable phases
(α'-martensite, α''-$Fe_{16}N_2$)

- **excellent magnetic properties** → (α''-$\mathrm{Fe_{16}N_2}$)

- **significantly improved corrosion and wear resistance, high hardness** → (ε-nitride)

- **various experimental approaches to the synthesis of iron nitrides** (i)evaporation in nitrogen atmosphere

(ii)reactive sputtering

(iii)laser nitriding

(iv)molecular beam epitaxy

(v)ion beam assited deposition

(iv)ion implantation

Precise control of impurity concentration and depth distribution

New phases formation that cannot be produced by other conventional methods

Formation of iron nitrides in thin film structures

Specific nitride phase at lower nitrogen fluences

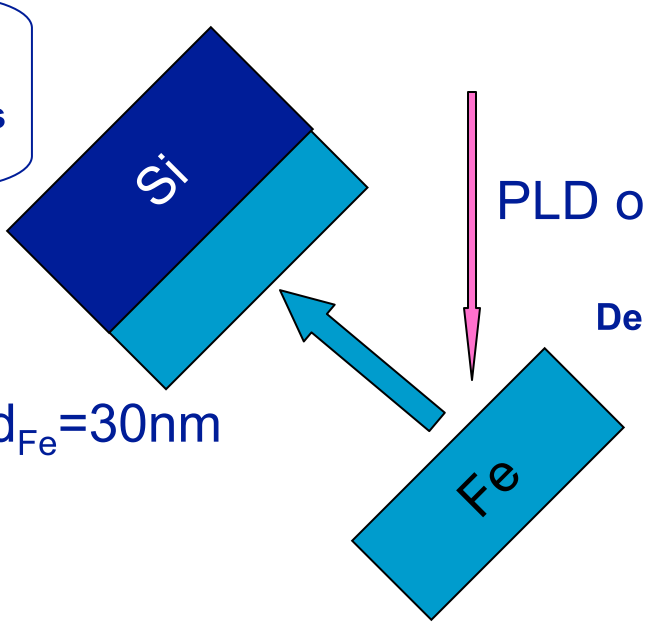

PLD of ^{57}Fe (95% enriched)

Deposition rate = 0.5 nm/s

d_{Fe}=30nm

Experimental details

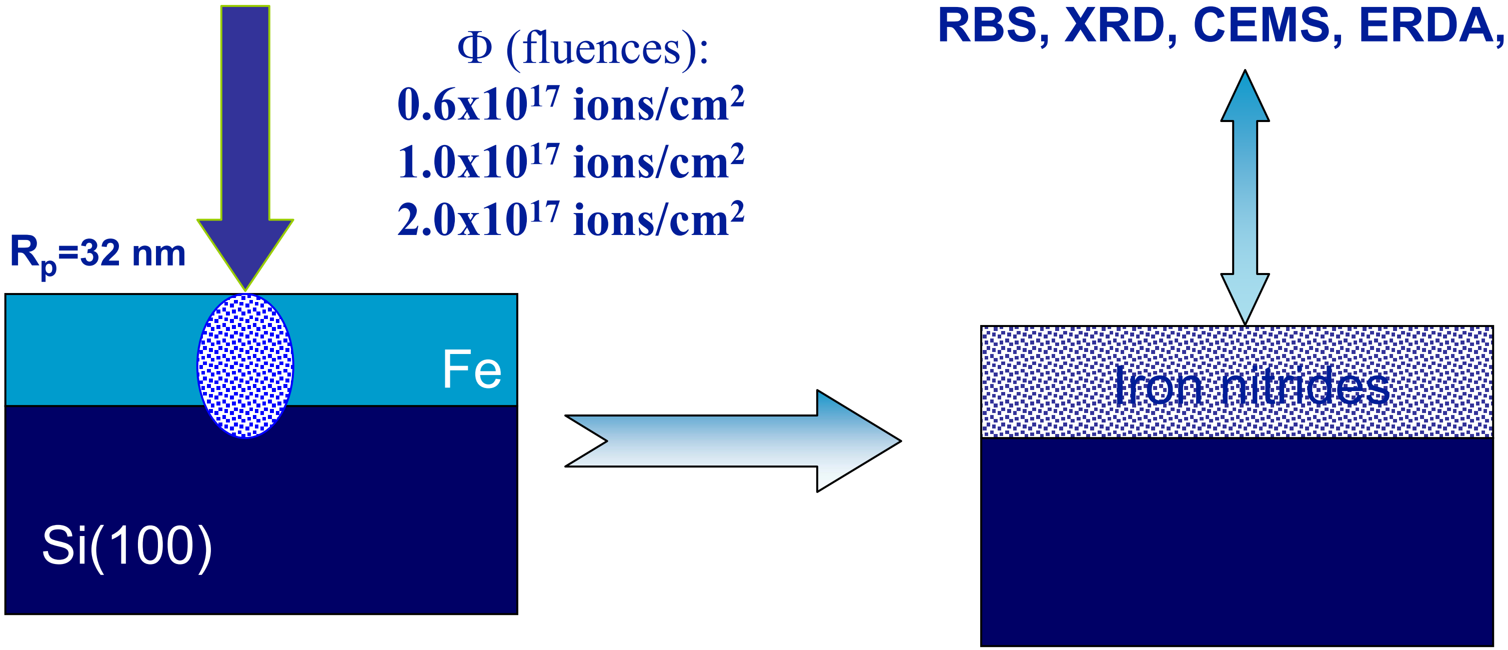

22 keV N^{2+} beam

R_p=32 nm

Φ (fluences):

0.6×10^{17} ions/cm^2
1.0×10^{17} ions/cm^2
2.0×10^{17} ions/cm^2

RT(room temperature)

RBS, XRD, CEMS, ERDA, AFM

Depth profiles: WiNDF and RUMP codes

RBS spectra (a); Fe and Si concentration profiles (b) of ^{57}Fe/Si bilayers irradiated with 0.6×10^{17} - 2×10^{17} N^{2+} ions/cm^2 at 22 keV

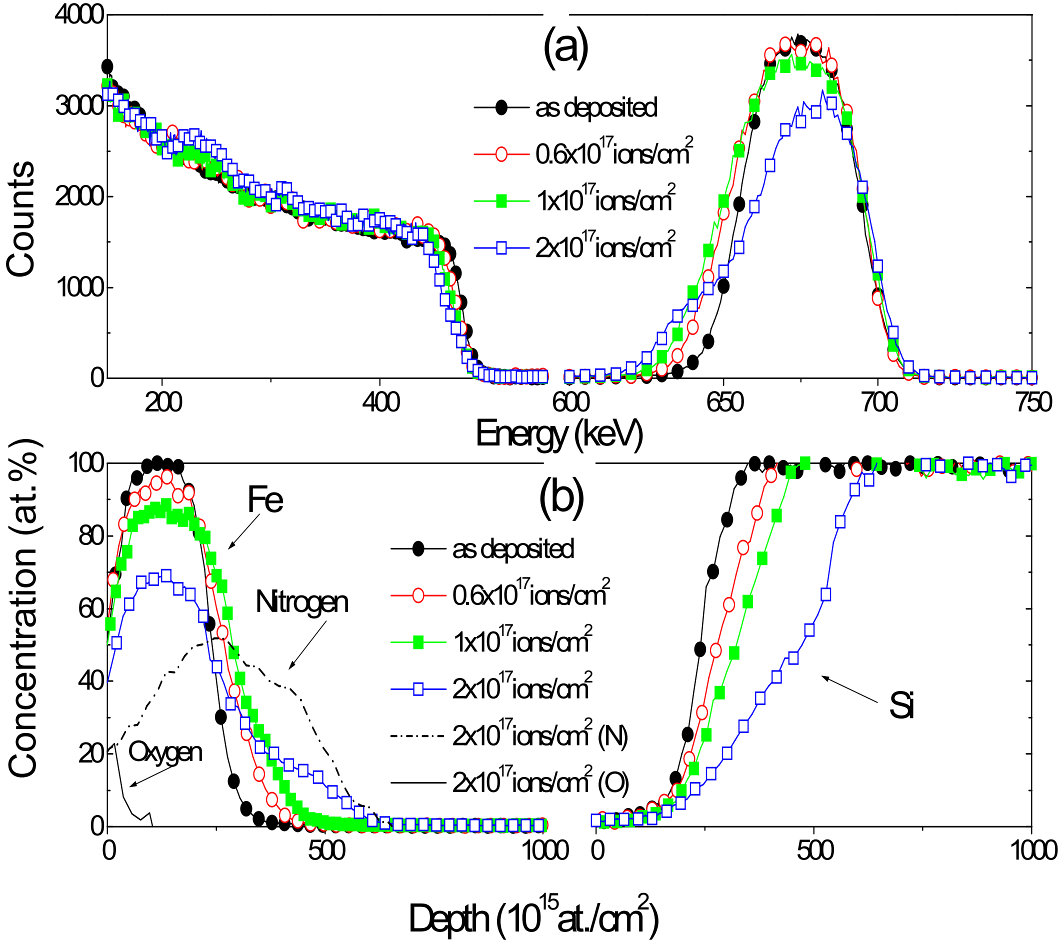

The profiles of Fe, Si, N and O for the high fluence irradiated sample

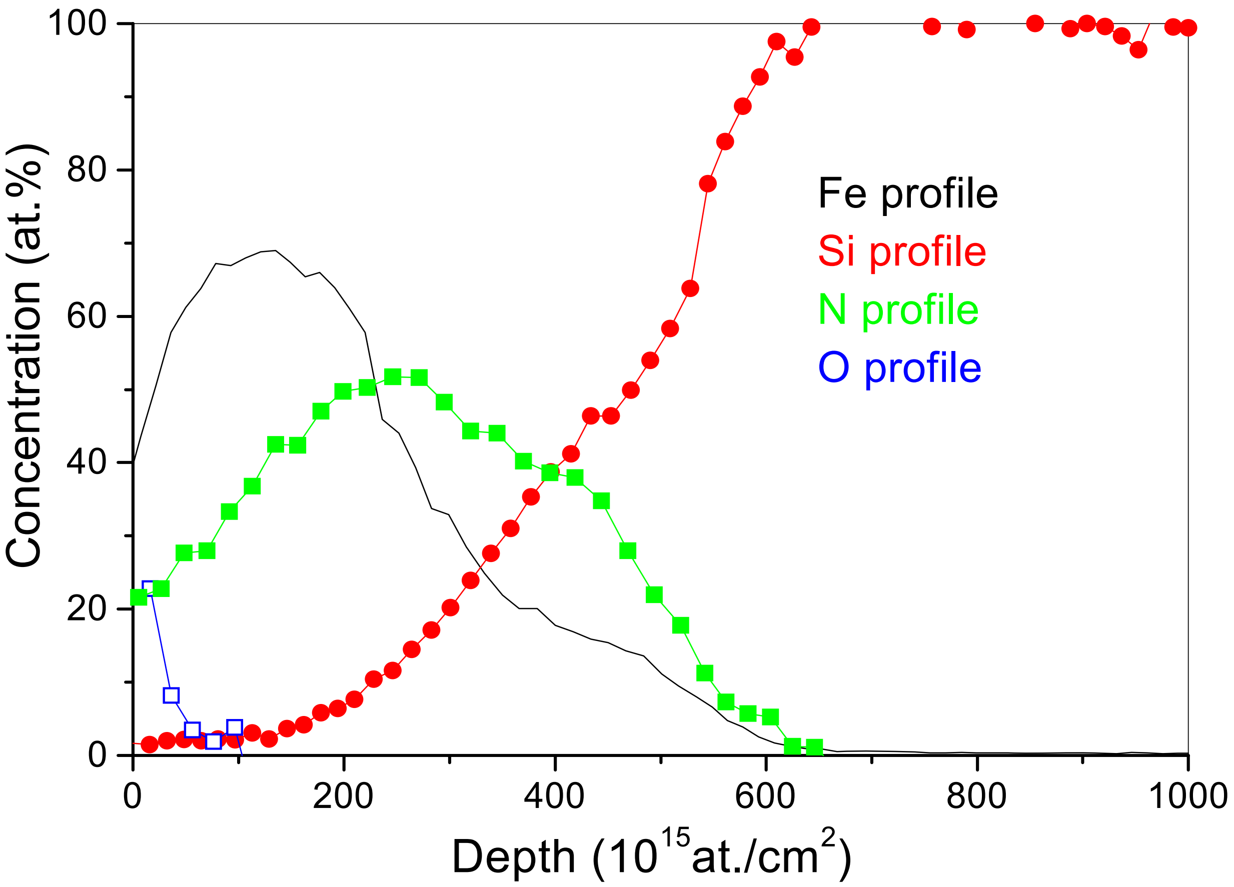

Nitrogen depth profiles obtained by ERDA

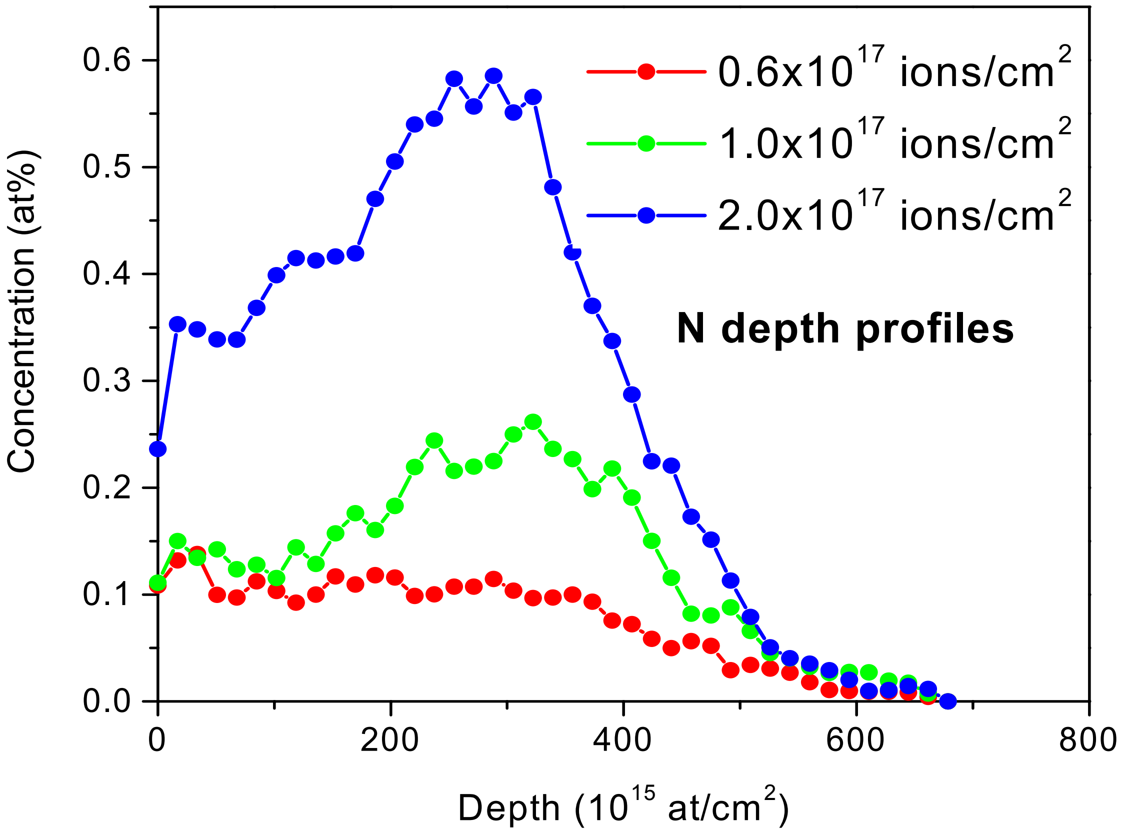

XRD analysis of the ^{57}Fe/Si samples before and after irradiation

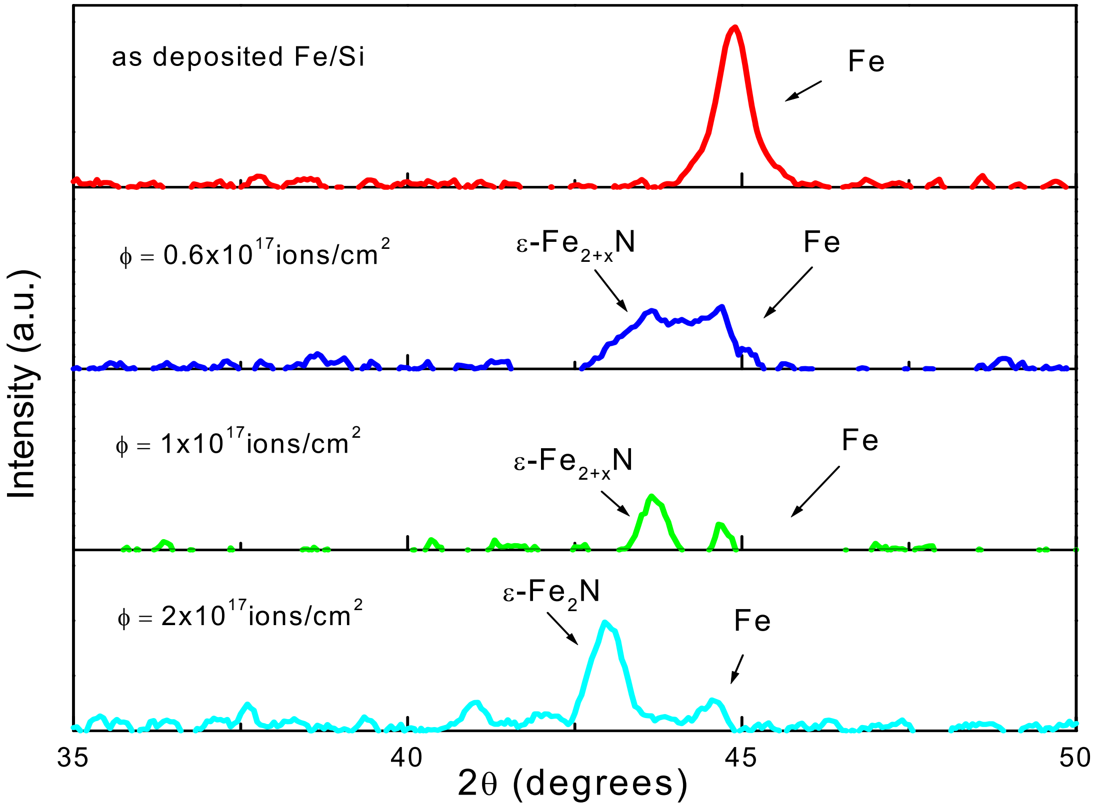

CEMS measurements of ^{57}Fe/Si bilayers

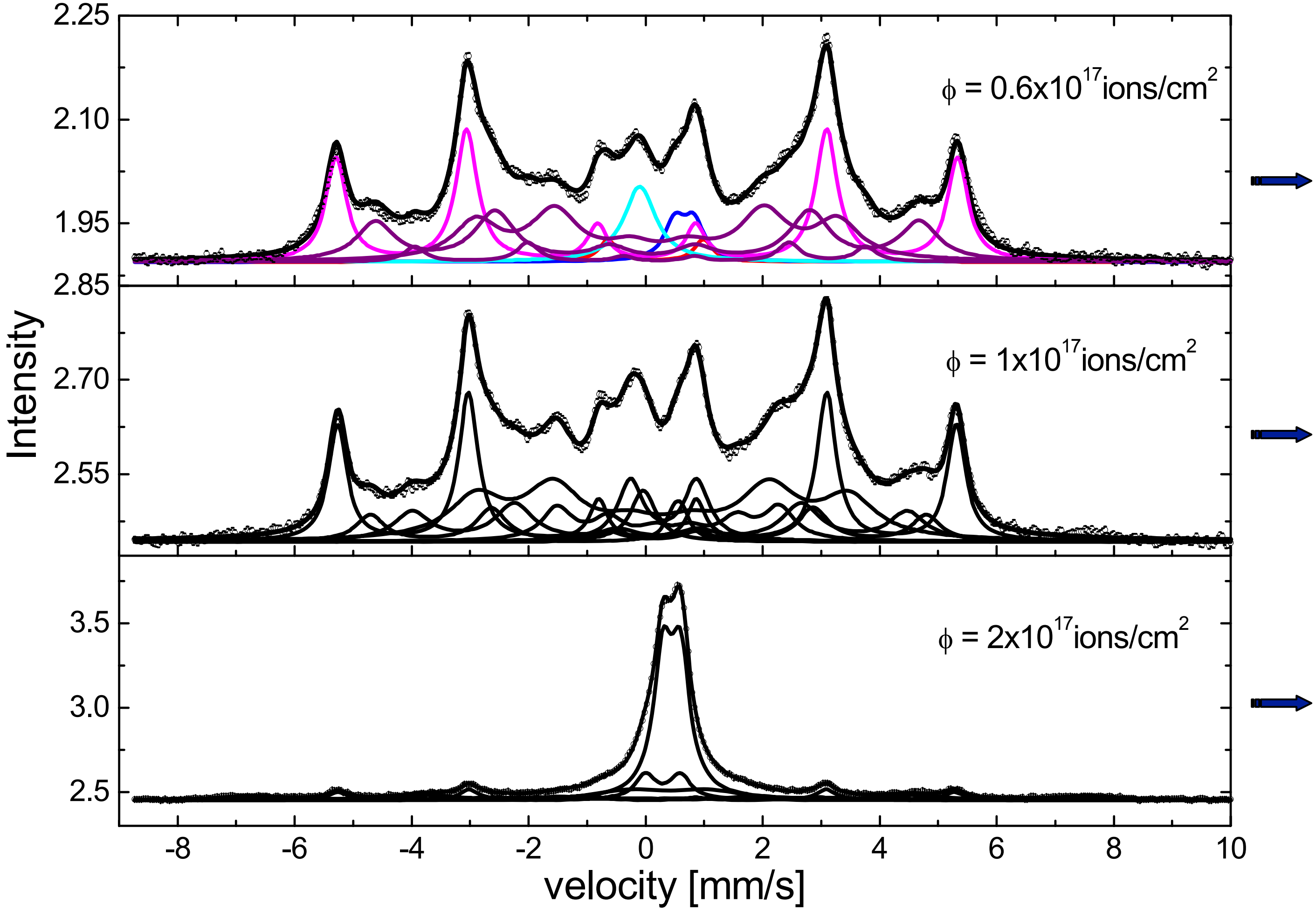

one doublet
and four sextets
H=33.0T δ=0mm/s
α-Fe (32.6%)
ε-Fe_{2+x}N (51%)

singlet, doublet,
five sextets
α-Fe (26.5%)
ε-Fe_{2+x}N (49%)
α'-(FeN) γ'-Fe_4N?

two doublets
four sextets
ε-Fe_2 N (61%)
α-Fe (7.6%)
α'-(FeN) ε-Fe_{2+x}N

Fraction of the nitride phase as observed by CEMS

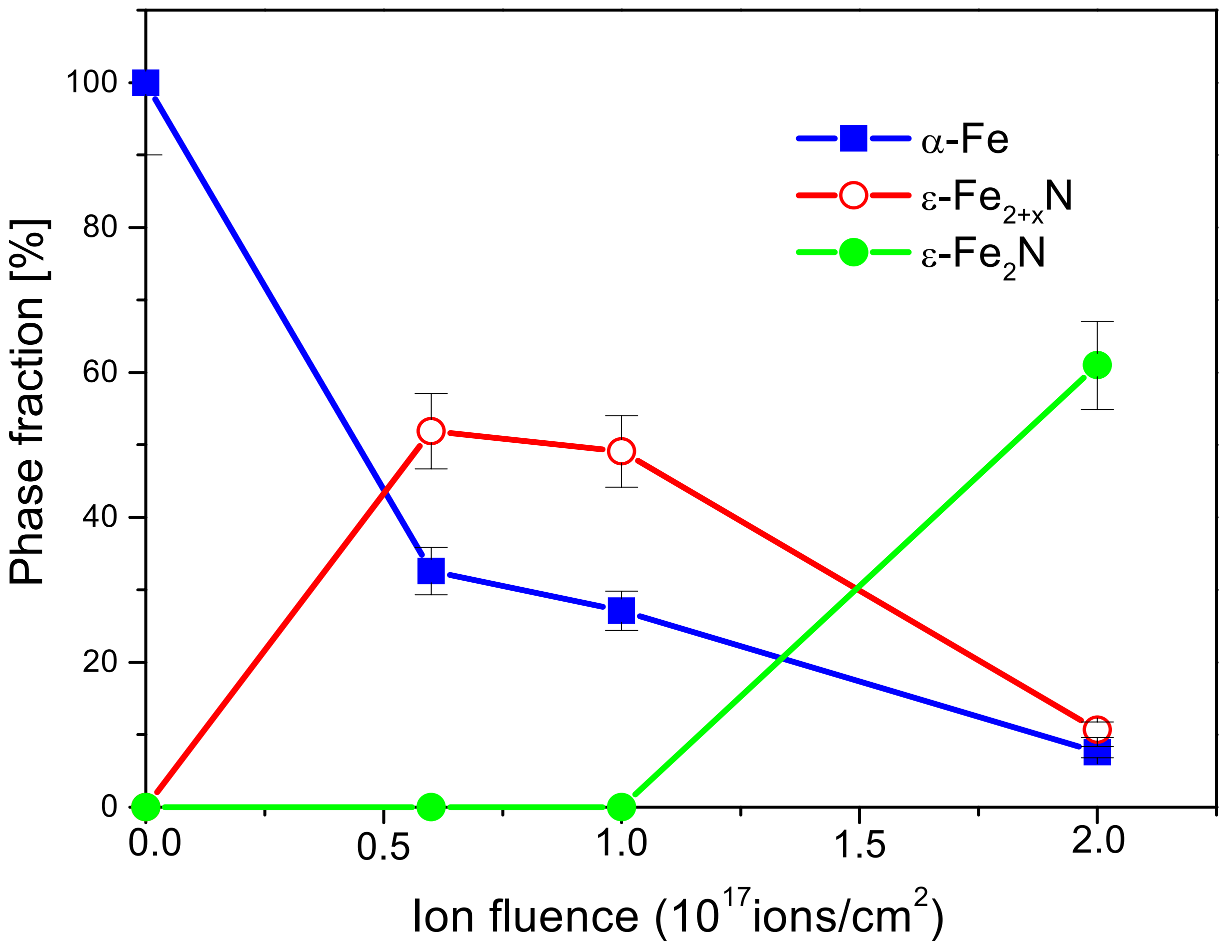

Phase fractions of various iron nitrides

Ion fluence ions/cm^2	Fraction of the nitride phase					
	α - Fe	α' - (FeN)	ε-$Fe_{2+x}N$	γ'-Fe_4 N	ε -Fe_2N	Oxide/ unresolved
0.6x10^{17}	**32.6%**		**51%**			**15.5%**
1.0x10^{17}	**26.5%**	**10%**	**49%**	**?**		**14%**
2.0x10^{17}	**7.6%**	**7.9%**	**10.7%**		**61%**	**12.7%**